Greenland Sea primary production with respect to changes in sea ice cover

Dissertation zur Erlangung des akademischen Grades
Doktor der Naturwissenschaften (Dr. rer. nat.)

vorgelegt dem Fachbereich 1 Physik der Universität Bremen

Erstgutachter : Prof. Dr. Astrid Bracher
Zweitgutachter: Prof. Dr. Antje Boetius
Datum der Abgabe: 21.02.2014

Alexandra Cherkasheva
geb. in Leningrad
2014

1st Reviewer: Prof. Dr. Astrid Bracher,
Institute of Environmental Physics, Universität Bremen, Bremen and Alfred-Wegener-Institute for Polar and Marine Research, Bremerhaven

2nd Reviewer: Prof. Dr. Antje Boetius,
Max Planck Institute for Marine Microbiology, Bremen, and Alfred-Wegener-Institute for Polar and Marine Research, Bremerhaven

Anlage zur Dissertation

Eidesstattliche Erklärung

(Gem. § 6(5) Nr. 1-3 PromO)

Hiermit versichere ich, dass ich

1) die vorliegende Arbeit ohne unerlaubte, fremde Hilfe angefertigt habe
2) keine anderen, als die von mir im Text angegebenen Quellen und Hilfsmittel benutzt habe
3) die den benutzen Werken wörtlich oder inhaltlich entnommenen Stellen als solche kenntlich gemacht habe.

Bremen, 15. Februar 2014

_____

Alexandra Cherkasheva

Dear Reader,

The current monograph presents the result of an interdisciplinary study that uses remote sensing, in situ and modeling techniques. As it explores the interaction between physical oceanography and marine biology and is to be presented in the Physics Department of the University of Bremen, the relevant concepts and notions of marine biology are described in detail for the benefit of the reader.

Table of Contents

Abstract

It has been estimated that phytoplankton contribute to about a half of the world's primary production and to over 90% of marine primary production. Phytoplankton are, therefore, responsible for releasing half of the world's oxygen and for removing large amounts of carbon dioxide from the surface waters. Without phytoplankton, atmospheric carbon dioxide concentration would increase by more than 200 ppm. In addition to this role, phytoplankton support essentially all life in the oceans despite their low biomass (1% of the Earth biomass). To evaluate how marine phytoplankton influence the carbon cycle, oxygen concentrations and affect the ocean food web, an accurate knowledge of marine primary production, seasonal cycle of phytoplankton and their inter-annual changes is required. Currently, the world marine primary production estimates range by a factor of two between different models. When only the Arctic Ocean is taken into account, this factor rises to fifty, because the optical properties of the water constituents as well as the vertical distribution of phytoplankton differ from those of the global ocean. Apart from that, the presence of sea ice complicates remote sensing in this region. Nowadays, Arctic phytoplankton deserve special attention as they are already living in waters with the most prominent climate change effect. The Arctic waters are beginning to show a shift towards a fresher surface layer, thinner sea ice, more open water area and are very likely to experience ice-free summers in the near future. These changes in turn alter solar irradiation, nutrient transport and plankton seasonality. Whether such an impact will result in an increase or a decrease of phytoplankton remains questionable. Since the polar regions are difficult to access with research vessels, there is a scarcity in field data and hence, remote sensing data, from optical satellites, provide an alternative. However, it is not recommended to use remote sensing data alone as the satellite ocean color algorithms used for estimation of phytoplankton stock are known to perform poorly at polar latitudes even if developed explicitly for the Arctic waters. Gaps in satellite data which occur at these latitudes because of the presence of sea ice, clouds and low sun elevation angles, are also a source of error.

The current thesis combines remote sensing, simulated and field data for the years 1998-2012, to investigate the seasonal cycle, variability and productivity of phytoplankton in the Greenland Sea, which is one of the most productive regions of the Arctic Ocean, as well as the most sampled region in terms of field data. Specific objectives for this case study in the Greenland Sea were: 1) to study the

interaction between phytoplankton and physical factors, such as sea ice concentration and thickness, water temperature and salinity; 2) to investigate temporal trends, seasonal cycle and spatial variability of phytoplankton; and 3) to obtain more accurate estimates of primary production.

First, we focused only on the northern part of the Greenland Sea (Fram Strait). The western, sea ice-dominated, part of the Fram Strait, proved to have short, late (mid-May) and time varying phytoplankton blooms. At the marginal sea ice zone of the western Fram Strait, a stratification induced by sea-ice melt was shown to have promoted phytoplankton growth, which resulted in the enhanced biomass observed in May. The eastern part, dominated by warm and salty Atlantic waters, experienced earlier (end of April) and longer blooms. Moreover, in the eastern Fram Strait, stratification due to solar warming proved to act as a guiding factor for the open ocean phytoplankton blooms, while the declining coastal ice was seen to promote the phytoplankton blooms along the coast of Svalbard. We have not observed a direct effect of the Arctic sea ice decrease in the time series of the Greenland Sea phytoplankton. However, we have observed that the enhanced stabilization of the water column, which was very likely caused by sea ice melt, promoted phytoplankton blooms. In the summer months, generally, the phytoplankton are concentrated in the upper ocean layer and are not limited by the light availability. The concentration of nutrients in this layer will, hence, determine the threshold up to which the primary production at these polar latitudes can increase in the future, provided the environmental changes continue.

Over the twelve years (1998-2009), a significant increase in phytoplankton bloom concentration was observed in the south-eastern part of the Fram Strait (which is mainly influenced by the Atlantic waters), where, for the same period, an increase in water temperatures and decline of coastal Svalbard ice was seen. We thus conclude that the observed increase in chlorophyll in the southern Fram Strait is most likely to have resulted from an increase in sea surface temperatures and from better availability of light for phytoplankton.

We have also studied the whole Greenland Sea to investigate and prove that the Greenland Sea chlorophyll vertical profiles largely deviate from the generalized schemes proposed earlier for global waters, which are usually used in primary production models. We developed a Greenland Sea specific algorithm which allowed accurate (only 4% underestimation when compared to in-situ data) estimation of the chlorophyll vertical profile based on the surface value. The global primary production model (Antoine and Morel, 1996) was then adapted to the Greenland Sea environment using this developed algorithm.

Our Greenland Sea-adapted version of the Antoine and Morel (1996) primary production model reproduced field data with higher accuracy and less bias (overestimation of in-situ data by 190 $mgC/m^2/day$ on average) as compared to the global version of the same model and the, more commonly used, satellite primary production model by Behrenfeld and Falkowski (1997a).

According to our Greenland Sea-adapted version of the Antoine and Morel (1996) model, annual Greenland Sea primary production was estimated between 161 and 194 TgC/yr (slightly higher than previously reported estimates which range between 148 and 162 TgC/yr). Time series of the primary production showed an increasing trend in the north-eastern open ocean area of the Greenland Sea (or south-eastern Fram Strait), rising to about 120 mgC/m^2 per day for the thirteen years of observations.

These newly derived Greenland Sea primary production estimates can be used in the future for validation of primary production obtained from biogeochemical models, which are based e.g. on the climatology of nutrients. On a local scale, it would be interesting for marine biologists to thoroughly compare our estimates with the benthic data, to study the part of the carbon cycle which links the increasing primary production of the Greenland Sea to the carbon stored in the sediments.

To my current knowledge, this thesis in the Greenland Sea, has for the first time: 1) studied the influence of the physical environment on phytoplankton using coupled sea ice-ocean-circulation model, microwave satellite and optical satellite data; 2) investigated the onset and duration of phytoplankton bloom based on satellite data; 3) developed a region-specific primary production model and, based on it, derived basin primary production estimates; and 4) modeled in-situ primary production from available in-situ irradiance, biomass, absorption and temperature profiles data.

List of publications

Peer-reviewed publications

Cherkasheva, A., Nöthig, E. M., Bauerfeind, E., Melsheimer, C., and Bracher, A. 2013. From the chlorophyll-a in the surface layer to its vertical profile: a Greenland Sea relationship for satellite applications. Ocean Science, 9 (2), pp. 431-445. doi:10.5194/os-9-431-2013

Cherkasheva, A., Bracher, A., Melsheimer, C., Köberle, C., Gerdes, R., Nöthig, E.-M., Bauerfeind, E., and Boetius, A., 2013. Influence of the physical environment on polar phytoplankton blooms: a case study in the Fram Strait. Journal of Marine Systems. doi: 10.1016/j.jmarsys.2013.11.008

Nöthig, E.M., Bracher, A., Engel, A., Metfies, K., Niehoff, B., Peeken, I., Bauerfeind, E., Cherkasheva, A., Gäbeler- Schwarz, S., Hardge, K., Hildebrandt, Kilias, E., Kraft, A., Lalande, C., Piontek J., Thomisch, K., Wurst, M. (in review). Plankton ecology and biogeochemistry in a changing Arctic Ocean - a case study in the Fram Strait . Arctic in Rapid Transition (ART) Special Issue

Conference and workshop contributions

Cherkasheva, A. , Bracher, A. and Melsheimer, C. 2010. Arctic marine primary production with respect to changes in sea ice cover. In: Oceanography from Space: Revisited. Barale, V. (ed.), Gower, J. F. R. (ed.), Alberotanza, L. (ed.), Oceanography from Space: Revisited, New York, Springer-Verlag, 374 p., ISBN: 9789048186808. hdl:10013/epic.35869

Cherkasheva, A., Nöthig, E. M., Bauerfeind, E., and Bracher, A., 2013. Towards accurate Greenland Sea primary production estimates: a parametrization of chlorophyll vertical profile. Liège Colloquium on Ocean Dynamics - ILCOD 2013, Liege, Belgium, 13-17 May 2013

Cherkasheva, A., Bracher, A., Melsheimer, C., Köberle, C., Gerdes, R., Nöthig, E.-M., Bauerfeind, E., and Boetius, A. 2013. Environmental controls of phytoplankton blooms at high latitudes: a case study at Fram Strait . Evaluation of Helmholtz Graduate School for Polar and Marine Research POLMAR, January 14, 2013, Bremerhaven, Germany.

Cherkasheva, A., Bracher, A., Nöthig, E. M., Bauerfeind, E., 2012. From the chlorophyll-a in the surface layer to its vertical profile: a Greenland Sea relationship for satellite applications. Franco-German Workshop 'Gateway to the Arctic', 17-19 October 2012, Bremerhaven, Germany

Cherkasheva, A., Bracher, A., Nöthig, E. M., Bauerfeind, E., 2012. Chlorophyll-a data as the main input parameter to the primary production models: case study for the Greenland Sea. Oceans of Change 2nd ICES/PICES Conference for Early Career Scientists, 24 - 27 April 2012, Majorca Island, Spain. hdl:10013/epic.40315

Cherkasheva, A., Bracher, A., and Melsheimer, C. 2011. Arctic primary production with respect to

changes in sea ice cover. PACES workshop on climate scenarios, September 5-6, 2011, Bremen, Germany.

Cherkasheva, A., Bracher, A., Melsheimer, C., Köberle, C., Gerdes, R., Nöthig, E. M., Bauerfeind, E., and Boetius, A., 2011. Influence of surface water stratification on phytoplankton blooms in the Arctic: a case study at Fram Strait. ICES/NAFO Symposium on the Variability of the North Atlantic and its Marine Ecosystems during 2000-2009. 10-12 May 2011, Santander, Spain. hdl:10013/epic.37650

Cherkasheva, A., Bracher, A., 2012. Influence of the stratification on the phytoplankton bloom in the Fram Strait. AWI Pol Biol Oz Seminar, 22 February 2011, Bremerhaven, Germany.

Cherkasheva, A., Bracher, A., and Melsheimer, C. 2010. Study of Arctic primary production with respect to changes in sea ice cover: first steps and future plans, IUP Ocean, Ice and Atmosphere Seminar, University of Bremen, December 2010, Bremen, Germany. hdl:10013/epic.36462

Cherkasheva, A., and Bracher, A. 2010. Chlorophyll-a and sea ice satellite data analysis. Case study for the Hausgarten region, AWI Pol Biol Oz Seminar, November 2010. hdl:10013/epic.36461

Cherkasheva, A. 2010. Arctic marine primary production with respect to changes in sea ice cover: challenges and first findings. AWI PhD Days 2010, 25-27 May 2010, Potsdam, Germany.

Melsheimer, C., and Cherkasheva, A. 2012. Remote Sensing of Sea Ice and Possible Implications for Arctic Primary Production. Sino-German Symposium 2012, 'Advances in observation and modelling of biogeochemical and oxygen dynamics in the ocean', 17-18 September 2012, Kiel, Germany

Nöthig, E. M., Bauerfeind, E., Haas, A., Boetius, A., Bracher, A., Cherkasheva, A., Kraft, A., Metfies, K., Peeken, I., and Schwarz, J. N. 2012. Variability of chlorophyll a distribution in the Fram Strait, Greenland Sea and Central Arctic Ocean, IPY 2012 Conference: From Knowledge to Action , Montreal, Canada, 23 April 2012 - 27 April 2012. hdl:10013/epic.39192

Nöthig, E. M., Bauerfeind, E., Haas, A., Bracher, A., Cherkasheva, A., Kraft, A., Peeken, I., Metfies, K., and Schwarz, J. N. 2011. Variability of chlorophyll a distribution in the Fram Strait and the Greenland Sea. ICES/NAFO Symposium on the variability of the North Atlantic and its marine ecyosystems during 2000-2009, 10-12.05.2011, Santander, Spain. hdl:10013/epic.37872

Peeken, I., Nöthig, E. M., Bauerfeind, E., Bracher, A., Cherkasheva, A., Engel, A., Gäbler-Schwarz, S., Kilias, E., Kraft, A., Metfies, K., Niehoff, B., Pfaff, S., and Wurst, M. 2011. Plankton Ecology and Biogeochemistry in a Changing Arctic Ocean (PEBCAO), first results from the AWI HAUSGARTEN area (Fram Strait). Arctic Frontiers Arctic Tipping Points. Tromsø, Norway, January 2011. hdl:10013/epic.36723

Chapter 1

Introduction

1.1 Motivation and the goals of the study

Marine phytoplankton are responsible for about half of the global primary production, which is the rate of conversion of inorganic carbon into organic carbon through the process of photosynthesis. They, therefore, are responsible for releasing half of the world's oxygen and are annually making about 50 billion metric tons of carbon available to the heterotrophs in the world ocean, an amount equivalent to the terrestrial production (Chavez et al., 2011). Despite the relatively equal productivities of land and ocean primary producers, the world ocean accounts for only 1% of the photosynthetic Earth biomass (Bidle and Falkowski, 2004). Although the biomass of marine phytoplankton is low, they profoundly affect global biogeochemical cycles and climate, and hence, essentially support all life in the world ocean.

One of the essential processes performed by phytoplankton is the 'biological pump', in which carbon dioxide is removed from the surface water by photosynthesis and transferred to the deep ocean where it is out of contact with the atmosphere, dead organisms, skeletal and fecal material. Without the contemporary biological pump, atmospheric carbon dioxide concentration would increase by more than 200 ppm (Gruber and Sarmiento, 2002; Maier-Reimer et al., 1996).

Phytoplankton represent the primary trophic level in marine pelagic ecosystems, through which most of the biological material produced by photosynthesis is channeled further through the foodweb via grazing by zooplankton. Because zooplankton act as a link between phytoplankton and higher trophic levels, the timing, intensity and the rate of phytoplankton growth were demonstrated to be important factors for fish recruitment and growth (Platt et al., 2003).

To parameterize how marine phytoplankton regulate atmospheric carbon dioxide and oxygen concentrations and affect the oceanic food webs, an accurate knowledge on the marine primary production estimates, seasonal cycle and inter-annual changes is required.

Current estimates of global marine primary production range over a factor of two (Carr et al, 2006). At high latitudes, the uncertainty in primary production estimates is even larger than globally, because

here, phytoplankton show special characteristics in response to the low-light adaptation, and in-situ data and ocean color observations are scarce.

Besides the difficulties in estimating the absolute values, knowledge on the variability of primary production is also limited. Despite more than 25 years of active research, our understanding of temporal and spatial variability in primary production is still incomplete (Robinson et al., 2009). In the polar regions this statement is clearly illustrated by a disagreement in the pattern of phytoplankton seasonal cycle postulated by different oceanographers (Figure 1.1). According to Chamberlin and Dickey (2008), at high latitudes, phytoplankton experience a single intense bloom in summer triggered by the increase in light intensities (Figure 1.1, top). A similar concept was described by Wassmann (2011). Recent work by Ardyna et al. (2013), however, states that two phytoplankton blooms (a massive spring bloom followed by a smaller autumn bloom) are generally observed in the Arctic Ocean (Figure 1.1, bottom).

The study of seasonal changes of populations of primary producers with respect to changes in environmental factors is a basis for our understanding of the ocean food webs. The marine environment influences the phytoplankton stock and their growth rate in a complex way which leads to challenges in interpretation, especially for the polar regions. An example is the interaction between sea ice and phytoplankton. Firstly, sea ice reduces light penetration into the water column, which has a negative effect on the underlying algae (Rysgaard et al., 1999; Smetacek and Nicol, 2005). Secondly, melting of sea ice increases the upper ocean stability since freshwater is released into the upper ocean layer. This can either promote blooms by keeping the phytoplankton closer to the surface where light levels are favorable for growth (Doney, 2006; Lancelot et al., 1993) or suppress them by increasing grazing pressure (Banse, 1992; Behrenfeld, 2010). Stratification can also suppress nutrient supply from deeper layers and thus limit further phytoplankton development. Finally, during the ice melt, phytoplankton and trace elements which were incorporated in the ice during formation, or accumulated as dust in the snow cover, are released into the upper ocean layer. This process could accelerate the spring bloom (Schandelmeier and Alexander, 1981; Smetacek and Nicol, 2005). The recent decrease in the minimum Arctic sea ice extent (Comiso et al., 2008; NSIDC, 2012), accelerated sea ice thinning (Giles et al., 2008), and freshening of the surface-layer waters of the Arctic Ocean (Proshutinsky et al., 2010) are likely to impact primary productivity and carbon export of the Arctic Ocean by altering solar irradiation, nutrient transport and plankton seasonality (Arrigo et al. 2012; Boetius et al. 2013; Vaquer-Sunyer et al. 2013; Wassmann 2011). Whether such an impact will result in an increase or a decrease of

phytoplankton remains questionable.

In order to make an effort towards solving the problems described above, the current case study for the Greenland Sea has three main objectives. These are:

I. to study the interaction between phytoplankton and physical factors, such as sea ice concentration and thickness, water temperature and salinity
II. to investigate temporal trends, seasonal cycle and spatial variability of phytoplankton
III. to obtain more accurate estimates of primary production.

We focus on the Greenland Sea region of the Arctic for several reasons. Firstly, the Greenland Sea is known to be one of the most productive regions of the Arctic (Arrigo and Van Dyiken, 2011; Reigstad, 2011; Sakshaug, 2004). Secondly, it is one of the few areas in the world where deep convective mixing occurs, possibly transferring significant amounts of carbon dioxide to great depths (Rey et al., 2000). Finally, it is one of the regions in the Arctic where the most in-situ chlorophyll-a (CHL) data are available (Arrigo et al., 2011). The Greenland Sea, was and is, in the focus of the hydrographic studies of the Alfred-Wegener-Institute (AWI), and transects across the Fram Strait have been run repeatedly for many years (e.g. Budeus and Ronski, 2009; Schauer et al., 2008). In this study, in-situ CHL data from R/Vs *Polarstern* and *Maria S Merian* 1991-2011 cruises are used together with the historic ARCSS-PP database (Arctic primary production in situ database).

In this study, in-situ measurements of CHL, but not of primary production, have been used. The standard field estimations of primary production involve incubations (24 or 12 hours) and require the use of radioactive isotopes (see section 2.5). Such field measurements of primary production are tedious and time-consuming. Hence, the measurements of phytoplankton biomass (given as CHL) are more common and are thus used in this study along with measurements of light field and particulate absorption to estimate the primary production.

Clearly, an ideal representation of primary production is at an ocean basin level (Robinson et al., 2009), especially when evaluating the significance of marine primary producers to the global carbon cycle and human-induced climate change. It is however slow to obtain basin-wide primary production estimates from the in situ data, owing to the enormous scales of time and space over which measurements must be taken. Technical difficulties and interpretation of results from different methodologies also challenge oceanographers attempting to provide accurate data on basin-wide primary production.

Satellite-based estimates of primary production have the potential to solve this problem, as the ocean color data, which gives information on phytoplankton biomass, is obtained on an about weekly scale with a 4.6 km spatial resolution (ACRI-STLOV et al., 2006) in most of the parts of the world ocean. Owing to the advances in ocean color remote sensing, by the mid-1990s, oceanographers concluded that oceanic production was twice that it was previously estimated (Chamberlin and Dickey, 2008). This is followed by a bigger influence of oceans on the global carbon cycle. Remote sensing methods are especially significant for estimating primary production in the remote polar regions which are difficult to access with the research vessels. However, it is inaccurate to use the remote sensing data alone, as the satellite ocean color algorithms are known to perform poorly at high latitudes even if developed explicitly for the Arctic waters (Cota et al., 2004; Matsuoka et al., 2007; Mitchell and Holm-Hansen, 1991; Sathyendranath et al., 2001) and due to the gaps in satellite data which occur due to the presence of sea ice, clouds and low sun elevation angles. In addition to that, in the absence of the explicit knowledge of the vertical distribution of biomass, remotely sensed CHL estimates in the Arctic Ocean are limited to the first optical depth which represents only the upper third of the euphotic zone phytoplankton biomass (Hill and Zimmerman, 2010). It is also a common knowledge that inaccuracy in estimating true ocean primary production is a problem for models based on remotely sensed CHL. The greatest degree of uncertainty comes from the accuracy of input variables, particularly CHL, rather than model simplicity (Saba et al., 2011). Hence, in the current study, we compiled the data retrieved from principally different sources: optical and microwave data from satellites, ship-borne optical and pigment measurements, and coupled sea-ice-ocean model data. This results in a more accurate estimation of phytoplankton biomass, primary production and their link to physical processes.

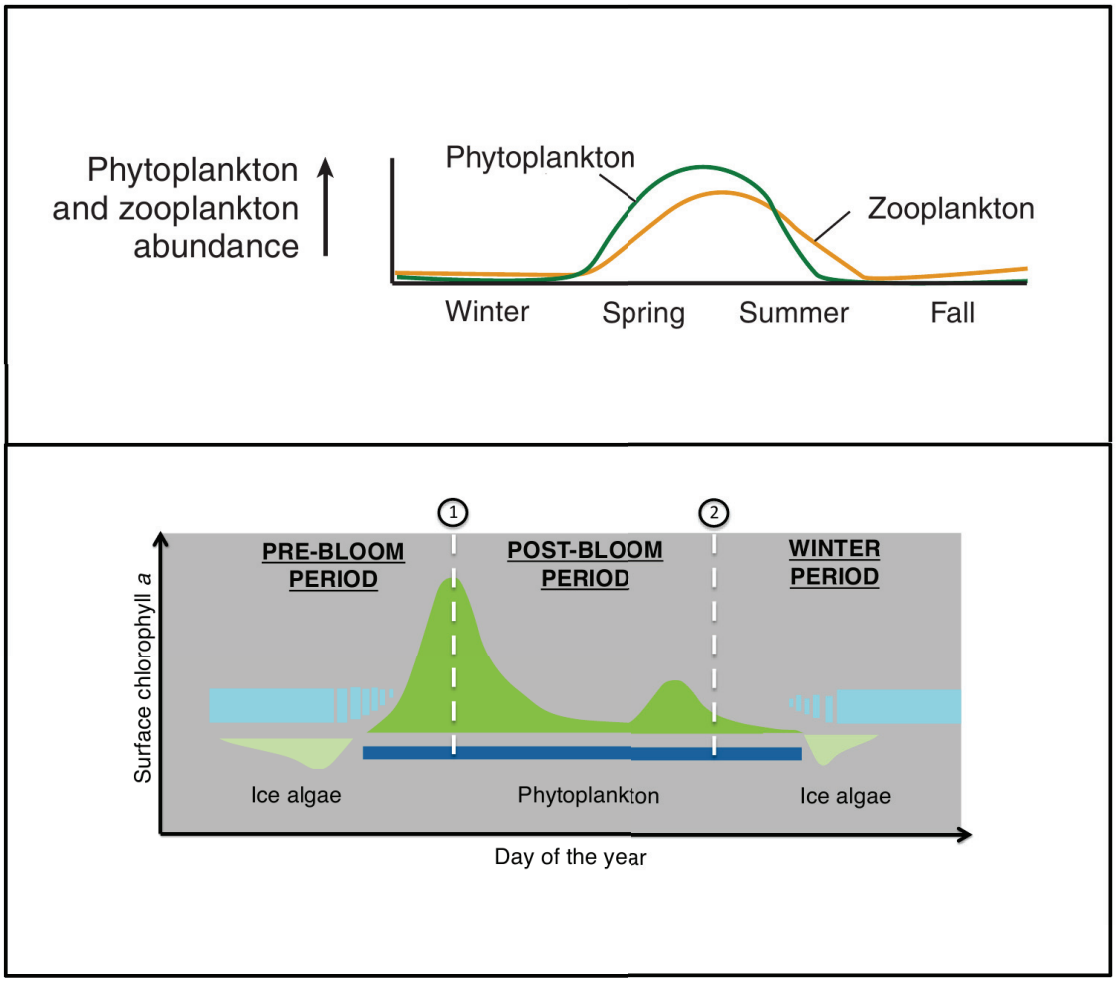

Figure 1.1 Top panel: phytoplankton seasonal cycle at high latitudes according to Chamberlin and Dickey (2008) as adopted from Segar (2007). Bottom panel: phytoplankton seasonal cycle in the Arctic Ocean according to Ardyna et al. (2013). First and second temporal delimitation are defined by the highest value of surface CHL and a threshold of 9 h of daylight, respectively.

1.2 Thesis Outline

The broad structure of the thesis is as follows. Chapters 2 to 3 provide the background information necessary for the four main thesis investigations that are presented in Chapters 4 to 7. Chapter 8 summarizes the main observations and results of the thesis and gives an outlook for possible future research.

In Chapter 2 an introduction to phytoplankton and marine primary production is presented. The factors controlling primary production are described and the methods used to estimate primary production are presented. Chapter 3 describes the oceanographic conditions of the Greenland Sea region and their potential effect on phytoplankton variability. A short review of studies dealing with phytoplankton in the Greenland Sea is also given here. Chapter 4 is the first of four major investigations. It describes the phytoplankton variability with respect to the changing polar marine environment in the Greenland Sea. This chapter provides an assessment of the impacts of various physical factors on the variability and trends of phytoplankton biomass. This chapter is based on Cherkasheva et al. (2013b), which was published in the *Journal of Marine Systems*. In Chapter 5 the duration and the intensity of phytoplankton blooms were closer analyzed in the temporarily ice-covered and open ocean areas of the Greenland Sea. This chapter is based on the contribution made in Nöthig et al. (in review), which is in review in the *Arctic in Rapid Transition (ART) Special Issue*. In Chapter 6, a parametrization and a description of the characteristic Greenland Sea CHL profiles are given based on CHL in-situ data from 1957-2010. CHL is a standard proxy for phytoplankton biomass. The parametrization was required in order to estimate the phytoplankton biomass in the water column from the satellite CHL value which originates from the surface ocean layer. This chapter is based on Cherkasheva et al. (2013a), which has been published in *Ocean Science*. Chapter 7 presents the output of a Greenland Sea-specific algorithm which transfers from the stock value, phytoplankton biomass, to the rate, primary production. Here, the relationship derived in Chapter 6 is used to obtain the local Greenland Sea algorithm for calculating primary production from satellite observations. The resultant satellite primary production is then validated with primary production values modeled using in-situ input data. Finally, Chapter 8 presents the conclusions and outlook of the thesis.

Chapter 2

Scientific backgrounds

2.1 Phytoplankton: main primary producers of the world ocean

Phytoplankton are not unique primary producers in the world ocean, and at a regional scale, other kinds of primary producers can substantially contribute to photosynthesis. For example, in shallow coastal waters and estuaries, seaweeds or macroalgae may be prevalent. Marine plants with roots and leaves include seagrass, salt marsh plants, and others. Coral reefs are mainly inhabited by zooxanthellae of corals. However, though many of mentioned organisms could have high photosynthetic rates locally and provide food and shelter to a wide variety of marine organisms, their contribution to the global primary production is much less than that of the marine phytoplankton. In the current study, the focus is on dominant primary producers in the world ocean, phytoplankton (Table 2.1).

Table 2.1 Primary Producers in the World Ocean. Adopted from Field et al., 1998.

Biogeographic region and its primary producers	**World Ocean Net Primary Production (units x 10^{15} grams carbon per year)**
Oligotrophic regions (phytoplankton)	11.0
Mesotrophic regions (phytoplankton)	27.4
Eutrophic regions (phytoplankton)	9.1
Coastal ocean and estuaries (kelps and seaweed)	1.0
Total	48.5

2.1.1 Classification of phytoplankton

Phytoplankton include both single-celled plants (eukaryotes) and bacteria (prokaryotes) and are defined as microscopic algae (or microalgae). Algae are the photosynthetic autotrophs lacking roots and leaves, and include, besides phytoplankton, seaweeds, or macroalgae. In other words, organisms are assigned to phytoplankton according to their microscopic size and their ability to convert inorganic carbon into organic compounds using dissolved substances and the radiant solar energy. These organisms, however, may be very different in terms of their shape (Figure 2.1), Deoxyribonucleic acid (DNA), pigment composition etc.

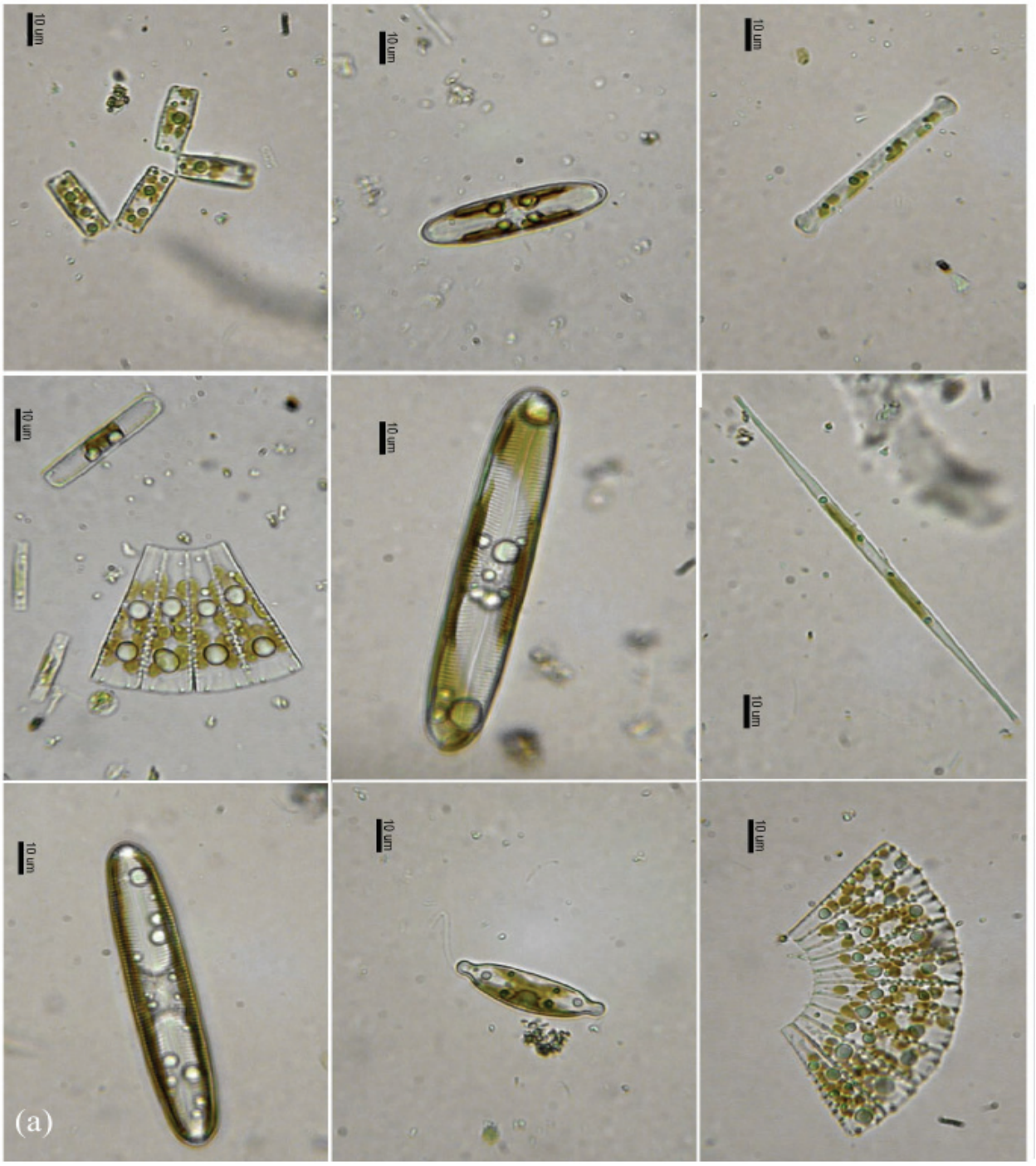

Figure 2.1 Example of the diversity in phytoplankton shapes: diatoms in approximately 20x magnification. From Segar (2007).

Since phytoplankton are easily separated using filters of different pore sizes, they (and other plankton) are often classified according to their size. Phytoplankton represent a continuum of sizes from ~0.6µm to chain forming species generating aggregates greater than 200 µm. Three size classes are usually being specified: pico- (0.2 - 2 µm), nano- (2 - 20 µm) and microphytoplankton (20 µm) (Sieburth et al., 1978). These broad classes occupy different physical and chemical niches based on their nutrient-uptake ability, light-harvesting efficiency, and sinking rate through the euphotic zone.

Besides size, phytoplankton are often classified according to their functional type. In this concept, each phytoplankton functional type represents an aggregation of organisms according to some well-defined property that sets a role or "function" for them in a system. Some important phytoplankton functional types include nitrogen fixers (which are able to utilize nitrogen gas dissolved in seawater), calcifiers (which produce calcium carbonate shells) and silicifiers (which have silica frustules that surround and protect the cells, and also tend to sink more rapidly than other phytoplankton).

From an optical point of view, colour of phytoplankton differs depending on the pigments that they have. Light-absorbing pigment chlorophyll-a, which exists in all phytoplankton, absorbs light in the wavelength range between 400 nm and 700 nm and most in the wavelength that penetrates deepest in the ocean, around 440 nm (Cannizzaro and Carder, 2005; Figure 2.2). Its concentration in seawater is easily determined by the instruments that detect fluorescence. This is the pigment we focus on as it is present in all phytoplankton and its concentration is used as a proxy for phytoplankton biomass. In addition to chlorophyll-a some phytoplankton groups also manufacture chlorophyll-b, chlorophyll-c, phycobilins (e.g. phycoerythrin and phycocyanin) and carotenoids (e.g. betacarotene). These accessory pigments have different wavelengths of maximum absorption, and give phytoplankton different colours such as green, brown or red. Thus depending on the phytoplankton group, they can absorb almost the full range of light and survive in the environment even when blue light is unavailable, such as under a phytoplankton bloom. For our study, it is important that phytoplankton pigments composition is affecting the phytoplankton absorption spectrum. Mind that a wavelegth-resolved satellite primary production model which we use (see sections 2.6.5, 7.2.2), assumes a certain standard absorption spectrum of phytoplankton, which may change if groups with a non-typical (e.g. regional) pigment composition are present.

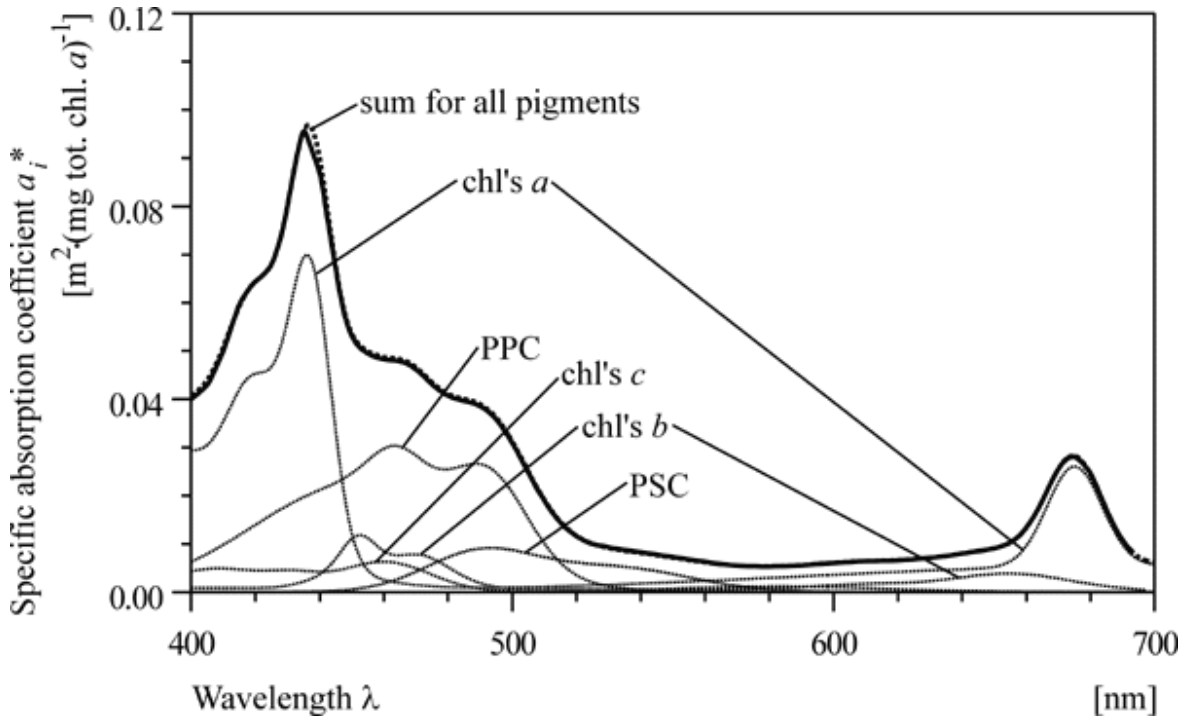

Figure 2.2 Specific light absorption spectra: modeled main groups of phytoplankton pigments, their sum (dashed line) and total spectrum determined on the bases of the measured data sets (solid lines). PPC stands for photosynthetic and PSC stands for photo-protecting carotenoids. Adopted from Wozniak et al. (1998).

2.1.2 Deriving phytoplankton biomass from satellite

Most phytoplankton absorb light much more strongly in the blue than in the green (Figure 2.2), which is the basis for the algorithms that retrieve phytoplankton concentrations from satellites. As the phytoplankton concentration increases, the water-leaving radiance (light backscattered from the ocean at the sea surface) in the blue spectrum is absorbed and decreases. Because phytoplankton also scatter light, as do all kinds of particles by which they are accompanied, an increase of phytoplankton increases the amount of light backscattered in the green spectrum. Therefore, by determining the ratio of water-leaving radiance in the blue (~440 nm) to the green (~550 nm) wavelengths range, a quantitative estimate of pigment concentration is derived (e.g. O'Reilly et al., 1998).

Since the ocean color satellite sensor is located above the atmosphere at a few hundred kilometers,

the water-leaving radiances measured by the satellite sensor contributes to less than 5% of the total light measured by the satellite (Brown, 2008). The total radiance received by the sensor above the atmosphere, L_T, can be broken down as follows (omitting spectral and angular dependencies (Martin, 2004)):

$$L_T=L_R+L_A+L_{RA}+tL_G+t_DL_F+t_DL_W \qquad [2.1]$$

Table 2.2 Symbols used for the definition of radiances (W m^{-2} sr^{-1} μm^{-1}) and transmittances (dimensionless) in equation above

Symbol	**Definition**
L_T	Total radiance at the top of the atmosphere
L_R	Radiance due to Rayleigh scattering
L_A	Radiance due to aerosol scattering
L_{RA}	Radiance due to aerosol-molecule interactions
L_G	Radiance due to sun glint
L_F	Radiance due to presence of foam at sea surface
L_W	Water-leaving radiance
t_D	Diffuse transmittance
t	Beam transmittance

The necessary operations to obtain the value of water-leaving radiance, also called 'marine radiance' (L_w), are the atmospheric corrections which are generally based on signal decomposition (equation [2.1]). These consist of eliminating the part of radiation that was backscattered by the molecules (L_R) and aerosols in the atmosphere (L_A and L_{RA}), and possibly also reflected at the ocean surface by sun glint (L_G) and foam (L_F), but have never penetrated the ocean surface.

Attenuation of light in the atmosphere happens due to scattering and absorption on various atmospheric constituents (molecules, particles and gases) - e.g. molecular scattering (Rayleigh scattering), scattering and absorption on aerosols, clouds and atmospheric gases. The spectral radiometers (as are MODIS, MERIS, etc) mostly work within the transparency windows of the atmosphere, i.e. the spectral intervals of very high gaseous absorption are avoided. For such sensors,

most atmospheric corrections would therefore address scattering mechanisms (Antoine, 2006). For some of the constituents, their distribution in the atmospheric column and their scattering properties are well known or can be assumed with high accuracy, so that the corresponding effect can be corrected for (as is for Rayleigh scattering and some of the atmospheric gases, e.g. water vapor). For others, either the distribution, scattering properties (as e.g. for aerosols) or the height of the atmospheric column are in general case not known (as for e.g. oxygen absorption bands in case of cloudy skies), so their effect on the top of atmosphere radiance measured by satellite varies. This variance and the sensitivity of the top of atmosphere radiance to it are used to retrieve the corresponding quantity (e.g. aerosol optical thickness or cloud properties retrievals) and knowing that, to determine atmospheric transmittance.

The above mentioned mechanisms altogether determine atmospheric transmittance and are responsible for the radiance reaching the surface. The effects of polarization and modification of the way in which illumination is reflected at the air-to-sea interface can also be taken into account (Gordon et al., 1988; Gordon and Wang, 1992 a, b). Most currently used techniques for atmospheric correction rely on the observation in at least two channels of the near infrared, for which the oceanic signal is zero (this is only true in open ocean waters). This is due to the very strong absorption of water itself, and to the low scattering of the various materials present in the water (except perhaps air bubbles). After correction for molecular scattering, the remaining signal at these wavelengths is entirely due to aerosols. From the intensity of this signal and its spectral dependence at the two wavelengths, the aerosol contribution can be extrapolated through visible wavelengths (for example, Andre and Morel, 1991; Antoine and Morel ,1998, 1999; Bricaud and Morel 1987; Gordon 1978; Gordon, 1997; Gordon and Wang, 1994; Fraser et al., 1997).

In addition to the atmospheric corrections made, some pixels are screened out due to the presence of sun glint and foam. For the sun glint masking in SeaWiFS and MODIS images, the combination of the wave facet model by Cox and Munk (1954) with vector wind speeds derived from NOAA numerical weather prediction models is used. An additional check on sun glint is provided by examination of near-infrared radiances, where if these radiances exceed a preset threshold, sun glint is assumed and the pixel is masked. There is an important difference between the spatial and angular distribution of the reflected radiances due to foam and sun glint, with foam pixels being more difficult to screen out. The sun glint radiances are distributed around a certain solar angle, so that depending on wind velocity these radiances may affect only a fraction of the image, which can be masked. The foam coverage also depends on wind speed, but because foam reflectance is more diffuse, it has a much weaker

dependence on solar angle, so that L_F can be nearly uniform across an image. In the processing, L_F is estimated, then either subtracted from L_T or if L_F is too large, the image is discarded. Estimation of L_F follows the model of Frouin et al. (1996) and Moore et al. (2000). In almost all cases, the correction for foam is small, perhaps because small winds are often accompanied by clouds (Martin, 2004).

After the corrections described above are made, the water-leaving radiances (L_w) obtained can be expressed through the following equation:

$$L_w\left(\lambda,\theta_s,\theta',\Delta\varphi\right)=E_d\left(0^+,\lambda\right)Geom\left(\theta'\right)R\left(\lambda\right)/Q\left(\lambda,\theta_s,\theta',\Delta\varphi\right) \qquad [2.2]$$

where λ is wavelength, θ_s is solar zenith angle, θ' is satellite viewing angle and ΔΦ is the relative azimuth difference angle. $E_d(0^+)$ is downwelling irradiance just above the sea surface, and R(λ) is diffuse reflectance of the upper ocean. Geom (θ') is the geometrical factor, accounting for all refraction and reflection effects at the air-sea interface (Morel and Gentili, 1996) , and Q (λ, θ_s , θ', ΔΦ) is the factor which describes the anisotropy in the marine radiance field. For the values of Q factor see Morel et al. (1995), Morel and Gentili (1991, 1993, 1996).

When retrieving the CHL values, rather than using observed radiances which are influenced by the geometry of the observation, we inverse the equation above and use the ratio of reflectances R, which are dependent on the wavelength alone:

$$R\left(\lambda\right)=L_w\left(\lambda,\theta_s,\theta',\Delta\varphi\right)Q\left(\lambda,\theta_s,\theta',\Delta\varphi\right)/E_d\left(0^+,\lambda\right)Geom\left(\theta'\right) \qquad [2.3]$$

An illustration of the ability for retrieving CHL concentration from two slightly different reflectance ratios is given in Figure 2.3.

Though the estimation of CHL in the open ocean (Case 1 waters) is well established using the reflectance ratios, it is not the case in coastal waters (Case 2 waters). This is mainly due to the presence of dissolved and particulate materials from rivers, land runoff, and resuspension of seafloor sediments which interferes with the reflectance measurement of phytoplankton. In these waters, the determination of CHL is more complicated, since it is not correlated to the amount of non-algae particles and CDOM (Coloured Dissolved Organic Matter).

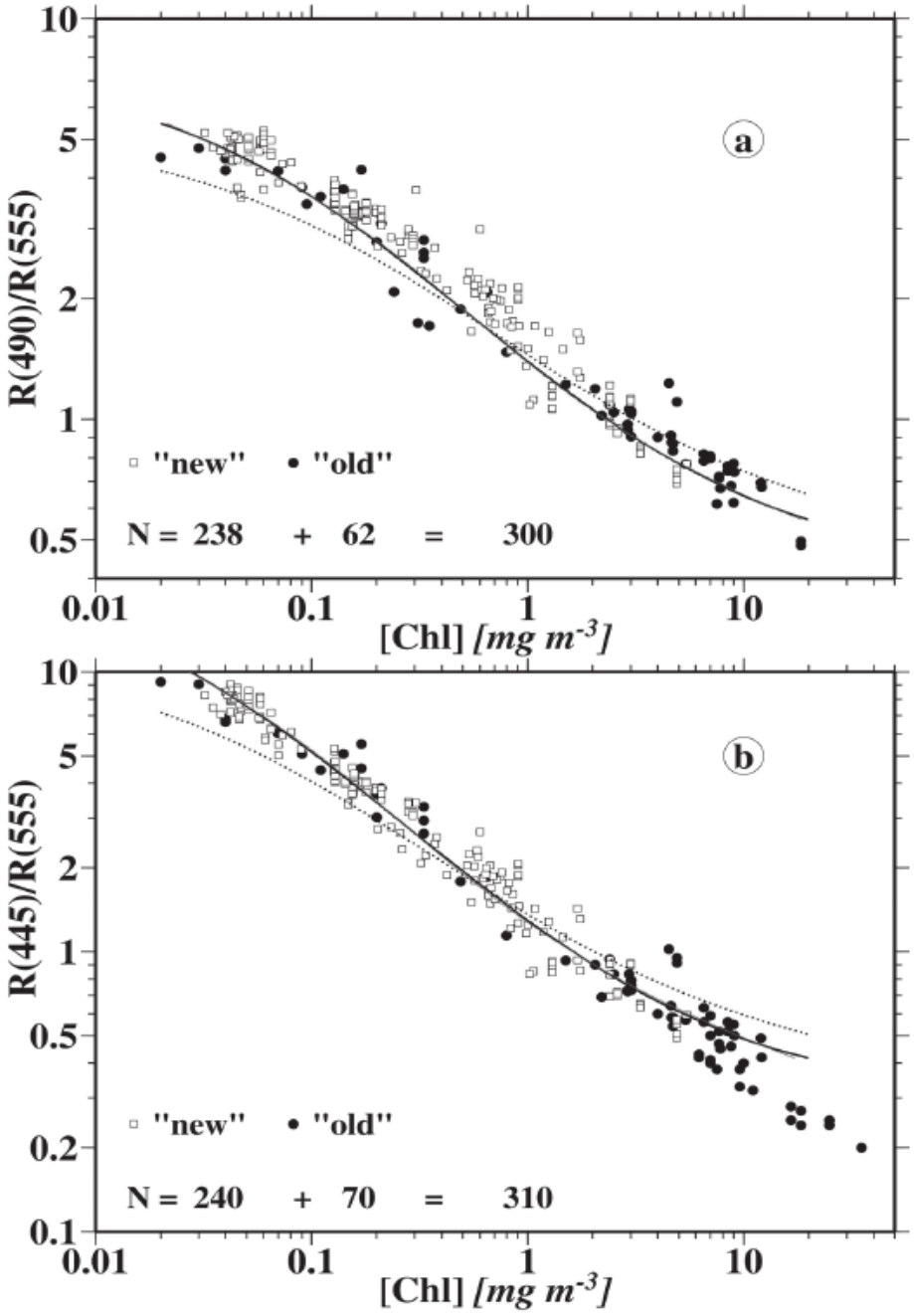

Figure 2.3. Illustrations of the relation of two different reflectance ratios (i.e., R(445)/R(555) (lower panel) and R(490)/R(555) (upper panel)) to the CHL concentration. The various symbols correspond to data collected in various parts of the world ocean, and the dashed lines correspond to the bio-optical model proposed by Morel (1988), whereas the solid curves correspond to the bio-optical model proposed by Morel and Maritorena (2001).

2.2 From biomass to primary production: a generalized scheme of photosynthesis

The knowledge of phytoplankton biomass is important to answer the questions about the phytoplankton seasonal cycle and the magnitude of phytoplankton blooms. However, if the research question is to quantify the amount of carbon which was fixed by phytoplankton and made available to heterotrophs or stored in the sediments, then the flux of biomass, i.e. primary production, should be estimated or derived.

The fixation of dissolved carbon dioxide by phytoplankton is made via photosynthesis. Photosynthesis produces the chemical energy that drives the cycling of organic matter in nearly all of Earth's ecosystems. The description by Kirk (1994) emphasizes the energetic aspects of photosynthesis in two fundamental sets of reactions: 1) the light reaction, or the set of chemical reactions that are driven by sunlight, where photons are absorbed, and electrons are transferred into chemical energy. Here the electron from the water molecule is taken up by the CHL-photosystem and oxygen is generated as a byproduct; and 2) carbon-fixation reaction, or the set of chemical reactions that use the chemical energy produced by the light reaction (converted into ATP (adenosine triphosphate) and NADPH (nicotinamide adenine dinucleotide phosphate) to manufacture sugars and other energy-yielding products. Overall, the light reaction and carbon fixation reaction are combined into a general equation for photosynthesis

$$CO_2 + H_2O + light \rightarrow C_6H_{12}O_6 + O_2 \qquad [2.3]$$

If the major limiting nutrients are included and the Redfield ratios (Redfield et al., 1963) for phytoplankton are applied (106 C : 16 N : 1 P), the equation reads:

$$106\,CO_2 + 122\,H_2O + 16\,HNO_3 + H_3PO_4 \rightarrow (CH_2O)_{106} + [NH_3]_{16} + H_3PO_4 + 138\,O_2 \qquad [2.4]$$

Even when written this way, it is a simplification of the photosynthesis equation. However, it

symbolizes the important aspects of photosynthesis, namely, that inorganic carbon dioxide and water are transformed using light energy into organic carbon compounds, yielding oxygen as a by-product. It also emphasizes the role of biologically important nutrients, which are the dissolved substances required for the growth of phytoplankton (see details below in section 2.4.2). In the oceanic environment, the availability of both, light and nutrients, governs rates of photosynthesis.

2.3 Terms 'primary production' and 'primary productivity'

There is a confusion between the terms 'primary production' and 'primary productivity', because term 'primary productivity' is often used in the scientific literature to denote both the process of photosynthesis itself and the rate at which it occurs. Therefore various authors (Davis, 1963; Flynn, 1988; Steeman Nielsen, 1965) have come to the conclusion that owing to casual use or misuse, one or other of the terms should be abandoned. On the other hand, the dictionary definitions (e.g., Little et al., 1983) make it clear that whereas production (like product) is a concrete term, productivity is qualitative and more abstract. In this study, the separation between the two terms which was proposed by Williams (1993), and is close to that based on dictionary definitions, is used: production (or the rate of production) is the defined property ('...the annual production was...'), whereas productivity (as fertility) qualitatively describes the level of production ('…a period of high productivity...').

2.4 Types of primary production

Commonly three types of primary production (PP) are defined based on how the respiration by organisms was accounted for in the measurement or in the model. The PP values obtained using the different definitions can differ up to an order of a magnitude. It is thus necessary to define the type of PP of interest prior to the measurement or modeling.

Gross Primary Production (GPP) is defined as the rate of conversion of inorganic carbon into organic carbon (i.e., photosynthesis). It yields the largest value. Net Primary Production (NPP) is the organic carbon remaining after the metabolic needs of phytoplankton have been met (or the Autotrophic Respiration (AR) has been accounted for).

$$NPP=GPP-AR \qquad [2.5]$$

Since NPP represents the organic carbon available to other trophic levels, that is, the heterotrophs, and is the relevant quantity when discussing the fate of carbon removed from the atmosphere (Chamberlin and Dickey, 2008), it is usually the preferred quantity to be obtained. The third type of PP is the Net Community Production (NCP), which describes the amount of organic carbon available for export after the needs of all trophic levels have been met. This distinction becomes important in field measurements because it is difficult to measure separate rates of autotrophic and heterotrophic respiration. The relation of NCP to NPP is the following:

$$NCP=NPP-HR \qquad [2.6]$$

, where HR represents the respiratory losses from heterotrophs.

In-situ measurements allow to distinguish between the different types of PP, for example by varying the incubation time (^{14}C assimilation method), which will be the shortest for GPP and longest for NCP. Some of the in-situ methods are able to measure only a single type of PP (such as O_2/Ar ratio, which measures NCP). A more detailed description of these methods is presented below in section 2.6.

The satellite models, such as the one used in this study, obtain either GPP or NPP simply by changing the value of some of the parameters in the model, which in our case is the quantum yield of carbon fixation (Antoine, 2006). Increasing the complexity of the model might allow one to determine NCP. Determining this quantity, however, in principle requires some knowledge of the food-web structure, which is generally not accessible when using satellite information. Like the majority of satellite models estimating PP (Chavez et al., 2011), the Antoine and Morel (1996) model yields the NPP values. Another classification of the PP is made depending on whether the new or recycled nutrients were used for growth. New production is defined (Dugdale and Goering, 1967; Eppley and Peterson, 1979) as the production realized from “new nutrients,” which are brought into the surface layers by physical mechanisms such as upwelling or eddy diffusion, as opposed to the regenerated production which uses nutrients that are derived from local recycling of organic matter. The motivation for distinguishing between new production and regenerated production is to track the fate of carbon in ocean food webs and to identify the carbon available for export to the deep sea. In the current study, we do not separate new and regenerated production, since the measurements of nutrients are not achievable

using the satellite sensors data.

2.5 Controls of primary production

There are a number of physical and biological factors that limit or alter the growth rates of phytoplankton. Those factors which have the highest impact in the region of study, along with their potential effect on PP, are discussed below.

2.5.1 Photosynthetic Light Limitation

In the water column, light intensity decreases with depth following approximately the Beer-Lambert Law:

$$E_d(z) = E_d(0) * \exp^{-K_d z} \quad [2.7]$$

where $E_d(z)$ is downwelling irradiance at a depth z, $E_d(0)$ is light intensity at the surface, and K_d is the diffuse attenuation coefficient of light.

In addition to that, water, suspended particles, and dissolved substances selectively absorb and scatter different wavelengths of light so that not only the intensity, but also the spectrum of light changes with depth. The wavelengths of light that are available for photosynthesis at a particular depth are referred to as Photosynthetically Available Radiation (PAR). PAR values are obtained by integrating spectrally resolved downwelling irradiance measurements for the wavelengths of the visible light (400-700 nm). The decrease in PAR with increasing depth has important impact on the growth of phytoplankton. Where PAR diminishes rapidly, phytoplankton growth may be confined to the near-surface waters. Where PAR penetrates more deeply, phytoplankton growth may occur at greater depths. The parameter which is commonly used to define the depth until which net photosynthesis occurs is called the euphotic depth (Z_{eu}), which corresponds to the depth where the PAR value falls to 1% of its value at the surface (Morel and Berthon, 1989). Z_{eu} rarely reaches more than 100 m (Segar, 2007).

With increasing PAR, the increase in PP will not be infinite. At a certain threshold, the intensity of light exceeds the photosynthetic capacity and additional increases in light will lead to the same level of

photosynthesis or even a decrease, a phenomenon known as photoinhibition. The various parametrizations of PP dependency on the light intensity were derived by e.g. Platt (1986), Steele (1962), Webb et al. (1974) and the examples are shown in Figure 2.4.

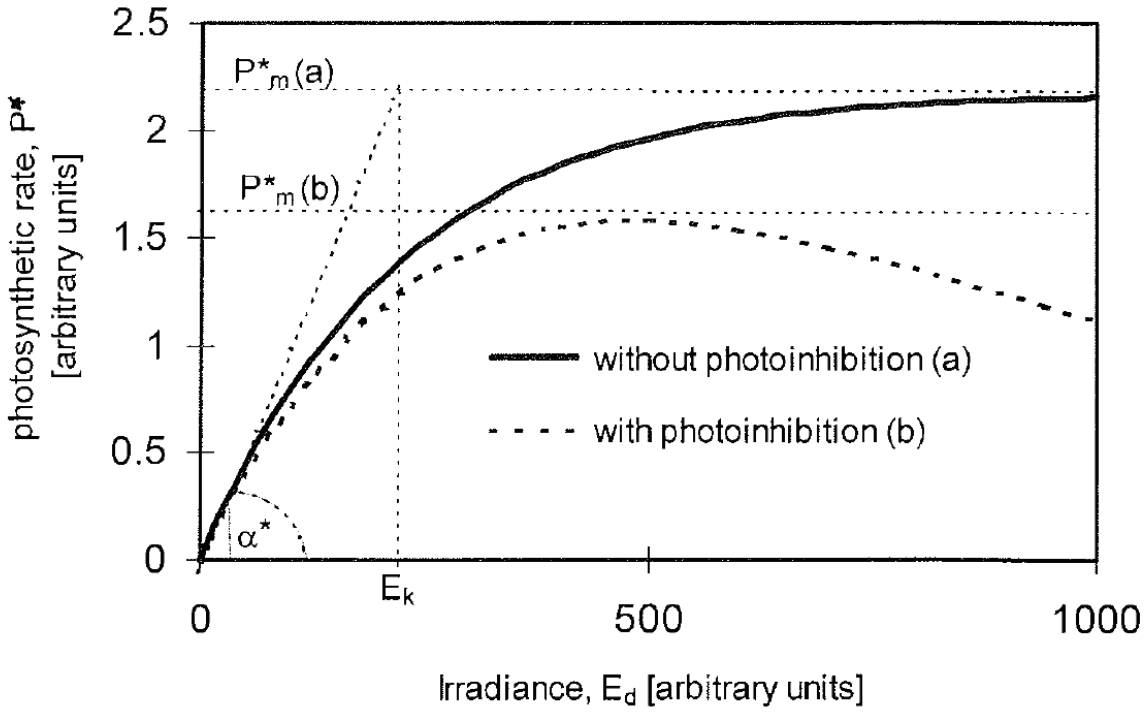

Figure 2.4 Two typical photosynthesis vs irradiance curves according to (a) Webb et al. (1974) and (b) Platt et al. (1980), where α is the slope of the curve of the origin, P^*_m is the maximum photosynthetic rate, and E_k is the irradiance at the onset of light saturation. In Chapter 7: P^*_m is referred to as $P^b_{max.,}$ and as irradiance is expressed in terms of Photosynthetically Usable Radiation (PUR) instead of PAR, irradiance at the onset of light saturation is KPUR instead of E_k. Figure adopted from Bracher (1999).*

The spatial distribution of PAR is obviously primarily driven by the inclination of the Earth's axis, with its maxima moving across the equator according to the seasons. The cloud distribution is superimposed on this annual pattern, which generates a patchy distribution that would be even patchier when considered on a daily scale. At high latitudes such as the Greenland Sea, the phytoplankton

remain in darkness during a significant portion of the year. In addition to that, the sea ice present here can decrease or even block the light penetration in the water column, suppressing the phytoplankton growth until the ice is partly or fully melted (Rysgaard et al., 1999; Smetacek and Nicol, 2005).

2.5.2 Dissolved Inorganic Nutrients

Dissolved Inorganic Nutrients (DIN) are the substances essential for phytoplankton growth, which are dissolved in the seawater (Figure 2.5). Phytoplankton absorbs them through their cell wall. The nutrients that are required in highest concentrations, or the macronutrients, include carbon, hydrogen, oxygen, nitrogen, phosphorus, silica, magnesium, potassium, and calcium. It is important to note, that some elements, such as silica and calcium, will be in greater demand by certain species, namely diatoms and coccolithophorids, respectively. Regional distribution of nutrients also plays a role. For example, in the Antarctic waters the concentration of phytoplankton is low, though the macronutrients are available. Here, the lack of iron, which is a micronutrient, is limiting phytoplankton growth. Basically any nutrient may hinder the growth of phytoplankton if it is not supplied in a quantity that meets their metabolic demands.

The primary processes influencing nutrient concentrations in the sea are the geophysical and geochemical processes. These processes not only control the addition of these elements to seawater but also their dispersion and removal. Rock weathering and the decay of organic material, together with waste discharge, are the major sources of most forms of nutrients in the sea (Chen, 2007). In addition to that, there are the antropogenic sources of nutrients entering oceans through rivers or precipitation, such as sewage and detergents, which are the main sources of oceanic phosphorous, and agriculture fertilizers, which are the sources of oceanic nitrogen.

Because rates of photosynthesis tend to be higher at the surface than at depth, nutrients tend to be removed more quickly at the surface. A part of the nutrients used by phytoplankton is then resupplied by a process called remineralisation. This process occurs when the dead phytoplankton are eaten by bacteria or zooplankton which then convert their organic matter back into carbon dioxide, release the nutrients they have used back into the water and use up oxygen. In addition to remineralisation, the replenishment of the supply of nutrients in the surface water depends upon the action of physical processes, namely vertical mixing and eddy diffusivity, lateral movements of deep water, diffusion out of sediments and transport of mineral dust. Zooplankton also supply the nutrients to phytoplankton by

excreting dissolved compounds, such as ammonium, which may be used by phytoplankton when other forms of nitrogen are not available

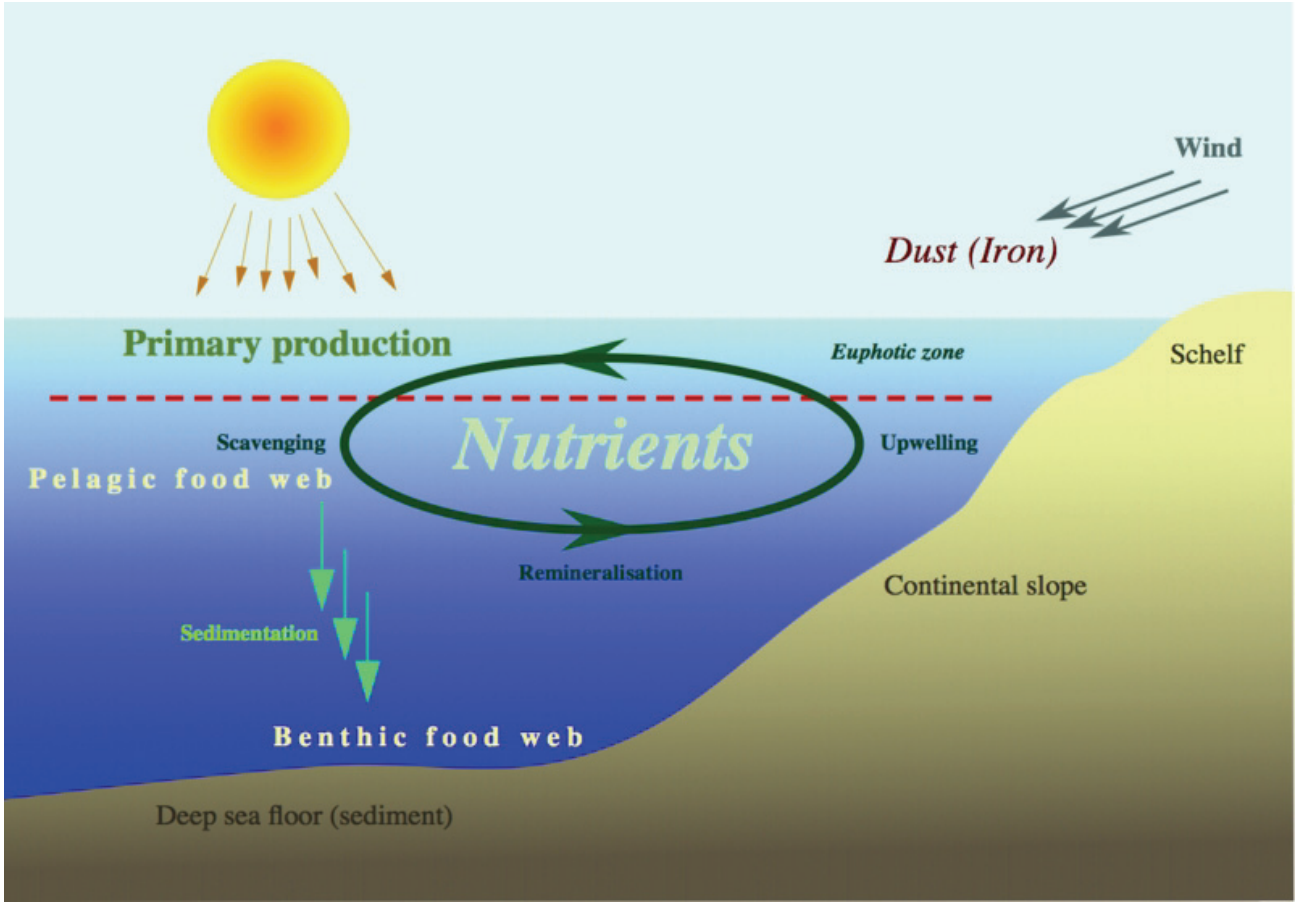

Figure 2.5 Generalized scheme of nutrient cycle in the oceans by Grobe, 2007.

2.5.3 Zooplankton Grazing

The grazing (i.e., consumption) of phytoplankton by zooplankton does not directly influence the PP. It has an indirect effect on PP by lowering the biomass, or the number of primary producers. For example, in cases of high concentrations of both, phytoplankton and zooplankton, high PP will be observed, but without an increase in biomass. The degree to which zooplankton feeding controls

phytoplankton growth rates and biomass depends on a great number of factors, including the size and type of zooplankton, their life cycle, and temperature, among others. Thus, while zooplankton grazing has some effect on primary productivity, the magnitude of these effects under a given set of circumstances may be uncertain.

One of the main hypotheses describing the interaction between phytoplankton, zooplankton and the seasonally varying physical processes is the ‘‘Dilution–Recoupling Hypothesis’’ (Banse, 1992; Banse, 2002; Behrenfeld, 2010; Evans and Parslow, 1985; Marra and Barber, 2005). When simplified, the underlying concept of the Dilution–Recoupling Hypothesis is that the complex food web of planktonic ecosystems allows a constant tight coupling (rapid response time) between phytoplankton growth and losses, but seasonal mixed layer deepening has the potential to slightly decouple phytoplankton and zooplankton through dilution of both phytoplankton and grazers. Thus, the end of mixed layer deepening (or the beginning of shallowing) should advocate a strengthening in predator–prey coupling.

2.5.4 Vertical Mixing

The intensity and seasonal cycle of the sea water vertical mixing influence both, the amount of light to which phytoplankton are exposed and the nutrient availability at a certain depth. Vertical mixing acts like a conveyor belt that carries phytoplankton deeper (to the nutrient-rich and less sunlit waters) or shallower (to the nutrient-depleted and more sunlit waters) in the water column.

The oceanographic concept that is relevant for the ocean depths where the vertical mixing significantly affects the plankton, is the mixed layer. The mixed layer is the upper ocean layer within which salinity, temperature and density are almost vertically uniform, due to the turbulences induced by winds, cooling/heating processes and other factors such as sea ice melt/formation and evaporation. The bottom of the mixed layer is characterized by a gradient in the vertical variation of water properties (temperature, salinity and density).

An example of the effect of the mixed layer depth on the phytoplankton growth is the initiation of the spring phytoplankton bloom in the seasonal seas of the ocean, which was parameterized in the 'Critical Depth Hypothesis' (Sverdrup, 1953). The emergence of plankton-rich waters in spring and early summer from the clear waters of winter, when light is low and storms are frequent, leads to the conclusion that the spring bloom is a consequence of improved upper ocean growth conditions in spring that stimulate phytoplankton growth. The fundamental principle of the critical depth concept is

that there exists, for any given date, a surface layer at which phytoplankton growth is precisely matched by losses of phytoplankton biomass within this depth interval. In Sverdrup (1953) hypothesis, the spring bloom is initiated when the surface mixed layer shoals to a depth less than the critical depth. With the shallowing of the mixed layer, which happens due to the warming of the surface layers and hence leads to stabilization of the water column, the overall irradiance experienced by phytoplankton will be higher than in a deep mixed layer. Thus, rates of photosynthesis within a shallow mixed layer will be greater than rates of photosynthesis within a deep mixed layer (Figure 2.6).

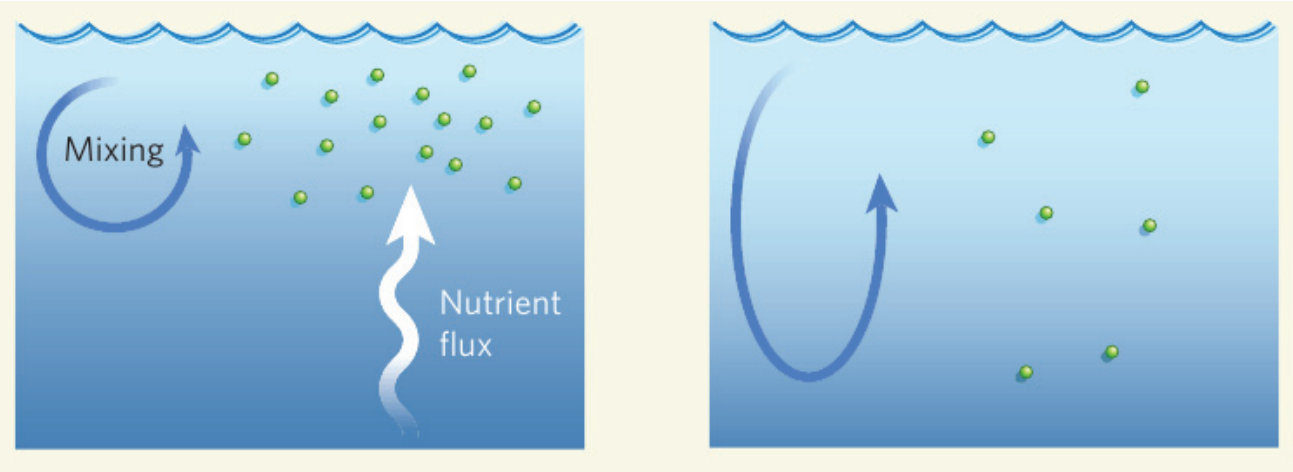

Figure 2.6 Vertical distribution of phytoplankton when the mixed layer is shallow (left) and the mixed layer is deep (right). On the right panel nutrients are assumed to be present in the whole water column (light-limited environment). Modified from Doney (2006).

2.6 Methods to estimate primary production

> "There exists perhaps no single method or series of observations that is going to provide oceanographers with an absolute measure of primary production in the ocean. All methods, all approaches, are approximations."
>
> (Marra, 2002)

Traditional in situ measurements of primary production in the ocean have concentrated on two separate aspects of photosynthesis, namely, the uptake (or consumption) of carbon dioxide or the evolution (or release) of oxygen. As it was shown above in section 2.2, these processes occur during the photosynthetic reaction and they thus provide a measure of PP.

2.6.1 ^{14}C assimilation

The method to estimate the uptake of carbon dioxide introduced by Steeman-Nielsen (1951), or the ^{14}C assimilation method, is the most commonly used, and also the most persistently criticized (Longhurst et al., 1995). In this method, water samples are spiked with a small amount of radioactive, inorganic carbon. Then the water samples in glass bottles are incubated in sunlight (either on deck, in the water column, or in a laboratory), and ^{14}C becomes fixed in the phytoplankton cells at a rate that is proportional to their rate of photosynthesis. Finally, the ^{14}C's uptake and its photosynthetic conversion to reduced particulate organic carbon measured after the incubation. When these experiments are carried out over the daylight hours, these incubations are considered NPP due to intracellular carbon refixation (Marra, 2009). The chief uncertainty of this method is believed to be the suppression of productivity by low concentration of toxins, often metals, introduced to incubations during sampling and handling (Fitzwater et al., 1982). There are also difficulties in interpretation associated with the choice of incubation time. Twenty-four-hour incubations, if begun at dawn, include nighttime losses of ^{14}C via respiration and are even sometimes considered as NCP (N.Cassar, personal communication). Shorter, daytime-only, incubations thus produce higher uptake rates than longer, twenty-four-hour incubations (by at least 15%; Karl et al., 1996). Thus these two estimates cannot be inter-compared.

2.6.2 Light-and-dark bottle (change in dissolved oxygen concentration)

The method relying on changes in the concentration of dissolved oxygen, the light-and-dark bottle method, requires clear and opaque bottles to be incubated for a period of time at different depths within the water column. The decrease in oxygen (which can be estimated using e.g. Winkler method) in the opaque bottle equates to respiration of the phytoplankton, bacteria, and other organisms. The change in oxygen in the clear bottle represents the net difference between rates of photosynthesis and respiration.

Note that this method is best suited for conditions where productivity is high and where in-situ incubations are logistically possible. The source for uncertainty lies in the assumption that respiration occurs at the same rate in the dark as in the daylight. In addition, both methods described above fail to duplicate mixing within the water column, a process that could have a considerable effect on the chemical and light environments phytoplankton experience throughout the day.

2.6.3 Depletion of dissolved inorganic nutrients

The concentration of DIN in seawater provides an indirect estimate for determining phytoplankton growth rates. The theory behind this is that phytoplankton must decrease the concentration of particular elements and that by measuring changes in the concentration of these elements over some period of time (and accounting for other processes), the growth of phytoplankton could be determined. As an early example, Cooper (1938), working in the Irish Sea, estimated primary production by comparing the winter maximum and summer minimum of phosphate, and scaling the difference approximately to the growth of phytoplankton for that year. Such estimates of PP are considered to be the fraction of total production, that is available for net transport up the food chain, i.e. NPP (Jennings Jr et al., 1984). The estimation of PP from nutrient depletion requires knowledge of nutrient assimilation and carbon fixation by phytoplankton. The composition of marine phytoplankton is usually assumed to be consistent with a ratio found by Redfield et al. (1963), C/N/P=106/16/1. However, according to a recent work by Martiny et al. (2013), the ratios found are at a variety of marine locations dramatically different from the Redfield ratio and the phytoplankton populations have been found to be more carbon-rich than previously thought (Figure 2.7).

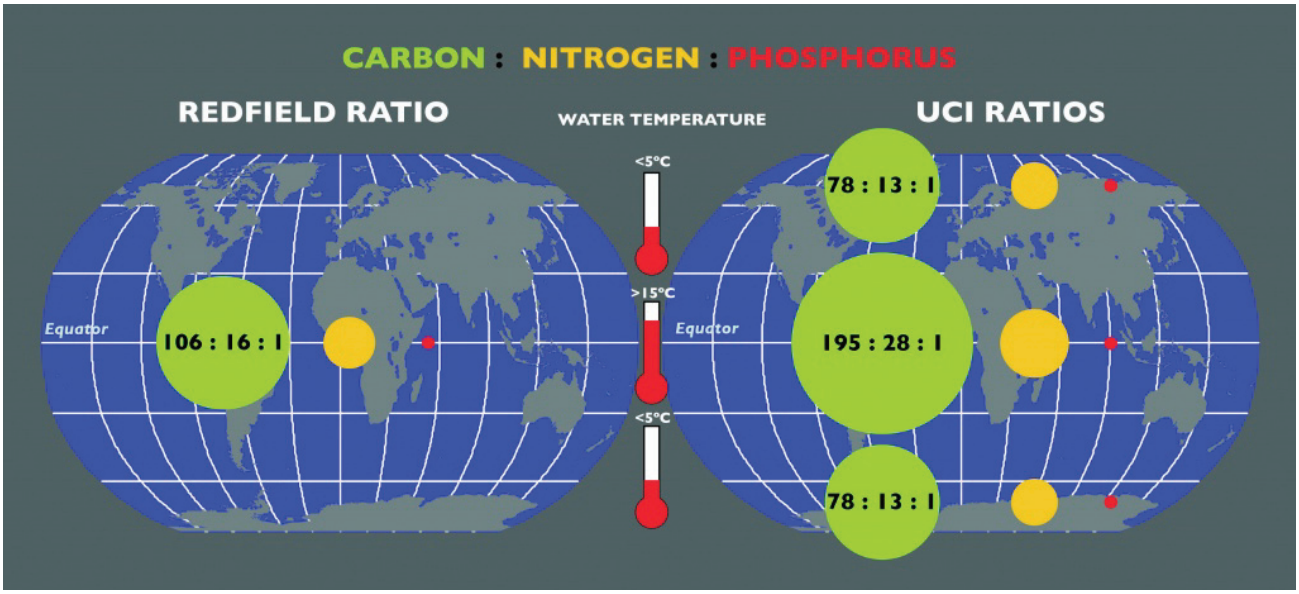

Figure 2.7 The variety of Redfield ratio at different marine locations. Green is for carbon, yellow is for nitrogen and red is for phosphorus. From Martiny et al. (2013).

An additional error is introduced by the fact that particulate nitrogen and phosphorus are remineralized more rapidly in the water column than silica, and they are more likely to be recycled within the euphotic zone. One aspect of this recycling is that some nitrogen is returned to the euphotic zone as ammonium by zooplankton excretion and microbial regeneration (Jennings Jr et al., 1984; Gilbert et al., 1982; Olson, 1980). This ammonium is utilized preferentially by phytoplankton, therefore the nutrient-based estimate of PP is an underestimate.

2.6.4 Fluorescence-based

During photosynthesis a photon of light hitting a CHL molecule puts the molecule into an excited energy state. Energy of an excited CHL molecule may be: 1) transferred to another CHL molecule 2) transferred to an electron transfer chain, and 3) got lost along the way through a fluorescence process. As a CHL molecule fluoresces, it loses energy at a less energetic wavelength, namely red light. Thus, CHL molecules fluoresce red when stimulated by blue light (stimulated fluorescence).

When the CHL molecule is not stimulated, but is just exposed to natural sunlight, it still shows

fluorescence (natural fluorescence), which is less than the fluorescence under stimulated blue light. The relationship between PP and natural fluorescence was first shown by Chamberlin et al. (1990).

The ratio of natural fluorescence (related to PP) to stimulated fluorescence (proxy of CHL) is now commonly measured by an instrument FRRF (Fast Repetition Rate Fluorometer) to estimate the GPP (Robinson et al., 2009; Sugget et al., 2003).

2.6.5 Satellite-based

The time- and labor-consuming field PP measurements produce the most accurate information on oceanic photosynthesis, especially the physiology of phytoplankton. These, however, have a number of limitations. When the in-situ PP measurement methods described above are performed simultaneously in the field, they differ by up to an order of magnitude (Robinson et al., 2009). Such a large variation in PP values is explained by the uncertainties in the measurements, as well as by the different measured quantities from which the final PP value is derived. Note that these measured quantities (parameterizing the relationship between fluorescence, carbon fixed, and oxygen released during photosynthesis) change depending on phytoplankton species and photoacclimation characteristics. It is also difficult to define a measurement method which can be used as a 'standard', as none of the currently available methods of determining PP provide a definitive measurement (Robinson et al., 2009). Another limitation is that by using such a small sampling, periods of unusually high or low productivity may be missed or may not be averaged into the results. An alternative or a supplement to field methods are the satellite-based models capable of providing basin-wide estimates of PP, which is an ideal representation of PP for addressing such problems as human-induced climate change.

In the last three decades, a great deal of effort has been expended to derive algorithms that estimate PP from satellite ocean color estimates of near-surface CHL. Such estimates also suffer from important inaccuracies, particularly near the shore, where suspended, nonliving colored materials influence the estimates. Satellite algorithms are typically applied to weekly or monthly composite data, reducing the effect of clouds and other errors, and are therefore less variable than PP data obtained by in-situ measurements. Regular satellite-based global time-series of CHL became available in 1997 with the launch of the Sea-viewing Wide Field-of-view Sensor (SeaWiFS). Earlier, the Coastal Zone Color Scanner (CZCS) operated with poor spatial coverage over 1978–1986.

With the launch of the CZCS, simple statistical relationships were proposed for calculating PP from

the surface CHL alone (e.g., Eppley et al., 1985; Smith and Baker, 1978). Such empirically derived algorithms are still considered useful when applied to annually averaged data (Iverson et al., 2000), but they are not sufficiently accurate to estimate PP at seasonal or more detailed timescales. The surface CHL explains only 30% of the variance in PP at the scale of a single station (Balch et al., 1992; Campbell and O'Reilly, 1988). Over the past three decades, scientists have improved the PP algorithms with the use of CHL integrated for the water column by assuming a vertical profile of CHL. Then a time dependent variable was needed, to transfer a biomass, which is a stock, into PP, which is a rate. Solar radiation is an obvious choice, and simple mechanistic models (see below) compute PP from biomass, PAR, and a transfer or yield function which incorporates the physiological response of the measured CHL to light, nutrients, temperature, and other environmental variables. As a variable accessible by remote sensing, sea surface temperature (SST) is often used to parameterize the photosynthetic potential, which cannot be directly measured from space. The empirical relationships of SST to the photosynthetic potential are used in several PP models (Antoine and Morel, 1996; Balch et al., 1989; Behrenfeld and Falkowski, 1997a; Howard, 1995; Morel, 1991; Ondrusek et al., 2001; Platt and Sathyendranath, 1993).

Several dozens numerical models have been described to estimate PP in marine waters, all differing to some extent according to their resolution in depth and irradiance, as well as parameters that they account for. The most commonly used classification of these models (see Carr et al., 2006; Friedrichs et al., 2009; Saba et al., 2011) was proposed by Behrenfeld and Falkowski (1997b) and is based upon the levels of model integration. The details are given in Table 2.3 and below, with the three categories ordered according to model complexity starting from complex to simple models:

I). Wavelength-Resolved-Depth-Resolved models (WRDR): The daily water column PP is calculated by integrating photosynthetic rates over wavelength, depth, and time. These models use absorbed radiation (Photosynthetically Usable Radiation, PUR) instead of PAR. The WRDR models convert PUR into net photosynthesis using specific empirical models which are based on photosynthesis-irradiance variables (Antoine and Morel, 1996; Morel, 1991; Sathyendranath et al., 1989; Sathyendranath and Platt, 1989), or variables characterizing the photosystems (Dubinsky, 1992; Sakshaug et al., 1989).

II). Wavelength-Integrated-Depth-Resolved models (WIDR): The daily water column PP is calculated by integrating photosynthesis rates over depth and time. This model category results from removing the wavelength-dependence such that net photosynthesis is described as a function of PAR

rather than PUR (Armstrong, 2006; Asanuma et al., 2003; Marra et al., 2003).

III). Wavelength-Integrated-Depth-Integrated models (WIDI): The daily water column PP is related to environmental variables measurable at the sea surface through vertically integrated functions. The simplest WIDI model calculates PP as a function of CHL alone (Eppley et al., 1985; Smith and Baker, 1978), or as the product of depth-integrated CHL and daily integrated surface PAR (Falkowski, 1981; Platt, 1986). More complex WIDI models incorporate estimates of the euphotic layer depth, depth-integrated CHL, and daylength along with the irradiance-dependant functions of photoadaptive parameters (Behrenfeld and Falkowski, 1997a; Platt and Sathyendranath, 1993; Wright, 1959)

The category TI (Time-Integrated models), is not separated here, as such models did not participate in the intercomparison activities of PP models.

Table 2.3 Classification scheme for daily PP models based upon levels of integration, with the generalized equations. Each category includes a photoadaptive variable (Φ, φ, P^b_{opt}) corresponding to the resolution of the described light field. Φ and φ are CHL-specific quantum yields for absorbed (PUR) and available photosynthetically active radiation (PAR), respectively. a is the phytoplankton-specific absorption which e.g. transforms PAR into PUR. In case of WIDI irradiance-dependent function (f(PAR(0))) and photoadaptive yield term (P^b_{opt}) are required to convert estimated biomass into the photosynthetic rate. CHL(z) and CHL(0) are depth-resolved and surface CHL concentration, respectively. DL is the daylength, Z_{eu} is the depth of the euphotic zone.*

I. Wavelength-Resolved-Depth-Resolved models (WRDR)

$$PP = \int_{z=0}^{Zeu} \int_{t=sunrise}^{sunset} \int_{\lambda=400}^{700} \Phi(\lambda,t,z)\, PAR(\lambda,t,z)\, a^{*}(\lambda,z)\, CHL(z)\, d\lambda\, dt\, dz$$

II. Wavelength-Integrated-Depth-Resolved models (WIDR)

$$PP = \int_{z=0}^{Zeu} \int_{t=sunrise}^{sunset} \varphi(t,z)\, PAR(t,z)\, CHL(z)\, dt\, dz$$

III. Wavelength-Integrated-Depth-Integrated models (WIDI)

$$PP = P^b_{opt}\ \ f[PAR(0)]\ \ DL\ \ CHL(0)\ \ Z_{eu}$$

The performance of satellite-based PP models were analyzed in a series of round-robin experiments aiming at an extensive comparative assessment of these models (Carr et al., 2006), and their validation against in situ measurements (Friedrichs et al., 2009; Saba et al., 2011). The mean RMSD (Root Mean Square Difference) of 21 ocean color models was 0.29 relative to in situ PP values collected in the tropical Pacific. In the latest round-Robin comparison, it was found that the model's success varies substantially from region to region (Saba et al., 2011), with RMSD ranging from 0.09 for the Southern Ocean to 0.53 for the Black Sea. In general, the performance is still limited by the accuracy of the input variables, particularly the uncertainties in satellite-based CHL values. The WRDR Antoine and Morel (1996) model used in this study performed the best in terms of RMSD in eight out of ten regions that were studied in Saba et al. (2011) and was recommended by the authors to be used for open ocean waters. For comparison purposes, we also use the WIDI Behrenfeld and Falkowski (1997a) model, which had higher RMSD when validated by in-situ data than Antoine and Morel (1996) model (0.08 difference in average RMSD across all regions between these two models, Saba et al., 2011).

Chapter 3

The physical environment of the Greenland Sea and its relation to phytoplankton variability: state of the art

The Greenland Sea is a highly dynamic area in terms of water mass exchange. Here, warmer surface waters of relatively high salinity, which are advected to the area from the North Atlantic, meet fresher and colder waters of Arctic origin (Rudels and Quadfasel, 1991). It is also the area where most of the Arctic drifting sea ice is advected. Two main ocean currents influence the exchange of water masses in the Greenland Sea (Forest et al., 2010). The current flowing in the western Greenland Sea, along the Greenland coast is the East Greenland Current (EGC), which carries southward the cold and low salinity waters originated in the central Arctic Ocean (Bourke et al., 1987). In the eastern Greenland Sea, the West Spitsbergen Current (WSC) transports relatively warm and salty Atlantic waters northward. In the northeastern Greenland Sea, a complex bathymetry leads to a split of the WSC into three branches: the first enters the Arctic Ocean north of Svalbard, the second continues north and further eastward around the rim of the Yermak Plateau, and the third recirculates to the west as the Return Atlantic Current (Gascard et al., 1995; Schauer et al., 2008). With the WSC and the EGC as the major current systems, the Greenland Sea is an important transition zone between the North Atlantic and the Arctic Ocean, were a voluminous exchange of oceanic water masses occurs (Quadfasel et al., 1987; Schauer et al., 2008) (Figure 3.1). Between the WSC and the EGC, mixed water masses are formed (Piechura, 2004). In addition, local oceanographic processes such as freshwater run-off, variable patterns of surface currents and wind driven circulation modify the hydrography and sea-ice distribution in these waters (e.g., Soltwedel et al., 2005). With regard to climate change, the core of the WSC displays a progressive warming of 0.06 °C per year since the beginning of continuous measurements by an oceanographic moored array at 78°50’ N in 1997 (Beszczynska-Möller et al., 2012; Schauer et al., 2008).

As is the case for most Arctic waters, the ice-affected western part of the Greenland Sea has pronounced water column stratification by salinity. The stratification here is influenced by the melting sea ice moving through the Fram Strait as it is a major gateway for the sea ice to leave the Arctic

Ocean. The amount of drifting sea ice varies throughout the year, and it in turn intensifies the strength of the stratification. Nutrient supply to the ocean surface layer (critical for phytoplankton growth) depends on the stratification and therefore also varies with season. At the same time a contrasting oceanographic regime with dominant thermal stratification characterizes the central basin of the Greenland Sea away from the seasonal ice zone and East Greenland Current. Clearly, the Greenland Sea has strong North to South and East to West gradients in oceanographic properties (Rudels and Quadfasel, 1991), as well as it is an area of substantial mixing by eddies (Johannessen et al., 1987). The effects on phytoplankton via nutrient and light availability are hence also likely to differ significantly on the scale of a few tens to hundreds of kilometers within the Greenland Sea, rendering the detectability of interannual to decadal trends.

Previous satellite-based phytoplankton studies showed that the variability in ice cover affects phytoplankton density in most geographical sectors of the Arctic Ocean except for the Greenland and Baffin Seas (Arrigo and Van Dijken, 2011; Pabi et al., 2008). Time series studies showed that in some regions phytoplankton blooms occur earlier because of the Arctic-wide seasonal sea-ice decrease (Wassmann and Reigstad, 2011), whereas at the Fram Strait, only a minor change or a slight delay in phytoplankton bloom timing was recorded (Harrison et al., 2013; Kahru et al., 2011). It has been demostrated, however, that empirical algorithms for estimating CHL from satellite information may not perform well in this environment even if they were developed explicitly for the Arctic waters (Cota et al., 2004; Matsuoka et al., 2007). This happens because the bio-optical properties of polar waters may differ significantly from those of the waters at lower latitudes (e.g. Matsuoka et al., 2007; Mitchell and Holm-Hansen, 1991; Sathyendranath et al., 2001).

Ecosystem models provide another important tool to test hypotheses related to the key factors that determine phytoplankton growth on interannual to decadal scales. For the Greenland Sea and Fram Strait, these factors include ice cover, stratification, wind, surface water transport and the activity of grazers (Skogen et al., 2007; Slagstad et al., 2011). Generally, such models agree that the interannual variability in the Greenland Sea can be linked to the transport of Arctic water through the Fram Strait, and the presence of sea-ice in spring (Skogen et al., 2007). An effect of atmospheric warming on phyto- and zooplankton growth was detected in the physically-biologically coupled model, suggesting that phytoplankton productivity in the Greenland Sea and western Fram Strait may increase in the future (Slagstad et al., 2011).

The Fram Strait located in the northern Greenland Sea, with a mean water depth of ~2500 m, is the

only deep water connection between the Arctic Ocean the North Atlantic Ocean, and is the focus for Chapters 4 and 5 of this thesis. Elevated concentrations of phytoplankton and higher trophic levels at the Fram Strait marginal ice zone were documented by, e.g., Smith et al. (1985) and Smith and Nelson (1985). One of the reasons behind this is that ice-melt induced stratification could support substantial phytoplankton blooms (Wu et al., 2007). The abundant ice flora and fauna, as well as sediments are drifting with the sea-ice from the central Arctic into the Fram Strait (Hop et al., 2006) and are adding to the physical factors supporting the growth of phytoplankton at the Fram Strait by seeding nutrients and phytoplankton cells. In addition, in some years the Arctic water outflow may add to the high CHL by transport of Pacific water with high nutrient concentrations (Slagstad et al., 2011). Previous field studies report that in the northeastern Fram Strait (78-81°N, June-July 1984) phytoplankton density is higher in the marginal ice zone, where physical processes such as enhanced water-column stability and upwelling result in favorable conditions for phytoplankton growth (Gradinger and Baumann, 1991; Smith et al., 1987). In the southern Fram Strait (75°N transect, May of 1993 and 1995), phytoplankton biomass is shown to follow hydrographical patterns, with elevated phytoplankton in the areas of low salinities and, hence, higher stratification (Rey et al., 2000).

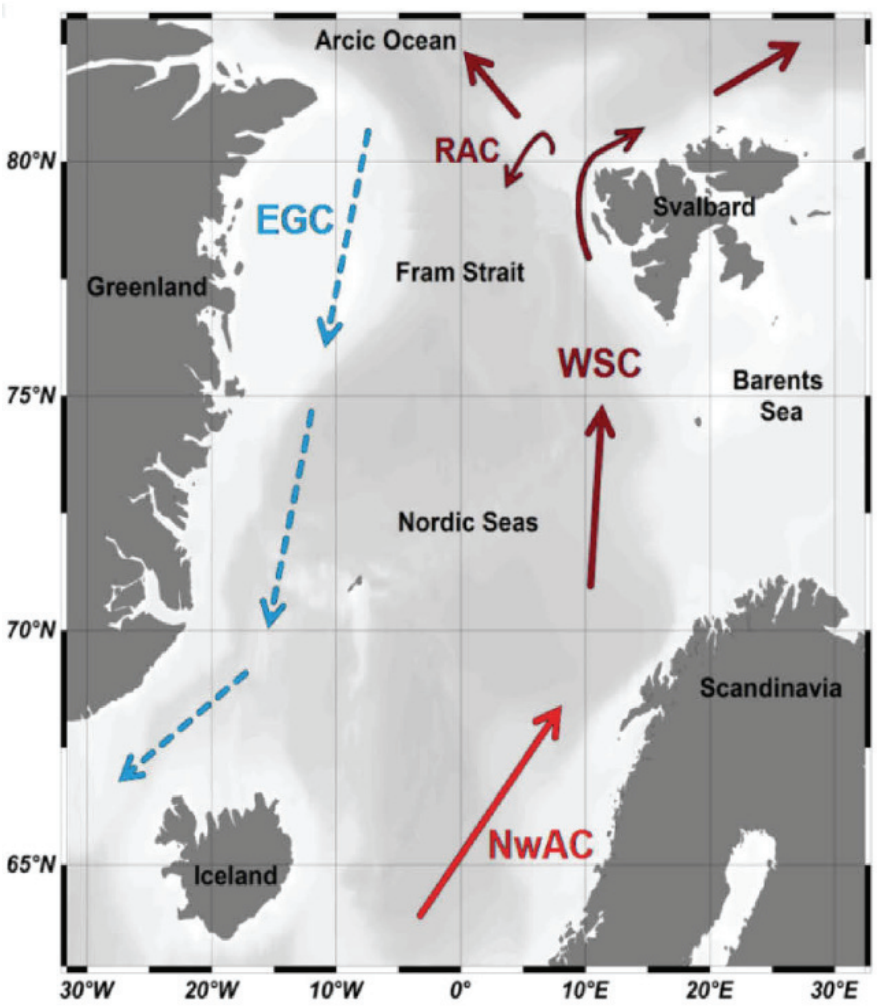

Figure 3.1 Schematic current system in the European Arctic. EGC - East Greenland Current; WSC - West Spitsbergen Current; NwAC - Norwegian Atlantic Current; RAC - Return Atlantic Current. From Kraft (2013).

Chapter 4

Influence of the physical environment on phytoplankton blooms in the northern Greenland Sea

4.1 Motivation

The Fram Strait is the main gateway for water, heat and sea-ice exchanges between the Arctic Ocean and the North Atlantic. This complex physical environment results in a highly variable PP in space and time. Previous regional studies have defined key bottom-up (ice cover and stratification from melt water for the light availability, and wind mixing and water transport for the supply of nutrients) and top-down processes (heterotrophic grazing for the control of biomass) (Gradinger and Baumann, 1991; Rey et al., 2000; Skogen et al., 2007; Slagstad et al., 2011; Smith et al., 1987; see also Chapter 3). The spatial, seasonal and interannual variations in these biophysical factors in the Greenland Sea suggest that a considerable spatial resolution (which can be provided by satellite measurements and/or coupled physical-biological models) is needed to decipher the interaction between key environmental factors governing PP, in order to better understand the future of productivity (Cavalieri and Parkinson, 2012; Rabe et al., 2013; Sakshaug et al., 2004; Wassmann and Reigstad, 2011). In this chapter, field data, remote sensing and modeling techniques were combined to investigate in detail the influence of melting sea-ice and ocean properties on the development of phytoplankton blooms in the Fram Strait region for the years 1998–2009. Satellite-retrieved CHL concentrations from temporarily ice-free zones were validated with contextual field data. These were then integrated per month on a grid size of 20 × 20 km, resulting in 10 grids/fields. Factors tested for their influence on spatial and temporal variation of chlorophyll-a were: sea-ice concentration from satellite and sea-ice thickness, ocean stratification, water temperature and salinity time-series simulated by the sea ice-ocean model NAOSIM. The latter simulated data sets were used because they provide time series information throughout the water column and parameters which have not been measured by satellite. The multi-parameter time series analysis enabled to test the following hypotheses: 1) processes associated with

the presence of drifting sea-ice promote phytoplankton growth within the Fram Strait; 2) effects of physical processes on phytoplankton variability are spatially inconsistent in this region.

4.2 Methods and Data

4.2.1 Data Acquisition

4.2.1.1 Chlorophyll-a in-situ measurements

In situ CHL data from R/Vs “Polarstern” and “Maria S Merian” 1998-2009 cruises were combined with the ARCSS-PP database covering years 1998-2003. The samples of RV “Polarstern” and “Maria S Merian” cruises were collected for 6 depths (0-100 m) in Niskin bottles, mostly between June-July. 0.5-2.0 L of water were filtered through Whatman GF/F glasfibre filters, and stored at -18ºC. Afterwards, in AWI laboratory, these filters were analysed with a spectrophotometer for higher values and with a Turner-Design fluorometer for lower values according to the methods described in Edler (1979) and Evans and O’Reily (1984). First the filters were transferred to plastic centrifuge tubes, then 8-11 ml 90% acetone was added. The filters were sonicated with an ultrasound device in an ice-bath for less than a minute, and then further extracted in the refrigerator for 2 hours. After refrigerated centrifugation for another ten minutes the CHL/acetone extract was measured in a dark laboratory room. The values from the fluorometer were calibrated using the values obtained from the spectrophotometer. In addition, calibration of the fluorometer was carried out with *Sigma* CHL. Refer to Matrai et al. (2013) and Hill et al. (2013) for details on the ARCSS-PP database (http://www.nodc.noaa.gov/cgi-bin/OAS/prd/accession/details/63065).

4.2.1.2 Satellite-borne chlorophyll-a measurements

Satellite CHL level-3 data were taken from the GlobColour archive (http://hermes.acri.fr). The GlobColour data sets are based on the merging of level-2 water leaving radiance data from three ocean color sensors over the whole globe. These sensors are MERIS, MODIS and SeaWiFS, which measure visible and infrared light, mainly sunlight scattered and reflected by the Earth's surface and clouds. Such remotely sensed information about open ocean water is complicated by the atmospheric

absorption and scattering processes, and is only available in the presence of sunlight and the absence of clouds and sea-ice. The satellite-retrieved CHL data set with 4.6 km spatial resolution was generated using GSM model (Maritorena et al., 2002) and algorithm, developed by Maritorena and Siegel (2005), which was applied to the merged level-2 water-leaving radiance data. The data product for open ocean (case 1 waters) was used. The daily data sets were used for validation purposes and the monthly data sets for the cross-correlation analysis.

4.2.1.3 Estimation of sea-ice and ocean properties

Daily Sea-Ice Concentration (SIC) maps were provided by the PHAROS Group of the University of Bremen. SIC data were retrieved from the Advanced Microwave Scanning Radiometer - Earth Observing System (AMSR-E) data with a spatial resolution of 6.25 km. AMSR-E measures microwave radiation that is emitted by the Earth's surface and by the atmosphere. This radiometer is independent of sunlight and clouds and thus provides daily maps with fine coverage for high latitudes. SIC is the percentage of a 6.25 by 6.25 km cell that is covered by sea-ice. The uncertainty of the data is 25% for 0% SIC and 5,7% for 100% SIC (Spreen at al., 2008)

Monthly sea-ice thickness as well as water temperature and salinity profiles down to 200 m depth were calculated with the North Atlantic/Arctic Ocean sea-ice Model (NAOSIM). NAOSIM is a coupled ocean-sea-ice model with 50 vertical layers driven by daily reanalysis data from the National Centers for Environmental Prediction (NCEP), developed at the Alfred-Wegener Institute for Polar and Marine Research (Köberle and Gerdes, 2003). It is derived from the Geophysical Fluid Dynamics Laboratory modular ocean model MOM-2 (Pacanowski, 1995) and a dynamic-thermodynamic sea-ice model with a viscous-plastic rheology (Hibler, 1979). NAOSIM has been used in a number of studies on the dynamics of northern high latitude oceans and was successfully validated by field observations (e.g., Gerdes et al., 2003; Karcher et al., 2003, 2005, 2012; Kauker et al., 2003; Köberle, and Gerdes, 2007). Specifically, the structure and development of water temperatures of 50-500 m in Fram Strait (and in the whole boundary current of the Arctic Ocean) for 1979-1999 were generally in good agreement with available observations. The interior Eurasian Basin of the Arctic Ocean, however, was colder than the observations (Karcher et al., 2003). The salinity sections, compared at East Greenland Shelf in September 2003 showed that the model mimicked the stratification on the shelf very well (De Steur et al., 2009). The simulated freshwater content, which is derived from salinity data, when compared to the

field observations for the period of 1992-2008 (Rabe et al., 2011) showed strong similarities in the large-scale pattern and amplitude. Regional differences were however apparent, in particular in the Beaufort Sea and the southern Canada Basin. Sea-ice concentration data were compared with satellite observations for the period 1978-2001 (Kauker et al., 2003), which demonstrated the capability of the model in reproducing the long-term mean state and the inter-seasonal variability in the Arctic and the North Atlantic. The observed and modeled sea-ice concentration variability were similar to a high degree, capturing even the small-scale features in the Greenland Sea. A detailed model description can be found in Fieg et al. (2010). Here we used the monthly data of the high resolution version of NAOSIM with 9 km grid spacing.

4.2.2 Satellite chlorophyll-a data quality, availability and time series analysis

4.2.2.1 Validation

To obtain a sufficient number of collocations we validated the satellite data for the whole Greenland Sea sector of the Arctic: north of the Arctic circle at 66°33'39"N and between 45°W and 15°E as in Arrigo et al. (2011). The rest of the time series analyses were performed for the Fram Strait area only, 76°N-84°N, 25°W-15°E.

In situ and satellite data were required to have been collected on the same day in order to be considered a valid match-up. Satellite values for match-ups were taken by averaging the valid pixels of a 3x3 pixel box centered on the location of the in situ data. More than half of the pixels in the box were required to be valid (i.e. not screened out due to clouds or sea-ice cover). Most of the validation methodology was adopted from GlobColour Full Validation Report (ACRI-STLOV et al., 2007). We validated the satellite data by the surface in situ CHL (<10 m) and alternatively by the in-situ CHL averaged over the penetration depth (5-28 m). According to Gordon and McCluney (1975) 90% of optical remote sensing information in the homogeneous ocean originates from the upper layer, defined by the parameter penetration depth. The penetration depth can be estimated as depth at which downwelling in-water irradiance falls to $1/e$ ($e \approx 2.72$) of its value at the surface (Gordon and McCluney, 1975). In our study the penetration depth was computed for every profile as the euphotic depth (Z_{eu}) divided by 4.6 (Morel and Berthon, 1989). Z_{eu} is defined as the depth where the

downwelling PAR irradiance is reduced to 1% of its value at the surface. We calculated Z_{eu} using the method described by Morel and Berthon (1989, Eq. 1a, 1b).

4.2.2.2 Temporal variability

The availability of the satellite GlobColour CHL data in Fram Strait was assessed as following. Firstly, in each pixel we calculated the number of days per certain month (April-August) with data per certain year (1998-2009). Only the months April-August were considered for further analysis since they had a sufficient number of valid data points (more than 1/3 of the area covered with data). We spatially averaged the obtained number of days with valid data over all the pixels in the Fram Strait area, and summed up the monthly numbers for each of the years.

In the analysis of satellite CHL monthly time series, the trend and its significance were assessed. Since the time series we examined were temporally and spatially averaged (hence experience no discontinuities and have a low probability of outlying observations) and presumably contain a seasonal cycle, we assumed that representing the data as a classical decomposition model is appropriate (Brockwell and Davis, 2002; Milke and Heygster, 2009):

$$X_t = m_t + s_t + Y_t, \quad t = 1,2,\ldots,n \qquad [4.1]$$

, where X_t is the value of time series at a time point t, m_t is a slowly changing function known as a trend component, s_t is a function with known period referred to as seasonal component, and Y_t is a random noise component, or anomaly.

Our aim was then to estimate the component m_t, which was done using three following methods.

1. The linear regression model was fitted to the original time series (using least squares estimation)

2. The seasonal component (s_t) was subtracted from the data to obtain the time series which contain only the anomaly and trend components. The seasonal component is the climatological monthly value for the period studied. Then the deseasonalized time series were further on referred to as anomalies of data and the trend was estimated by fitting a linear regression model as in the previous method. This approach was used by e.g. Milke and Heygster (2009).

3.The simple moving average filter of *n* surrounding elements was applied to eliminate the seasonal component and to dampen the noise, where *n* is the width of the smoothing window. The window was

set to five months (yearly cycle of current dataset), since we were interested in long term trend (Box and Jenkins, 1976; Velleman and Hoaglin, 1981). The first element of the moving average was obtained by taking the average of the initial five points of the number series. Then the subset was modified by "shifting forward", i.e., excluding the first number of the series and including the next number following the original subset in the series. This created a new subset of numbers, which was averaged. This process was repeated over the entire data series. Then the trend was estimated by fitting a linear regression model as in the previous methods. The estimation of a time series trend using a moving average was used by e.g. Carroll et al. (2011a) and Carroll et al. (2011b).

The alternative methods to estimate trend in the long-term data (used for example, when time series have jumps or gaps) include fitting of the higher order polynomial or stepwise trend fitting (Brockwell and Davis, 2002).

For all the three methods applied, the magnitude of the trend was assigned as the difference between the first and last y-values in a trend line. The significance of the trends was evaluated using t-tests. The time series smoothed with a moving average were used for the standard analysis of the trend, see results in Table 4.2.

To assess the spatial variability of CHL, the standard deviation was calculated as:

$$\sigma_{CHL} = \sqrt{\frac{1}{N}\sum_{i=1}^{N}\left(CHL_i - \overline{CHL}\right)^2} \qquad [4.2]$$

where for a current month of the current year N is the number of valid data pixels, CHL is the spatially averaged CHL value and CHL_i is the CHL of each data point *i*.

4.2.3 Calculation of simulated density and stratification

The Thermodynamic Equation Of Seawater - 2010 (TEOS-10) was used to calculate potential density profiles from potential temperature and salinity simulated by NAOSIM (Feistel, 2010). Upper ocean stratification was then determined by calculating the depth where the potential density was 0.125 kg m^{-3} higher than at the surface (Levitus, 1982) and alternatively by the maximum density gradient method (Method 5 in Zawada et al., 2005). The Fram Strait is a region of sea ice melt, where the

shallow meltwater layer of low density appears locally. In this case, the stratification value obtained using the criteria we used, does not correspond to the conventional mixed layer, which is situated deeper. To avoid the confusion of stating that the shallow freshwater layer is the mixed layer, we use the term 'stratification' instead.

4.2.4 Statistical analysis of relationship between chlorophyll-a and environmental factors

Monthly satellite-retrieved sea ice concentrations (SIC) were spatially averaged for the part of the Fram Strait that was not constantly ice-covered, and for the period of April-August 1998-2009. Of all months, July 2009 (see basemap in Figure 4.6) showed the lowest SIC (20%). Only the area not covered with sea-ice in July 2009 was used for further analysis. In this area, ten sites were chosen in such a way that they covered 1) the marginal ice zone (sites A, C, G, see Figure 4.6 for locations); 2) open ocean (sites D, E, H, I); 3) the coast of Svalbard (sites B, F, J). Their centers were equally spaced in latitude and longitude (1° latitude step, 4° longitude step) so that they did not intersect. For the parameters of interest all pixels within a 20 km radius around the individual sites were averaged into one value. Then a cross-correlation analysis of the data was performed. The data included monthly resolution time-series of satellite CHL and SIC, and simulated sea-ice thickness, surface water temperature and salinity as well as stratification for April-August 1998-2009. In addition, the connection between the timing of the bloom onset and the sea-ice was roughly estimated. For this purpose, satellite CHL and satellite SIC time series were used to calculate for each site and each year if the large increase in CHL between April and May (CHL>0.5 mgCHL/m^3) coincided with the presence of ice in April (SIC>5%).

All the analyses were restricted to the period April through August due to limitations of satellite-retrieved CHL data by light availability, cloud and ice cover at other times of the year. The analysis considers data from April 1998 onwards, when SeaWiFS provided ocean color data. The time series analysis was restricted to the years until 2009 because no simulated data sets were available afterwards.

4.3 Results

4.3.1. Satellite chlorophyll-a data quality and availability

We validated the satellite CHL: 1) by the surface in-situ CHL and alternatively 2) by the in-situ CHL averaged for the penetration depth (see Section 4.2.2.1). The surface CHL data included the underway ship measurements, and the profiles data used here were not required to reach the euphotic layer depth as opposed to the second method used. This resulted in a high number of in-situ data points collocated to the satellite data after applying the match-up criteria (N=108). The correlation was significant ($p<0.001$) with R=0.58 (R - correlation coefficient), and RMSD=0.58 (RMSD - Root Mean Square Difference). In-situ data were underestimated by satellite data by a factor of 3 (slope=0.33). A better agreement with satellite data was reached when the in-situ CHL was averaged for the penetration depth, for which 54 out of 526 available in situ data points were used after applying the match-up criteria. For these points penetration depth spanned from 5 m to 28 m. The correlation coefficient (R) equaled 0.64, and RMSD equaled 0.35. The correlation was significant ($p<0.001$). In-situ CHL data were underestimated by satellite data by a factor of 1.4 (slope=0.69, Figure 4.1).

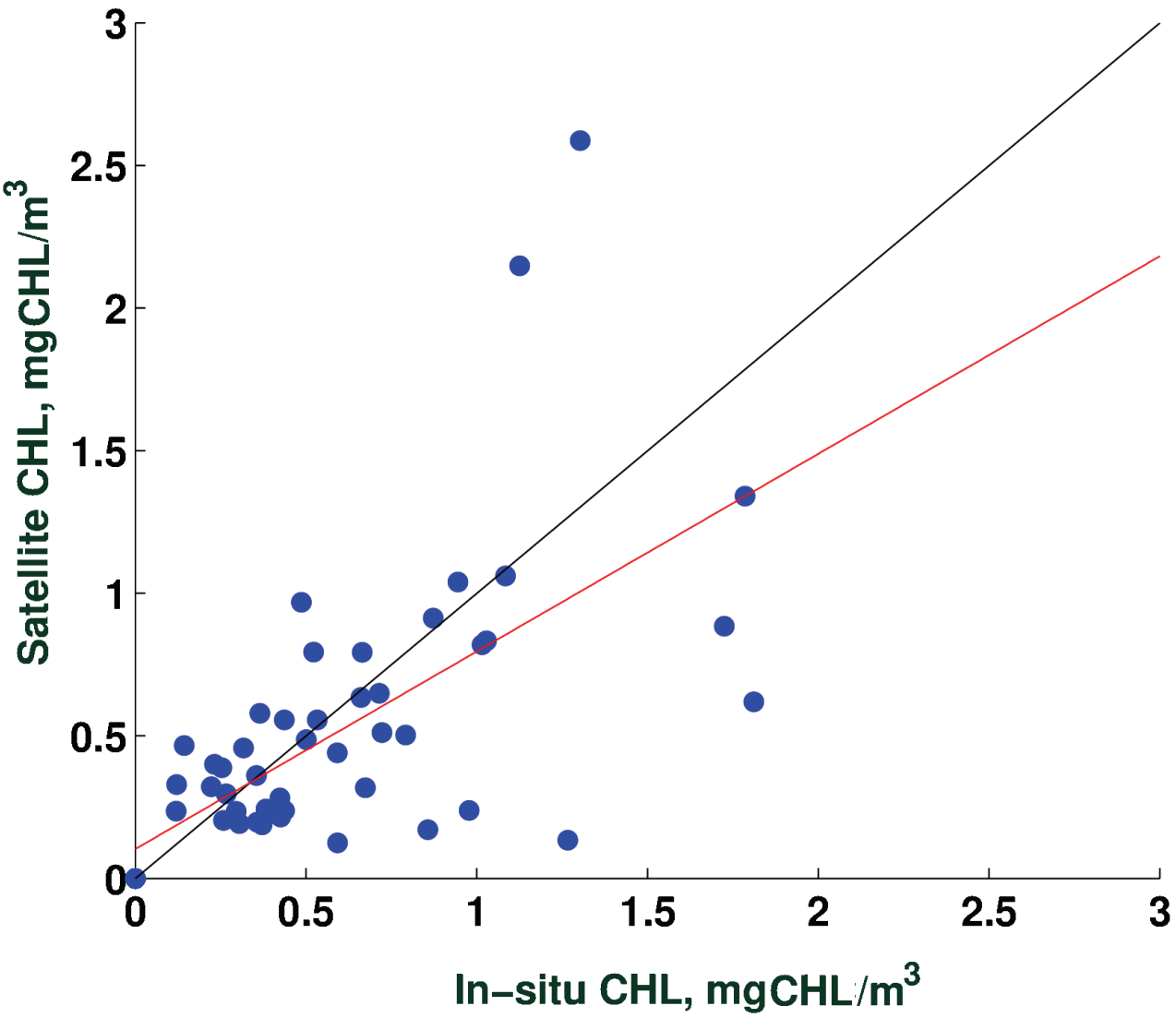

Figure 4.1 Satellite GlobColour CHL versus in situ data of RV 'Polarstern', RV 'Maria S. Merian' cruises and ARCSS-PP database for the period 1998-2010. Black line: one-to-one line, red line: linear regression line calculated in this study. In-situ data have been averaged over the penetration depth defined according to Gordon and McCluney (1975). Correlation statistics: N=54, R=0.64 (R^2=0.41), RMSD=0.35, OFFSET=0.1, SLOPE=0.69.

The satellite data availability test (Figure 4.2), showed that the number of days with data available within a specific year sharply increases from 11 to 22 days after 2001. This is due to the launch of the

two new sensors in 2002 (MEdium Resolution Imaging Spectrometer (MERIS) on 1 March and MODerate resolution Imaging Spectroradiometer on Aqua satellite (MODIS/Aqua) on 4 May) while the GlobColour data before 2002 are based on SeaWiFS measurements only. The years 2003-2005 have the most data, reaching a maximum of 25 days in 2004. The months with largest number of days with data in 1998-2001 are June and July, while after 2002 predominant months are hard to define. Noteworthy, the monthly mean we used for the further analysis was composed from on average 2 days for the years 1998-2001 and 5 days for the years 2002-2009.

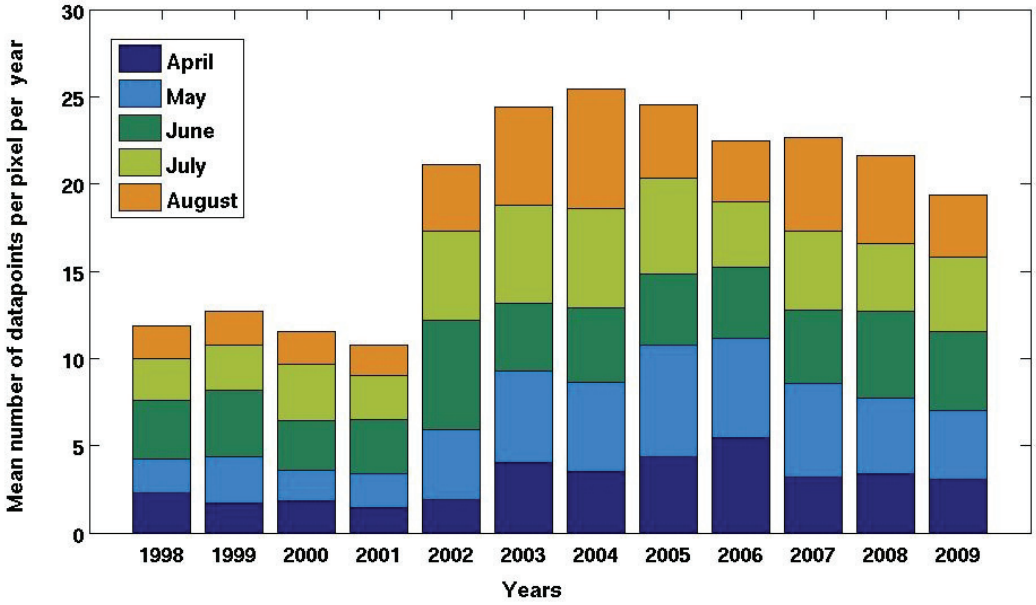

Figure 4.2 Availability of satellite GlobColour CHL data in the Fram Strait area (76°N-84°N, 25°W-15°E). Each bar represents mean number of pixels with data for the Fram Strait per year.

4.3.2 Time series analysis: basic statistics and temporal trends

The climatology of 1998-2009 CHL for the whole study area (76°N - 84°N, 25°W – 15°E) (Figure 4.3) shows the timing of the bloom varying for the different parts of the Fram Strait. Overall, the spatial variation of our data was high, and ranged for the whole area between 0.15 mgCHL/m^3 and 1.4 mgCHL/m^3, with values below 0.8 mgCHL/m^3 seen only in 2009. If one defines the start of the bloom

as the time when the CHL concentration increases to the threshold of 1.0 mg/m^3 (as, e.g., in Wu et al., 2007), then the start of the bloom in the eastern Fram Strait area generally occurred in May (except for the coast of Svalbard where the bloom were observed already in April). In the western part of the Fram Strait the bloom started even later than that, in July.

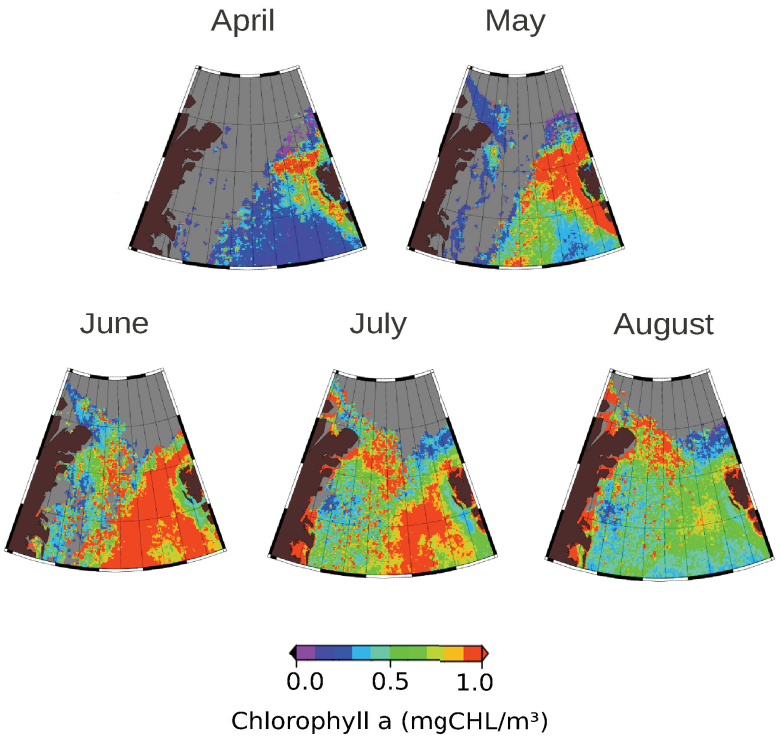

Figure 4.3 1998-2009 climatology of satellite GlobColour CHL, which is the MERIS-MODIS-SeaWiFS merged data with 4.6 km resolution within the Fram Strait, area: 76°N-84°N, 25°W-15°E.

The time-series of April-August CHL was first averaged over the whole area of Figure 4.3 and is shown in Figure 4.4a. A clear seasonal signal can be observed in the mean CHL concentrations with lowest concentrations in April and highest concentrations in May to July in the investigated period. The interannual variation can be summarized as follows: the years before 2002 were characterized by an earlier CHL maximum. After 2002, almost all maxima were observed in July, with the exception of the year 2007 when the maximum occurred in June. Comparing average CHL across all months, we notice an increasing trend in overall CHL from 1998 to 2009 (Figure 4.4a) with a maximum monthly value

observed in 2008.

This trend shows an increase of 0.18 mgCHL/m^3 over the twelve years analyzed (p=0.14, see Table 4.1). In the anomalies a weaker trend is present (Figure 4.4b) with an increase of 0.13 mgCHL/m^3 (p=0.05) over the same period. Applying the moving average of five months to the data also resulted in an increase of 0.22 mgCHL/m^3 (significant with p<0.01). The trend for the interannual variation based on single months (Table 4.1) showed the largest (+0.41 mgCHL/m^3) significant (p<0.01) trend for July (Figure 4.4c). All following trend analyses were calculated by applying the moving average of five months to the data.

Table 4.1 Trend analysis of remotely sensed CHL time-series (N=60) averaged for the Fram Strait area (76°N-84°N, 25°W-15°E). Monthly averaged data were used. Significant trends (p<0.01) are marked in bold. The time series for individual months were taken from the original time series. Original stands for original monthly mean time series, anomalies for the original time series with the seasonal cycle subtracted, and moving average stands for the original time series smoothed with a moving average of five months (section 4.2.2.2)

Trend characteristics	Overall (April 1998 – August 2009)			Individual months, 1998-2009				
	original	anomalies	moving average	April	May	June	July	August
magnitude	0.18	0.13	**0.22**	-0.03	-0.22	0.15	**0.41**	0.28
p-value	0.14	0.05	**<0.01**	0.67	0.25	0.31	**<0.01**	0.02

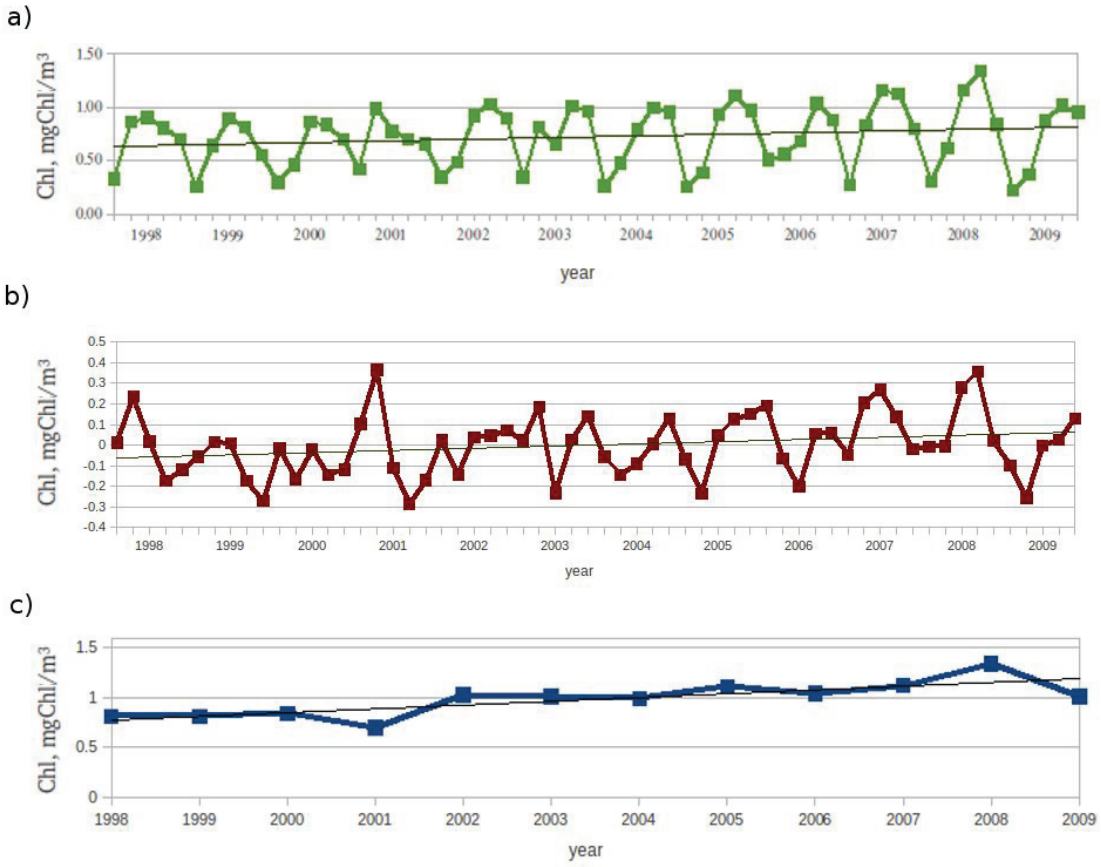

Figure 4.4 Time-series of the monthly satellite-retrieved GlobColour CHL averaged for the Fram Strait area 76°N-84°N, 25°W-15°E for April-August of 1998-2009 (a), its anomalies (b), and July values only (c)

The standard deviation characterizing the spatial variability of the CHL data showed a decreasing trend of -0.2 mgCHL/m^3 (or -41%, $p<0.01$, not shown). In the standard deviation time series of the other parameters, a decreasing trend was identified for the stratification only (-6 m according to Levitus (1982) method and -5 m according to maximum density gradient method, both $p<0.01$). The stratification patterns have thus spatially become more uniform and so did the phytoplankton patterns.

When the area was divided in subsections (Figure 4.5), significant increasing trends in mean CHL over the twelve years were observed mainly in the southern part (Table 4.2, sites D, G, H, I). They coincided with the significant increase in sea surface temperature (observed everywhere, 1.6°C on

average) and significant decrease in shelf Svalbard ice concentration (sites B, F, J, -13% on average). The sea surface salinity and water stratification either decreased or increased, depending on the site, not showing significant trends for the entire region.

Apart from the temporal trends, Table 4.2 explores the spatial patterns in the CHL data and in the physical parameters. The highest annual mean, standard deviation and maxima of CHL at the given latitude were observed at the marginal ice zone (sites A, C, G). Sea-ice was concentrated both around the marginal ice zone and at the coast of Svalbard (site B, F, J), with the thickest ice situated at the coast of Svalbard (68 cm at site B). The warmest and saltiest waters were associated with the ice-free ites (D, E, H, I). Stratification - regardless of its definition (see section 4.2.3) - showed a mean surface layer depth of 20-30 m in the entire region. However, both the sign and the absolute value of the difference resulting from the two methods for calculating stratification were spatially varying. Random (April 1998) examples of the temperature, salinity and density vertical profiles centered at the marginal ice zone site (G), open ocean site (I), and coastal site (J) at 75°N were plotted with the estimated depth of the surface layer (Figure 4.6).

Table 4.2 Statistical characteristics of the remotely sensed CHL time-series (mgCHL/m^3, N=60) and the environmental parameters, which were assumed to influence CHL variability, for ten sites of the Fram Strait region. Monthly averaged data were used and the trend analysis was based on the time series smoothed with the moving average filter. The locations of the sites A-J are indicated in Table 4.3 and Figure 4.5. Significant trends (p<0.01) are marked in bold. SIC – remotely sensed Sea Ice Concentration (%). Simulated parameters: SIT – Sea Ice Thickness (cm), SSS - Surface Salinity (‰), SST - Sea Surface Temperature (^oC), Stratification ($\Delta\sigma_{max}$) – stratification estimated using maximum density gradient (m), Stratification (Levitus) - stratification estimated using Levitus (1982) 0.125 kg/m^3 difference in density from the surface value method (m)

Parameter	Statistics	Site									
		A	B	C	D	E	F	G	H	I	J
CHL	mean	0.79	0.73	0.78	0.76	0.68	0.76	0.75	0.56	0.57	0.64
	st dev	0.41	0.31	0.49	0.50	0.34	0.35	0.60	0.41	0.35	0.26
	max	1.65	1.31	2.44	2.22	2.09	2.14	2.81	2.54	1.41	1.38
	min	0.16	0.19	0.11	0.10	0.17	0.25	0.11	0.07	0.10	0.19
	trend	0.03	-0.04	0.13	**0.33**	0.05	-0.04	**0.43**	**0.46**	**0.16**	0.05
	p	0.60	0.45	0.06	**0.00**	0.27	0.41	**0.00**	**0.00**	**0.00**	0.22
SIC	mean	9.71	1.47	3.48	0.03	0.19	13.16	2.40	0.00	0.01	3.62
	st dev	12.49	1.78	4.77	0.09	0.53	8.96	8.50	0.00	0.05	5.55
	max	50.73	7.27	17.90	0.46	2.82	42.97	62.14	0.02	0.34	33.12
	min	0.00	0.00	0.00	0.00	0.00	2.19	0.00	0.00	0.00	0.00
	trend	5.70	**-4.14**	1.72	-0.03	**-0.83**	**-23.75**	-1.34	0.00	**-0.06**	**-10.70**
	p	0.11	**0.00**	0.21	0.04	**0.00**	**0.00**	0.55	0.01	**0.00**	**0.00**
SIT	mean	0.02	0.06	0.01	0.00	0.01	0.05	0.00	0.00	0.01	0.07
	st dev	0.06	0.12	0.05	0.01	0.05	0.11	0.01	0.01	0.02	0.15
	max	0.37	0.68	0.42	0.05	0.34	0.56	0.07	0.05	0.12	0.66
	min	0.00	0.00	0.00	0.00	0.00	0.00	0.00	0.00	0.00	0.00
	trend	0.00	-0.04	0.00	0.00	**-0.04**	-0.04	0.00	0.00	**-0.01**	-0.07
	p	0.76	0.08	0.69	0.07	**0.00**	0.27	0.81	0.81	**0.01**	0.09
SSS	mean	34.53	33.92	34.38	34.78	34.71	34.43	34.78	34.98	34.96	34.49
	st dev	0.48	0.85	0.80	0.34	0.39	0.39	0.41	0.16	0.25	0.42
	max	35.13	35.07	35.11	35.16	35.12	35.02	35.11	35.22	35.22	35.08
	min	32.96	31.82	31.59	33.75	33.58	33.22	33.05	34.46	33.96	33.25
	trend	-0.38	**-0.75**	0.00	-0.11	0.07	0.25	-0.02	-0.08	0.10	**0.46**
	p	0.02	**0.00**	0.99	0.32	0.49	0.04	0.89	0.05	0.06	**0.00**
SST	mean	5.83	4.67	6.18	6.88	6.79	3.92	6.39	7.08	7.66	5.83
	st dev	2.80	2.42	2.92	2.83	2.82	2.05	3.25	3.40	3.18	2.89
	max	10.82	9.23	10.70	10.96	10.90	7.02	11.25	11.54	12.12	9.89
	min	0.29	0.65	-0.01	1.34	1.45	-0.27	0.60	1.03	1.44	0.10
	trend	**1.96**	**1.58**	**1.86**	**1.59**	**1.91**	**1.53**	**1.43**	**1.55**	**1.91**	**2.07**
	p	**0.00**	**0.00**	**0.00**	**0.00**	**0.00**	**0.00**	**0.00**	**0.00**	**0.00**	**0.00**
Stratification ($\Delta\sigma_{max}$)	mean	21.06	24.24	22.67	22.33	26.25	28.29	19.48	21.28	21.48	28.99
	st dev	9.26	11.67	12.97	10.98	15.13	12.23	7.76	10.49	11.66	13.09
	max	53.87	51.84	47.64	44.87	65.65	44.91	48.55	51.67	58.59	54.52
	min	5.00	5.00	5.00	5.00	5.52	6.52	5.00	5.00	5.00	6.21
	trend	-4.76	-5.28	**-6.56**	0.07	3.17	-5.35	-0.87	3.39	3.37	-2.92
	p	0.01	0.02	**0.00**	0.97	0.12	0.02	0.43	0.03	0.06	0.22
Stratification (Levitus)	mean	22.50	19.96	22.95	23.96	22.92	20.92	21.51	21.12	23.16	19.52
	st dev	10.66	8.53	12.84	12.01	11.45	8.95	11.15	9.77	10.41	8.53
	max	55.00	48.64	59.88	50.85	54.27	52.88	52.45	53.58	57.02	51.61
	min	5.00	5.00	5.00	5.00	5.00	5.00	5.00	5.00	5.00	5.00
	trend	-4.01	-1.77	**-8.08**	-3.63	2.64	**-4.08**	-2.67	-2.46	-0.52	3.79
	p	0.08	0.20	**0.00**	0.11	0.11	**0.01**	0.13	0.15	0.77	0.02

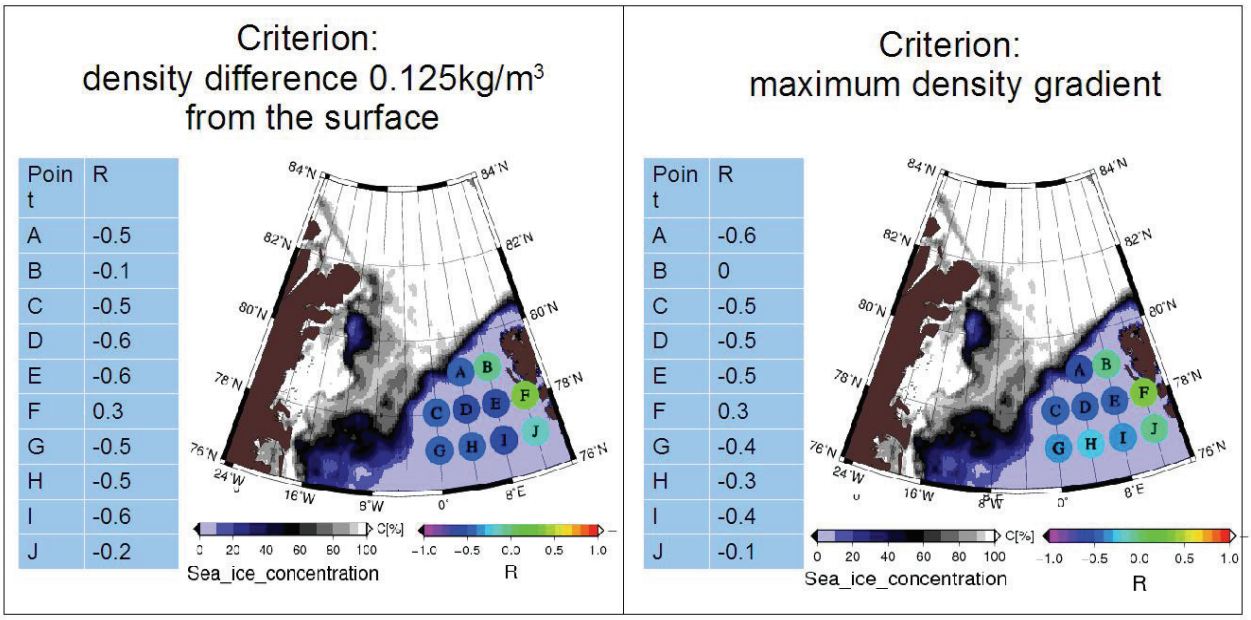

Figure 4.5 Circles on the map show location of the ten sites where the statistical analysis was applied. Colour of the circles indicates correlation coefficients between 1998-2009 time-series of satellite-retrieved GlobColour CHL and simulated water stratification. The exact number of the correlation coefficient is given in the table on the left. Left and right maps differ in the method of calculating the stratification. Base map is the satellite-retrieved sea-ice concentration for July 2009.

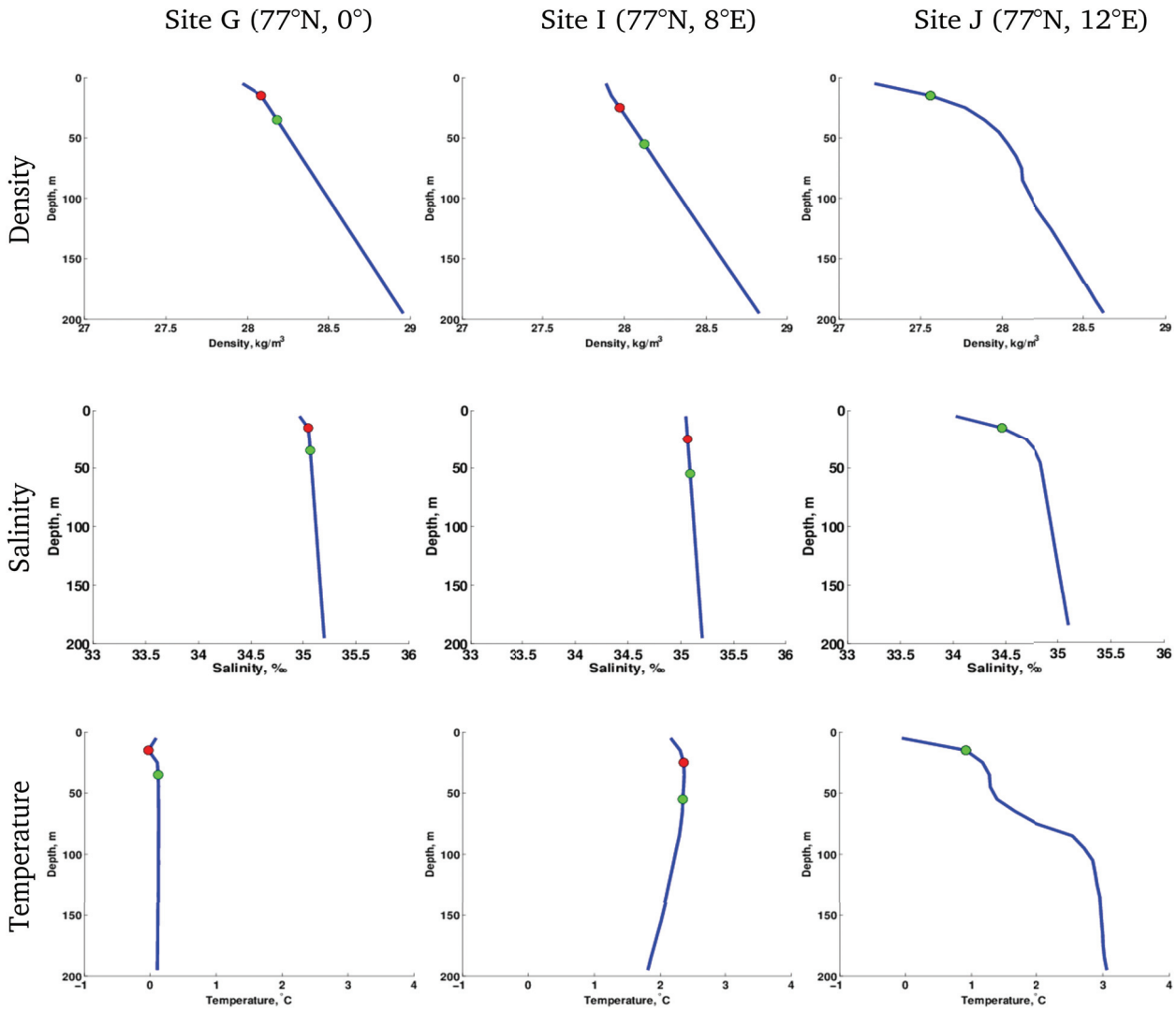

Figure 4.6 Examples of water density, salinity and temperature vertical profiles for the marginal ice zone (site G), open ocean (site I), and coast of Svalbard (site J). The circles indicate stratification computed using: 1) maximum density gradient (red circle), and 2) Levitus (1982) 0.125 kg/m^3 difference in density from the surface value (green circle). At site J both criteria match the same point. Data of NAOSIM for April 1998.

The coastal sites show no difference between the two criteria, while the sites at the marginal ice zone and in the open ocean show that the Levitus (1982) definition gives a deeper surface layer. The stratification is influenced from both vertical salinity and temperature gradients at the marginal ice zone site, from the temperature gradient at the open ocean site (salinity profile is close to uniformity) and from the salinity gradient at the coastal site (temperature increases with depth).

4.3.3 Statistical analysis of relationship between chlorophyll-a and environmental factors

The correlation coefficients between CHL and several physical parameters, and the spatial locations of the studied sites are presented in Table 4.3. The results of a cross-correlation analysis show that ocean stratification estimated according to Levitus (1982) is the parameter, which showed highest correlation to CHL explaining up to 36% of the observed variance (with the highest average correlation coefficient (r) of -0.6 for open ocean sites; Fig. 4.5). For the open ocean and marginal ice zone sites significant negative correlations (shallow mixed layers, more CHL) were observed, while for the coastal sites r was closer to zero (sites B and J), or even positive (site F) and not significant. Besides the observed relationship with ocean stratification, the CHL time-series also correlated relatively strongly (significant for 7 out of 10 sites) to the sea surface temperature variability (increasing SST, more CHL). Significant positive correlation was observed for all open ocean sites and all but one marginal ice zone sites, but significant negative correlation was observed for one coastal site. For observed sea-ice concentration, simulated sea-ice thickness and sea surface salinity no significant correlations with CHL variability were identified for the region with temporary sea-ice cover included in the analyses.

Table 4.3 Correlation coefficients for the parameters analysed with respect to remotely sensed CHL time series covering the months April to August 1998-2009 (N=60) for the ten sites of the Fram Strait region, with the geographic locations of their centers. Significant correlations (p<0.01) are marked in bold. SIC – remotely sensed Sea-Ice Concentration. Simulated parameters: SIT, SSS, SST, Stratification ($\Delta\sigma_{max}$) – stratification estimated using maximum density gradient, Stratification (Levitus) - stratification estimated using Levitus (1982) 0.125 kg m^3 difference in density from the surface value method. Monthly averaged data were used. Areas A-J are indicated on the map in Figure 4.5.

Site	Lat	Long	Correlation coefficient (*r*) of chlorophyll *a* time-series with					
			SIC	SIT	SSS	SST	Stratification ($\Delta\sigma_{max}$)	Stratification (Levitus)
A	79°N	4°E	-0.1	-0.1	-0.2	0.1	**-0.6**	**-0.5**
B	79°N	8°E	0.1	-0.1	-0.2	-0.3	0	-0.1
C	78°N	0°	-0.2	-0.2	-0.2	**0.4**	**-0.5**	**-0.5**
D	78°N	4°E	-0.1	-0.1	-0.2	**0.5**	**-0.5**	**-0.6**
E	78°N	8°E	-0.1	0	-0.3	**0.4**	**-0.5**	**-0.6**
F	78°N	12°E	0.1	0.2	0.2	**-0.5**	0.3	0.3
G	77°N	0°	-0.1	-0.1	-0.2	**0.4**	**-0.4**	**-0.5**
H	77°N	4°E	-0.1	-0.1	0.1	**0.5**	**-0.3**	**-0.5**
I	77°N	8°E	-0.1	0	0.3	**0.6**	**-0.4**	**-0.6**
J	77°N	12°E	-0.1	0	-0.1	0	-0.1	-0.2

When only the months of April and May and not the summer months were studied, a link between the SIC and the timing of CHL bloom onset was observed (Table 4.4). The presence of sea-ice in April (sea-ice event) was usually followed by a large increase in CHL from April to May (CHL increase) at the sites located closest to the ice edge (or marginal ice zone sites, namely A, C and G). At site A, 88% (seven out of eight) of the years with the ice edge present were followed by an early CHL increase, at site C the same was observed for 50% (three out of six) of the years, and at the site G for 60% (three out of five) of the years. At all other sites, a lower percentage of years with the ice edge close by were followed by a CHL increase in April (17% or less). At the open ocean sites not directly situated at the ice edge (D, E, H, I), the sea-ice concentration was never higher than 5%, therefore no match was observed. At the coastal sites (B, F, J) the presence of coastal ice was observed often in April (in four years on average), but did not result in an increase in CHL in most cases.

Table 4.4 Years when sea-ice concentration in April was >5% (I) or/and years when the increase in CHL from April to May was >0.5 mgCHL/m^3 (C) at the ten sites used for the cross-correlation analysis (for site locations see Table 4.3 and Figure 4.5). The percentage of the years with the sea-ice concentration in April >5% followed by the increase in CHL from April to May >0.5 mgCHL/m^3 (% of yrs I&C) was calculated by normalizing the number of the years with both I and C by the number of years with I. Remotely sensed sea-ice concentration and CHL data with monthly averaging were used

Site	Year												# yrs I	# yrs C	% of yrs I&C
	98	99	00	01	02	03	04	05	06	07	08	09			
A	I, C	C	C	I, C	I, C	I, C			I, C	I, C	I,C	I	8	9	88
B	I		C	C			C	C					1	4	0
C	C			I, C	I	I, C				I, C	I	I	6	4	50
D	C												0	1	0
E			C	C									0	2	0
F	I	I	C	C	I	I	C	C	I	I	C		6	5	0
G	I, C			C	I	I, C		I		I, C		C	5	5	60
H													0	1	0
I													0	0	0
J	I	I		C	I	I, C	C	C	I	I			6	4	17

4.4 Discussion

The sections below first discuss the phytoplankton variability in the Fram Strait and then address its relationship to the environmental factors.

4.4.1 Quality of satellite chlorophyll-a data

Globally only about 15% of field data can be used for the validation of satellite-born CHL measurements, because many satellite data are screened out because of cloud cover, sun glint, time difference or other rejection criteria (Brown, 2008). At polar latitudes, where the poor spatial coverage by satellite optical sensors remains a problem for remote sensing-based CHL measurements, obtaining 54 points out of 526 observations (=10%) for satellite CHL validation allowed to detect a significant correlation ($R=0.64$, $N=54$, $p<0.001$) between in situ and satellite-borne data. Our results for the Fram

Strait/Greenland Sea sector show that satellite CHL underestimates the concentration in the field by a factor of 1.4 when using in-situ CHL data averaged over the penetration depth, which showed better agreement with satellite CHL than the surface in-situ CHL data. Compared to other parts of the Arctic, this uncertainty is the same magnitude as observed for global as well as Arctic-adapted algorithms for the Labrador Sea (factor of 1.5, Cota et al., 2003), and better than for the Beaufort Sea (factor 3-5, Ben Mustapha et al., 2012). Compared to the GlobColour data validation (slope=0.87; ACRI-STLOV et al. 2006), the underestimation is somewhat stronger (slope=0.69) in Fram Strait. This may be explained by the presence of blooming phytoplankton species, which have a specific absorption spectrum differing from the spectrum used as the basis of global empirical satellite CHL algorithms. For example, *Phaeocystis pouchetii* and *Phaeocystis globosa* are forming colonies which bloom in major nutrient-enriched areas such as Greenland Sea (Schoemann et al., 2005), and show low specific absorption as compared to other phytoplankton species (Astoreca et al., 2006; Bracher and Tilzer, 2001; Lubac et al., 2008).

An average of data over two to five days per pixel per month is a low number considering the revisit time of the sensors merged for GlobColour data. At the latitudes of interest the revisit time for MERIS, MODIS and SeaWiFS is less than one day. Therefore by merging the data of three sensors, daily coverage can be obtained, and the revisit time cannot be the reason for the small number of days with data. The reason for data loss is likely sea-ice cover, clouds, sun glint or low illumination. However, even with monthly data composed from 2-5 days, phytoplankton blooms should be detected as the sub-arctic blooms are reported to last more than one month, for example, 70-90 days in the Irminger Sea (Waniek and Holliday, 2006), and more than 50 days on the Newfoundland and Labrador Shelves (Wu et al., 2007).

4.4.2 Environmental controls of the variability in the phytoplankton abundance in the Fram Strait

The importance of the marginal ice zone for the productivity of polar regions is well established. Fram Strait marginal zone is associated with abundant ice flora and fauna, as well as sediments, drifting with the sea-ice from the central Arctic into the Fram Strait (Hop et al., 2006), where a positive trend in sea-ice export was observed in recent years by Smedsrud et al. (2011). Elevated concentrations of phytoplankton and higher trophic levels at the marginal ice zone were documented by, e.g., Hunt et al.

(2002, 2008), Smith et al. (1985) and Smith and Nelson (1985). Ice-melt induced stratification – as observed in this study- can support substantial phytoplankton blooms (Wu et al., 2007). In addition, in some years the Arctic water outflow may add to the high CHL by transport of Pacific water with high nutrient concentrations (Slagstad et al., 2011). Combination of these processes resulted in the highest mean CHL at the ice edge (Table 4.2, sites A, C, G) as compared to that observed at other sites at the same latitude. For the Fram Strait marginal ice zone, we could not confirm the finding by Wu et al., (2007) for the Labrador Sea, that an "early ice retreat will result in an early and prolonged spring bloom". Our results rather match the conclusions by Hunt et al. (2002, 2008) for the Bering Sea, indicating that late ice retreat leads to an ice-associated bloom (Table 4.4). However, in Fram Strait the ice distribution reflects more the ice transport from the Central Arctic, and less seasonal melting. Further, the ice-associated blooms observed in this study occurred later (in May) than those observed by Hunt et al. (2002, 2008) in the Bering Sea (late March). In the observed area in Fram Strait, the April CHL value at the marginal ice zone reached 0.5 mgCHL/m^3 only in two years out of twelve at site A, and never at sites C and G. We conclude that the reason for this late ice-associated bloom is the light limitation of phytoplankton in Fram Strait at 76-84°N (MIZEX'87 Group, 1989), while in the Bering Sea light at latitudes of 55-58°N is available much earlier. Accordingly, the cross-correlation analysis of environmental factors potentially influencing phytoplankton accumulation at the marginal ice zone sites showed that stratification was significantly correlated to CHL (Table 4.4), with the shallowest surface layer corresponding to the highest CHL.

Interestingly, the CHL variability at the open ocean sites distant to the ice edge was also significantly correlated to stratification, as it was the case for the marginal ice zone sites. Looking at the example of the density profile for the open ocean site I (Figure 4.6), the gradual increase in density with no changes in salinity suggests that stratification is a consequence of the warming of the ocean surface due to solar radiation, rather than by the sea-ice melt. In the Arctic Seas such solar-induced stratification was previously observed by Wassmann et al. (2006) in the southern and central parts of the Barents Sea, influenced by Atlantic waters. Since for the majority of the open ocean area (sites C, D, E, G, H, I) the surface water salinity time-series was not correlated to CHL, but temperature and stratification were significantly related (Table 4.3), we suggest that here surface temperature is the key parameter that influences stratification most strongly. This agrees with the results of Karstensen (2011) for the Irminger Sea, which showed that 90% of the density changes in the upper 100 m layer of subpolar Atlantic waters are due to changes in temperature. Hence, seawater temperature may also be a

good indicator for onset of the phytoplankton bloom in open ocean zones in Fram Strait.

For the coastal sites (B, F, J) no significant relationship between stratification (any of the methods used) and CHL variability was found. In contrast to the link observed at the marginal ice zone, CHL concentrations at the coastal sites were higher when sea-ice was absent in April (Table 4.4), indicating a stronger nutrient than light limitation. This landfast ice, as opposed to the drifting sea-ice, is probably not enriched with nutrients and seed organisms. Coastal ice is also the thickest ice observed in the area and thus may rather delay the phytoplankton bloom. However, poor quality of the GlobColour CHL product in the coastal area is another possibility for our different results at the shelf of Svalbard. No validation data were available at the coast to investigate the latter in detail. The other, more general uncertainties that have to be kept in mind include the limitations of the cross-correlation analysis, and choice of the parameters studied. In the current analysis we restricted the physical variables analysis to the ocean and sea-ice properties. The atmospheric properties, such as Arctic Oscillation Index (AO), North Atlantic Oscillation Index (NAO), Arctic Climate Regime Index (ACRI), air temperature and wind speed, though, have previously been found to have an impact on marine organisms productivity (Carroll et al., 2011a; Pabi et al., 2008; Slagstad et al., 2011).

Our finding of increased stratification in the non-coastal ocean corresponding to enhanced CHL is consistent with Sverdrup's Critical Depth Hypothesis on the development of phytoplankton blooms (Platt et al., 1991; Sverdrup, 1953). The Critical Depth Hypothesis was recently disputed by Behrenfeld (2010). Behrenfeld's study was carried out in the North Atlantic, south of our study area (40-65ºN).

However, at the latitude of Fram Strait the phytoplankton blooms are likely most limited by light availability and thus cannot start when the depth of the stratified layer is at its maximum (in winter). Accordingly, the Fram Strait blooms happen after May except for the coast of Svalbard (Figure 4.4). According to Behrenfeld (2010), grazing pressure plays a central role in the North Atlantic phytoplankton population dynamics and will intensify with the shallowing of the mixed layer as the mobile predators concentrate into the shrinking volume. Indeed, in the late summer months in Fram Strait, an intense grazing pressure by mainly small copepods and protozooplankton is limiting CHL concentrations (Moeller et al., 2005). An important question remains the control of the phytoplankton by nutrient supply, which probably is also limited by strong stratification in summer, especially in the absence of ice.

4.5 Conclusions

The time series analysis for the ten ice-free fields at Fram Strait showed a regional separation according to different physical processes affecting phytoplankton distribution. At the marginal ice zone the melting sea-ice was promoting phytoplankton growth by stratifying the water column and potentially seeding phytoplankton communities. In this zone, the highest mean CHL concentration averaged for the productive season (April-August) of 0.8 mgCHL/m^3 was observed. In the open ocean the phytoplankton variability was correlated highest to stratification formed by solar heating of the upper ocean layers. Coastal zone around Svalbard showed processes associated with the presence of coastal ice were rather suppressing than promoting the phytoplankton growth. During the twelve years of observations, CHL concentrations significantly increased in the southern part of the Fram Strait, associated with an increase in sea surface temperature and a decrease in Svalbard coastal ice.

Chapter 5

Comparative analysis of the phytoplankton bloom development between the eastern and western parts of the Fram Strait

5.1 Motivation

The current chapter further explores the regional differences of the phytoplankton bloom variability in the Fram Strait. The time-series, onset and duration of the phytoplankton bloom are comparatively studied in a region roughly corresponding to that studied in Chapter 4, and an equally-sized region westward to that.

Phytoplankton blooms are recognized as rapid and temporary increase in the amount of cells of marine algae (mono-species or multi-species) in certain areas (Smayda, 1997). Phytoplankton blooms are common events: periodic spring blooms occur in most parts of the world ocean when increased sunlight causes the thermocline layer to be formed. Fall blooms are also abundant, though weaker than spring blooms, and are triggered by the nutrient-rich waters brought to the surface layer because of the cooling of the ocean surface. Sub-arctic blooms are reported to last more than one month, for example, 70-90 days in the Irminger Sea (Waniek and Holliday, 2006), and more than 50 days on the Newfoundland and Labrador Shelves (Wu et al., 2007).

An analysis of the phytoplankton bloom duration and timing was performed at the Fram Strait area in the northern Greenland Sea: 76°N-84°N, 15°W-15°E. The Fram Strait was divided into two neighboring regions equal in size (Figure 5.1): 1) the Western Fram Strait with high sea ice concentrations and with cold, low salinity EGC (15°W-0°, 76°N-84°N) further referred to as region #1, and 2) and the Eastern Fram Strait with the warm, saline WSC (0°-15°E, 76°N-84°N), further on referred to as region #2. Region #2 roughly corresponds to the area studied in Chapter 4. Because of the ice melt, region #1 is characterized by a freshwater layer in the surface waters and has a lower surface density than region #2 (Beszczynska-Möller et al., 2011). The mixing (or density profile) is seasonally

less uniform in region #1, as compared to region #2, as the amount of sea ice changes throughout the year. This is also the reason why the amount of light phytoplankton are exposed to is less uniform in region #1. It is important to remember that the satellite optical CHL data used here cannot give information on phytoplankton in the ice covered area. Thus, the data coverage of the region is not equal: data are concentrated in the non-sea-ice-covered southern part of region #1 and are located over the whole region #2. Still, some parts in region #1 which are covered by sea ice concentrations that are less than 100% (see example in Figure 5.1) and are ice free for several days in a month, are then seen by the satellite sensor and contribute as well to the monthly composites of satellite CHL.

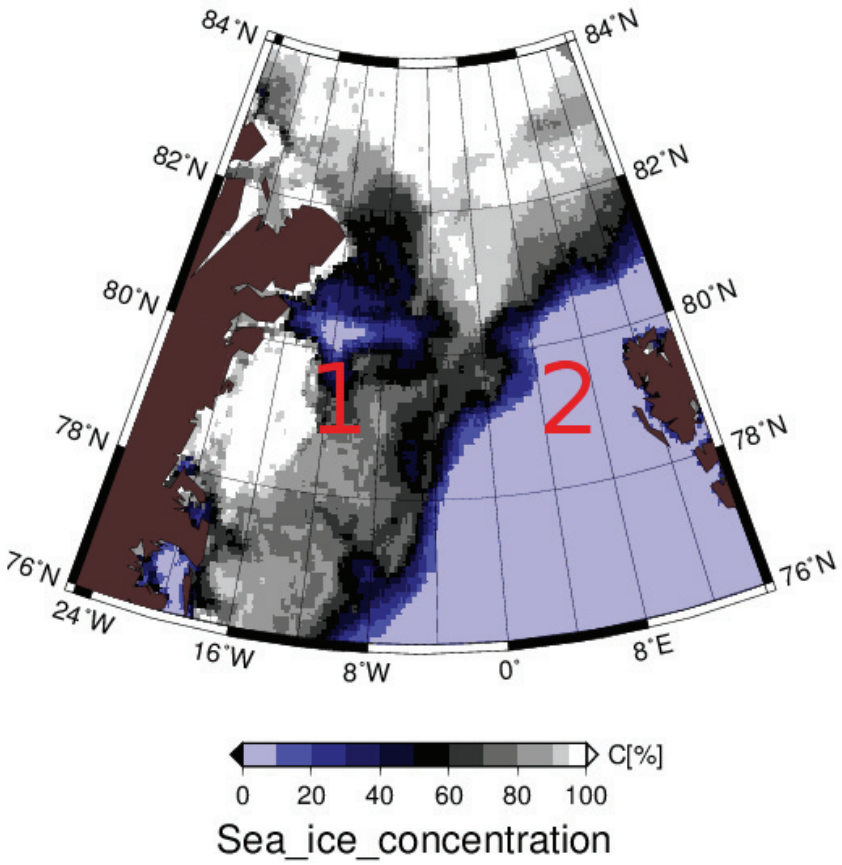

Figure 5.1 Location of region #1 (15°W-0°, 76°N-84°N) and region #2 (0°-15°E, 76°N-84°N), where the analysis of phytoplankton bloom duration and onset was performed. Base map is the SIC map of August 2011 produced by the PHAROS group of the University of Bremen.

5.2 Data and Methods

For the estimation of the timing of phytoplankton blooms, fine temporal resolution of satellite data is required. Consistent with Chapter 4 analysis, we have used GlobColour GSM (Garver-Siegel-Maritorena model) level-3 data with 4.6 km spatial resolution. For the detailed description of satellite CHL data refer to section 4.2.1.2. We used 8-day averages of GlobColour CHL data. 8-day maps have more data gaps than the monthly maps, but still enough information for generating every 8-day file from the beginning of April to the end of August 1998-2012.

The threshold for the onset of the bloom was set to 1 mgCHL/m^3 as in Wu et al. (2007). The examples shown in Figures 5.2 and 5.3 help in the explanation of the method used. For each year, the earliest 8-day map of the data in spring in which more than 5% of the pixels reached the threshold, was assumed to be the onset of the bloom (day 137 of the year 2005 in Figure 5.2). Similar to that, for the ending of the bloom in summer, first the latest 8-day map which had more than 5% of the pixels with data reaching the threshold was calculated (day 233 of the year 2005 in Figure 5.2). The ending of the bloom was then assumed to happen in the next 8-day period (day 241 of the year 2005 in Figure 5.2). In case that the latest 8-day map, which had more than 5% of the pixels with data reaching the threshold occured in the last week of August (which is the latest 8-day file with data), this last week was assumed to be the ending of the bloom (day 241 of the year 2003 in Figure 5.3).

The date assigned to the onset/ending of the bloom was chosen to be the fourth date of the 8-day file. Note that by using the described method, two-maxima blooms are regarded as a single-maximum bloom (Figure 5.2) and that the 8-day files with little data in the middle of the bloom are ignored (see day 169 of the year 2003 in Figure 5.3). Having the information about the onset and the ending of the bloom, the bloom duration was estimated as the difference between these two. Note that the precision of our bloom timing estimate depends also on availability of satellite data in the 8-day periods. The cases where the whole region was covered by pixels with high CHL, or when only several pixels of high CHL were available, produced the same results (presence of phytoplankton bloom) by our method. See the gray bars in Figures 5.2 and 5.3, which show for the years 2005 and 2003, respectively, satellite CHL data availability of the region#2 subset (76°-80°N, 0°-8°E).

In addition to that, the averaged monthly CHL time-series for each region were studied to assess the intensity of the bloom, variability and trends. The trend and its significance was assessed using the

same methodology as in section 4.2.2.2. The temporal trends for: 1) original time series, 2) anomalies of the time series, and 3) time series smoothed with a simple moving average were calculated.

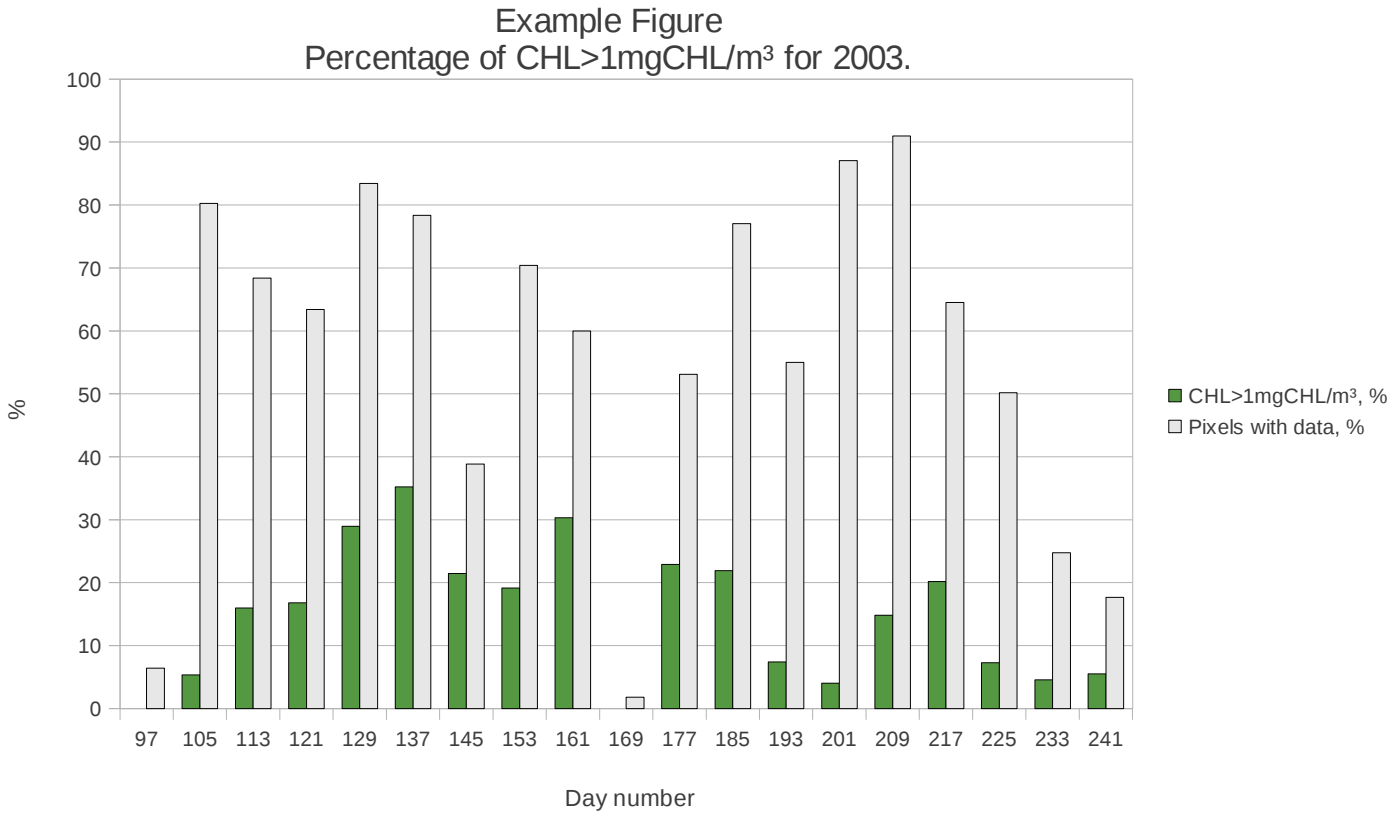

Figure 5.2 Example for the choice of the onset and the ending of the phytoplankton bloom dates for the subset of region #2. Green bars are the percentage of the pixels with data, which have the value higher than 1 mgCHL/m^3. Gray bars are the percentage of the pixels with data from the whole area (proxy for the reliability of the estimate). Analysis is based on the 8-day GlobColour CHL data. Data of 2003, 76°N-80°N, 0°E-8°E.

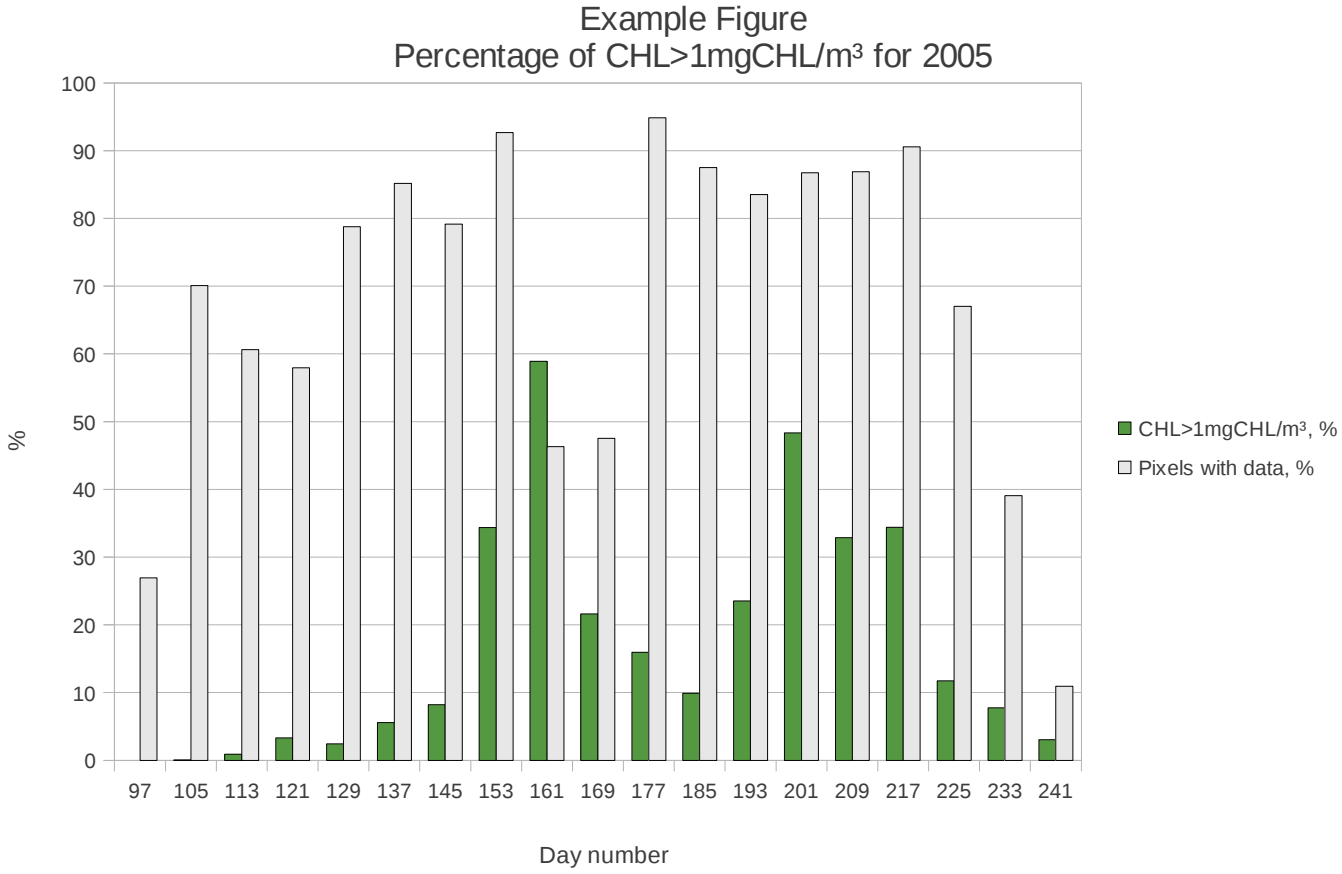

Figure 5.3 As for Figure 5.2, but data of 2005 are shown

5.3 Results and Discussion

The core differences observed between the two regions are the following. Consistent to what was earlier observed in Chapter 4 (Figure 4.3) in the western part of Fram Strait (region #1) phytoplankton bloom is delayed, compared to the eastern part (region #2). In region #2 the phytoplankton bloom starts earlier (Figure 5.4), on average, in the second half of April. It also lasts longer here, in nearly all the years reaching four months (120 days) or more (Figure 5.5). In the region #1, bloom starts on average in the middle of May. Here, in only two years did bloom reached four months (120 days), and once longer than that in 1998. The later start of blooms and shorter duration of bloom in region #1 may be caused by the varying exposure to sunlight of the phytoplankton in this sea-ice dominated part of the Greenland Sea. The bloom duration is more variable in region #1 (with about two months difference between shortest and longest bloom) than in region #2 (with about one month difference between shortest and longest bloom), which is likely to be associated with the more variable mixing and light exposure pattern in region #1.

The monthly mean time series of CHL (Figure 5.6) for both of the regions show that the maxima of CHL were larger in 2008-2012 than in all the previous years. However, a linear fit to the data shows only a significant increasing trend for region #2 (+0.56 mgCHL/m^3, $p<0.01$, see Table 5.1) as here the maxima in 1998-2003 are quite low as compared to region #1. Besides, the higher maxima in 1998-2003, region #1 are remarkable in having the peak of the bloom in 2008-2012 in June only, while in the previous years the month of peak of bloom was variable and ranging from May to July. The trend of increasing values towards 2012 is also clearly seen in the anomalies (Figure 5.7). It is of significance for region #2 alone as well (+0.54 mgCHL/m^3, $p<0.01$). Region #2 increasing trend is as expected and indicated by the results of Chapter 4, which used the same dataset, but did not cover the years 2010-2012. When the moving average of five months was applied to calculate trends, both of the regions showed significant increases in CHL for the period of the analysis (region #1: +0.21 mgCHL/m^3, $p<0.01$, region #2: +0.56 mgCHL/m^3, $p<0.01$). However consistent with mean and anomaly time series the increase in region #2 is larger and occurred mainly due to intensive blooms in 2009-2012 (Figure 5.8).

Trend characteristics	West (region#1)			East (region #2)		
	original	anomalies	moving average	original	anomalies	moving average
magnitude	0.2	0.19	**0.21**	**0.56**	**0.54**	**0.56**
p-value	0.21	0.14	**<0.01**	**<0.01**	**<0.01**	**<0.01**

Table 5.1 Trends calculated for the April 1998 - August 2012 time series of satellite GlobColour GSM CHL monthly data (N=75). West stands for western Fram Strait (15°W-0°, 76°N-84°N), region #1, and east stands for eastern Fram Strait (0°-15°E, 76°N-84°N), region #2. Significant trends (p<0.01) are marked in bold. Original stands for original monthly mean time series, anomalies for the original time series with the seasonal cycle subtracted, and moving average stands for the original time series smoothed with a moving average of five months (section 4.2.2.2)

In both regions the years 2009-2012 have positive anomalies, showing that values higher than the mean were prevalent in these years (Figure 5.7). In region #2 in all the other years, positive anomalies are occurring in April mostly, and the majority (73%) of the anomalies throughout the year are negative. On the other hand, in region #1 about the same number of positive and negative anomalies are present. The most abnormal bloom of all studied was observed in 2006 in region #2. It started earliest in the region (day 97 of the year) and had the longest duration in our series of observations (144 days). It is the only year in the region when the average CHL in April is higher than the average CHL in May. Such an early and intense bloom can be associated with the thermal stratification, which stabilizes the water column and concentrates the phytoplankton in the surface sunlit portion of the water column. Indeed, the highest observed values of temperature in the core of the Atlantic Water were measured in 2006 (Walczowski et al., 2012; Walczowski and Piechura, 2007). The long and intense bloom apparently was associated with increased export of organic material to the deep waters, as in 2006 where the benthic data showed a major deviation (Kraft et al. (2013); personal communication A. Boetius). In region #1, which does not experience an impact of Atlantic waters, 2006 was rather an average year.

In a broader context, consistent with previous studies (Kahru et al., 2011; Harrison et al., 2013) we have noted only a minor change in phytoplankton bloom timing for the last fifteen years. Besides, this analysis confirmed that the regional separation we have chosen based on oceanographic conditions of Fram Strait is present as well not only generally in the in the phytoplankton variability (as was

previously seen in Chapter 4), but also in the timing and duration of the phytoplankton bloom. Specifically, we have observed late (middle of May) and time varying phytoplankton blooms in the western part and earlier (end of April) and longer blooms in the eastern part. The increasing trend for 1998-2012 in the eastern Fram Strait and the absence of such trend in the western Fram Strait was also observed in the in-situ CHL data. Increase of CHL in the eastern region can partly be linked to the warm anomaly in WSC in the last decade (Chapter 4; Nöthig E.-M. et al., in review).

If the daily coverage of optical data for this region is provided by satellites (which is not yet the case as much data are excluded in the quality control procedures, due to contamination by clouds, sun glint, and sea ice) then the more precise estimation of bloom timing will be possible (+/- a day instead of current +/- a week).

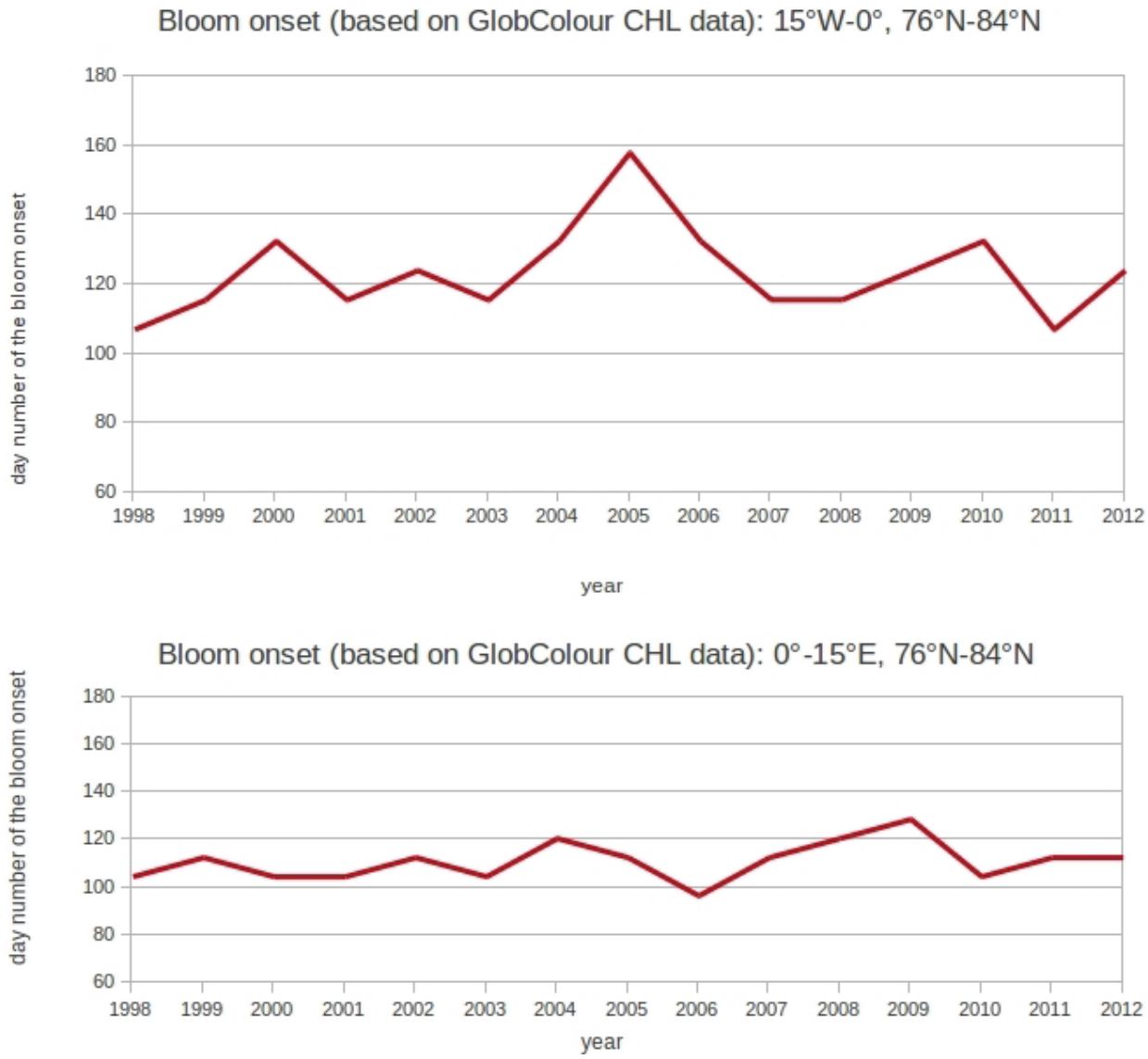

Figure 5.4 Date of phytoplankton bloom onset for years 1998-2012 calculated using as a threshold for the bloom onset 5% of the available pixels with values higher than 1 mgCHL/m^3. This analysis is based on satellite GlobColour GSM CHL 8-day data. Top: western Fram Strait (15°W-0°, 76°N-84°N), region #1. Bottom: eastern Fram Strait (0°-15°E, 76°N-84°N), region #2.

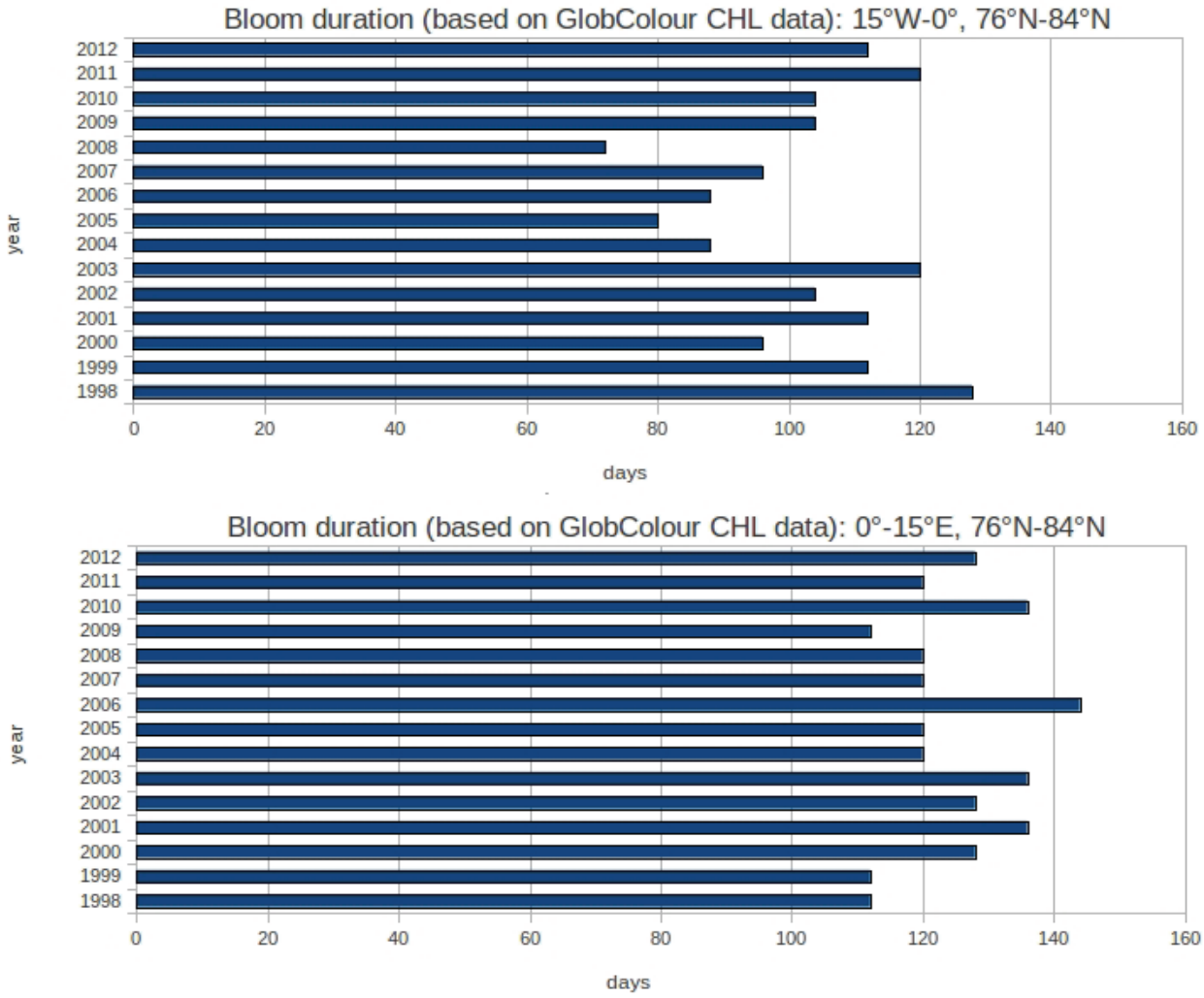

Figure 5.5 Duration of the phytoplankton bloom for years 1998-2012 calculated using as a threshold for the bloom onset 5% of the available pixels with values higher than 1 mgCHL/m^3. This analysis is based on satellite GlobColour GSM CHL 8-day data. Top: western Fram Strait (15°W-0°, 76°N-84°N), region #1. Bottom: eastern Fram Strait (0°-15°E, 76°N-84°N), region #2.

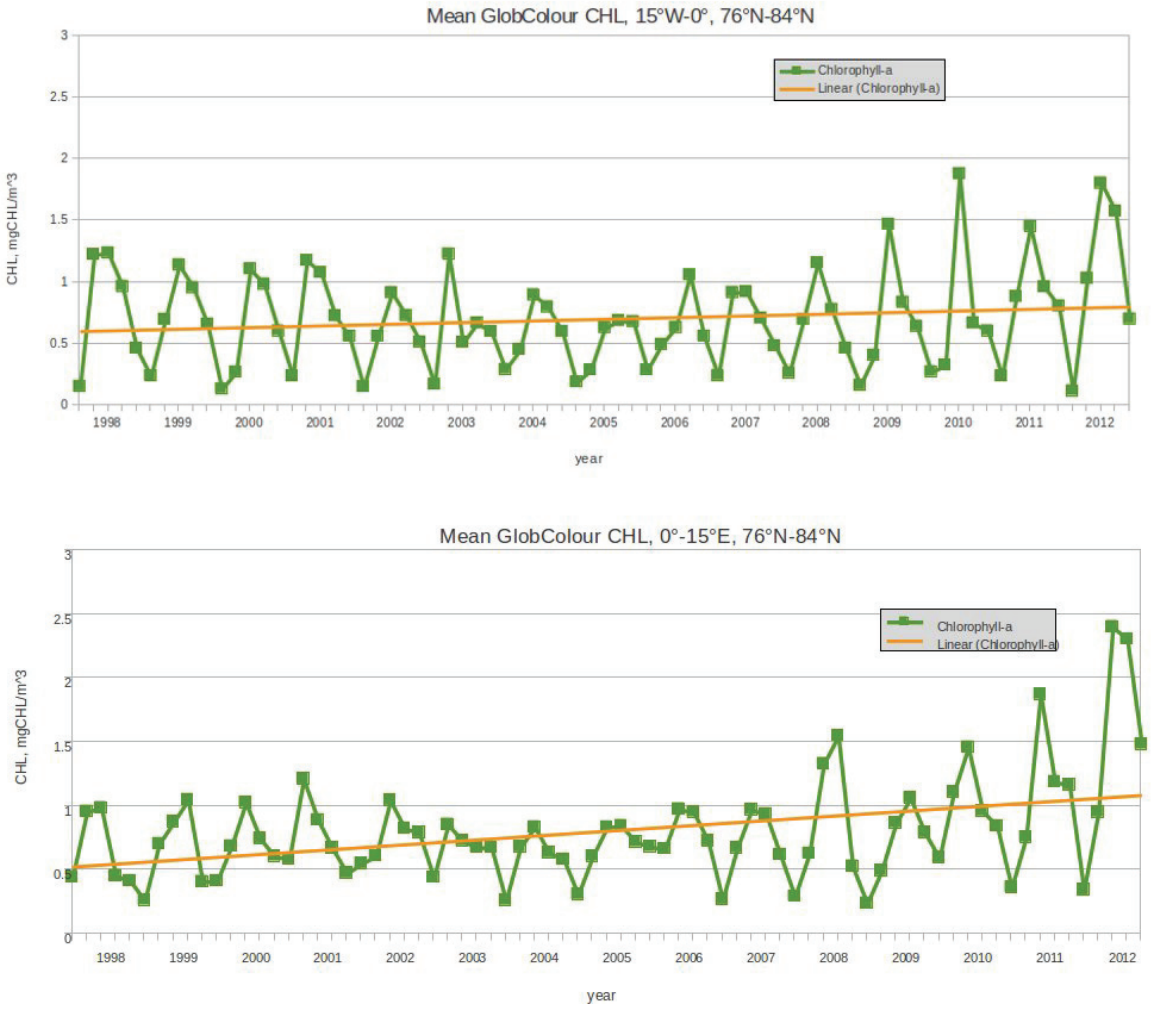

Figure 5.6. Time series of satellite GlobColour GSM CHL monthly mean data for years 1998-2012. Top: spatially averaged for the western Fram Strait (15°W-0°, 76°N-84°N), region #1. Bottom: spatially averaged for the eastern Fram Strait (0°-15°E, 76°N-84°N), region #2.

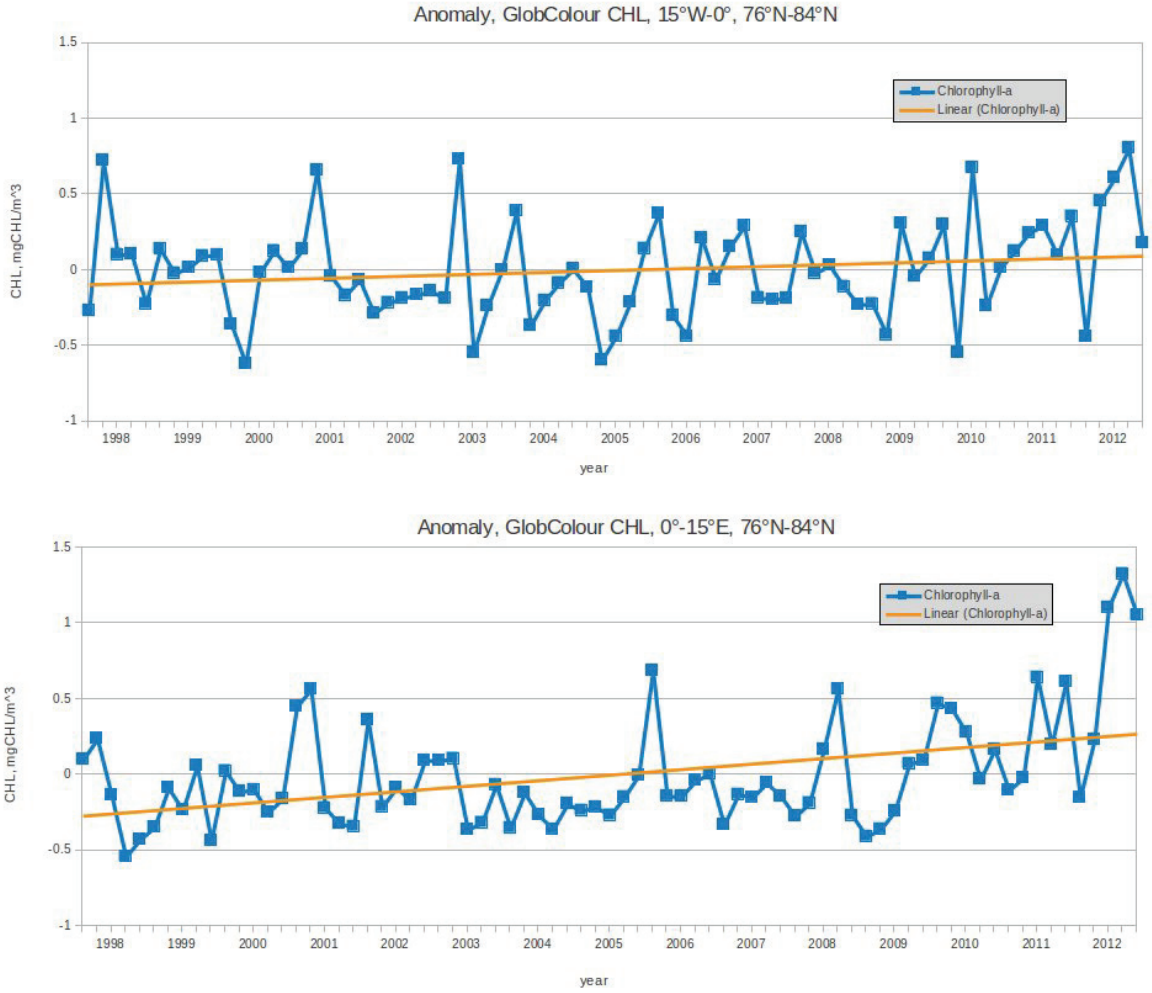

Figure 5.7 Time series of satellite GlobColour GSM CHL monthly anomalies for years 1998-2012. Top: for the western Fram Strait (15°W-0°, 76°N-84°N), region #1. Bottom: for the eastern Fram Strait (0°-15°E, 76°N-84°N), region #2.

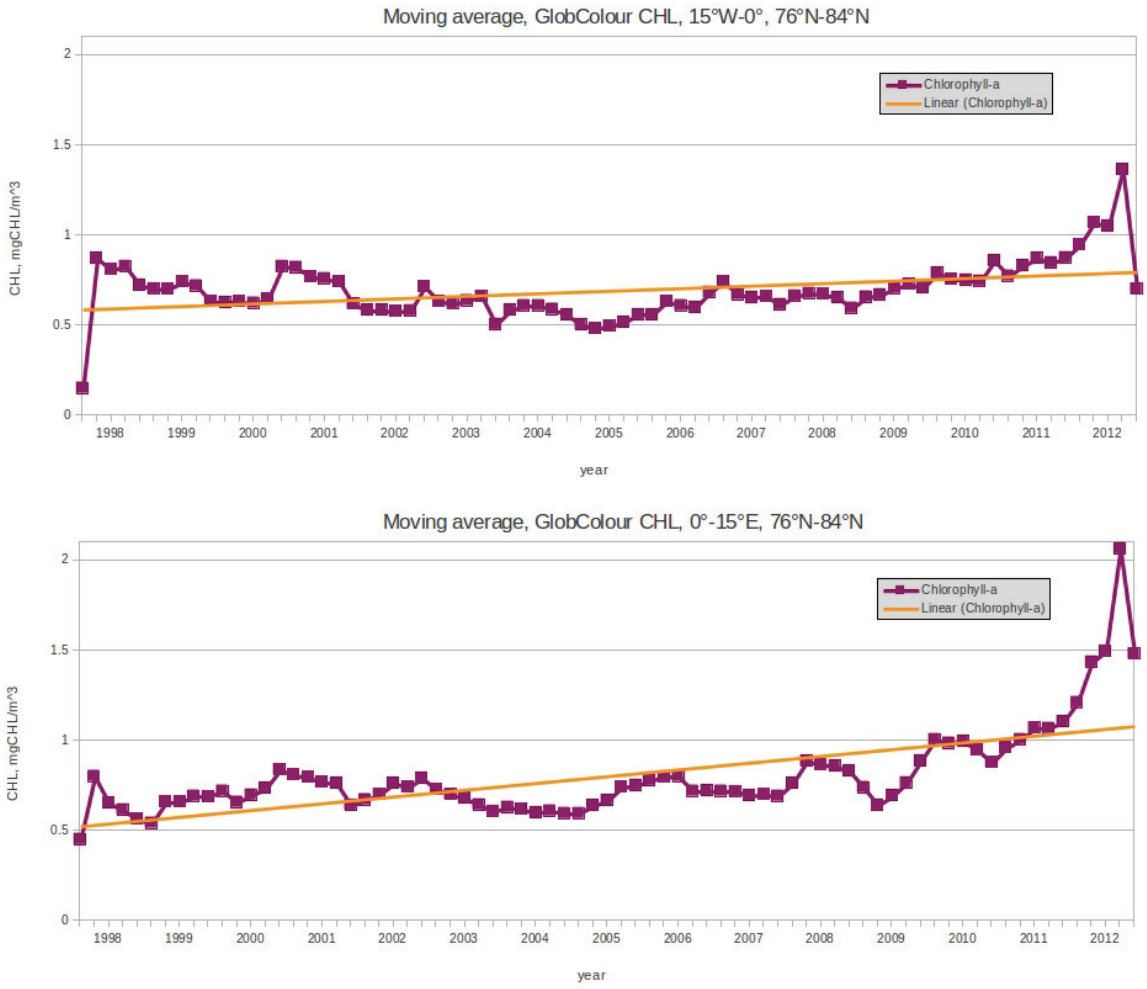

Figure 5.8 Time series of satellite GlobColour GSM CHL smoothed with a moving average filter of five months for years 1998-2012. Top: for western Fram Strait (15°W-0°, 76°N-84°N), region #1. Bottom: for eastern Fram Strait (0°-15°E, 76°N-84°N), region #2.

Chapter 6

Parameterization and analysis of chlorophyll-a vertical profiles

6.1 Motivation

The current uncertainty in the global marine PP estimates is high, with values ranging over a factor of two (Carr et al., 2006). The most challenging regions for PP modeling are poleward of 40° in all basins (Carr et al., 2006), where the range of PP estimates is even higher. In the Arctic Ocean the uncertainties are mainly caused by the unique optical properties of the Arctic waters and the presence of a Subsurface CHL Maximum (SCM) (Arrigo et al., 2011; Matsuoka et al., 2007, 2011; Weston et al., 2005). The SCM is often not correctly seen by the satellite as it lies below the surface layer visible to the satellite sensor. To include the information on the SCM into PP models accurately, one needs to find the appropriate relationship between CHL in the surface layer and its vertical profile. There have been a number of methods developed to handle this. The PP model by Behrenfeld and Falkowski (1997) considers the CHL profile to be uniform throughout the water column. The model by Antoine and Morel (1996) and Antoine et al. (1996) goes further by assuming that the CHL profile changes its shape according to the concentration of the surface layer. On the contrary, the recent Arctic PP model by Arrigo et al. (2011) adopts a fixed shape of CHL profile for a specific month and region.

The current study uses CHL data from R/Vs *Polarstern* and *Maria S Merian* 1991-2010 cruises together with the data from the ARCSS-PP database (Hill et al., 2013; Matrai et al., 2013). We combine the methods of Morel and Berthon (1989) and Arrigo et al. (2011), by looking for the relationships that describe 1) the change of the CHL profile depending on its surface concentration, and 2) the seasonal cycle of the CHL profile. Finally, we are also interested in identifying the differences between the Greenland Sea relationship of this study and the global one of Morel and Berthon (1989).

6.2 Methods

6.2.1 Data description

The borders for the Greenland Sea sector of the Arctic were chosen close to Arrigo et al. (2011): north of the Arctic circle at 66°33'39"N and between 45°W and 20°E. We combined the CHL data from R/Vs *Polarstern* and *Maria S Merian* 1991-2010 cruises with the ARCSS-PP database (1957-2003). The data covered the months from April till October.

The samples of R/V *Polarstern* and *Maria S Merian* cruises were collected for 6 depths in Niskin bottles, 0.5-2.0 L of water were filtered through Whatman GF/F glasfibre filter, stored at -18°C and afterwards analysed in AWI laboratory. The filters were extracted in 90% acetone and analysed with a spectrophotometer for higher values and with a Turner-Design fluorimeter for lower values according to the methods described in Edler (1979) and Evans and O'Reily (1984). The values from the fluorimeter were calibrated with the values obtained from the spectrophotometer. In addition, calibration of the fluorimeter was carried out with Sigma CHL standard. The samples were taken while the ship was underway (surface sampling) and while stationary (vertical profile sampling, henceforth “stations”). In this study we considered only the samples from stations as we are interested in information on the vertical profile. Refer to Matrai et al. (2013) and Hill et al. (2013) for details on the ARCSS-PP database.

The irradiance profiles were measured with the hyperspectral radiometer (RAMSES, TriOS GmbH, Germany). The instrument had a cosine collector fixed in front of it and covered a wavelength range of 350 nm to 950 nm with an optical resolution of 3.3 nm and a spectral accuracy of 0.3 nm. All the measurements were obtained with an automated integration time of the respective sensor between 4 ms and 8 s. A reference irradiance device was placed above the water surface to monitor the downwelling incident sunlight and allow the normalization of the in-water measurements according to Stramski et al. (2008). The irradiance profiles were collected simultaneously with the CTD (Conductivity Temperature Depth) profiles.

6.2.2 Data quality control and preprocessing

The data quality control procedure for the CHL data consisted of filtering out all profiles which either had less than three depths or belonged to the month of October since the number of data points in October was fewer than 20. In cases where several profiles were measured at one location and in one day we took only the profile with the most sampled depths. If either the location or the day changed we considered it to be a new profile. Profiles that did not reach the surface were extrapolated to the surface as described below. To avoid negative values we put 0.01 mgCHL/m^3 as the lowest value for the surface. Finally, we gridded the extrapolated profiles to 1 m increments for further statistical analysis.

By linearly extrapolating the profiles that have a steep change between the two shallowest measurements additional errors could be introduced. Therefore, we additionally investigated three other ways of handling the difficulty of the majority of profiles that did not reach the surface. These included: 1) taking the value of the shallowest depth as the surface CHL; 2) extrapolating only those profiles which changed with a rate less than 0.1 mgCHL/m between the 2 shallowest measurements and treating other profiles as described in point 1; 3) as in point 2, but with a stricter rate threshold of 0.05 mgCHL/m. Comparing the results of these three different extrapolation methods showed that there was hardly any influence on the shape of the final median profiles. We therefore decided to apply the simple linear extrapolation to the profiles by using the change between the two shallowest measurements.

6.2.3 Calculation of the main profiles parameters

Firstly, Z_{eu} (euphotic layer depth) and CHL integrated for Z_{eu} (C_{tot}) were calculated. Except for the nine light profiles we selected from those 23 profiles we measured in 2010 during RV 'Polarstern' ARK-25 cruise, no other database with co-located light and CHL profiles were available. Thus the euphotic depth was inferred from the CHL profile, using a bio-optical model for light propagation. Following Morel and Berthon (1989), the model of Morel (1988) was used (Eqs. [6.1a] and [6.1b]) for the estimation of both Z_{eu} and C_{tot}.

$$Z_{eu} = 568.2\ C_{tot}^{-0.746} \qquad [6.1a]$$

when Z_{eu}<102m

$$C_{tot} = 39.0 C_{pd}^{0.48}$$

$$Z_{eu} = 200.0\ C_{tot}^{-0.293} \qquad [6.1b]$$

when Z_{eu}>102m

To determine the C_{tot} value a given profile was progressively integrated with respect to increasing depth (z). The successive integrated CHL values were introduced in Eq (1a), thus providing successive 'Z_{eu}' values that were progressively decreasing. Once the last 'Z_{eu}' value, as obtained, became lower than the depth z used when integrating the profile, these C_{tot} and Z_{eu} values from the last integration were taken. Profiles which didn't reach Z_{eu} were excluded.

The Morel (1988) model for the Z_{eu} estimation has later been revised by Morel and Maritorena (2001), yielding to only minor changes in Z_{eu} (slightly increased Z_{eu} values in oligotrophic waters, with mean CHL in Z_{eu}<0.3 mg/m^3). As the revised version does not differ appreciably from Morel (1988) for the more productive waters such as Greenland Sea, we used the latter one to be consistent with Morel and Berthon (1989) analysis.

The Z_{eu} values obtained from nine co-located light and CHL profile measurements from 2010 were used to verify the Z_{eu} values obtained by the method of Morel and Berthon (1989), Z_{eu}^{CHL}. In order to calculate Z_{eu} from the light measurements (here called Z_{eu}^{PAR}), the following method was applied. PAR profiles were obtained by integrating spectrally resolved downwelling irradiance measurements for 400-700 nm. Downwelling irradiance measurements were corrected for incident sunlight following Smith and Baker (1984). To calculate Z_{eu} from those PAR profiles which didn't reach 1% of the surface PAR value an exponential function was fitted. The individual profiles are given in the Figure 6.1. The relative error (δ) of Z_{eu}^{CHL} was computed using the following equation:

$$\delta = \left(Z_{eu}^{CHL} - Z_{eu}^{PAR}\right) / Z_{eu}^{PAR} \qquad [6.2]$$

The average value of δ, which equaled 23%, gives us confidence in our determination of the euphotic depth derived from CHL profiles, since it is better than what has been determined in other studies: Milutinovic (2011) estimated δ values of 24%-36% by comparing global collocated datasets of

Z_{eu}^{PAR} and Z_{eu}^{CHL}, with the latter inferred by combining the methods of Morel and Berthon (1989) and Morel and Maritorena (2001). Lee et al. (2007) validated Z_{eu}^{CHL} measurements by the Z_{eu}^{PAR}, using the Morel and Maritorena (2001) model, obtained from data of Monterey Bay, Gulf of Mexico, and the Arabian Sea, resulting in an average error of 33%. Our lower average error than that estimated by Milutinovic (2011) and Lee et al. (2007) is likely to be explained by the low number of light measurements in our database. Generally, some discrepancies between Z_{eu}^{CHL} and Z_{eu}^{PAR} are to be expected: Z_{eu}^{CHL} is determined from a few measurements in the profile, while Z_{eu}^{PAR} is determined from continuous measurements. In addition, Z_{eu}^{CHL} is based on assuming Case1 waters, and should differ from Z_{eu}^{PAR} in regions with high CDOM concentrations. Henceforth, Z_{eu}^{CHL} is referred as $Z_{eu.}$

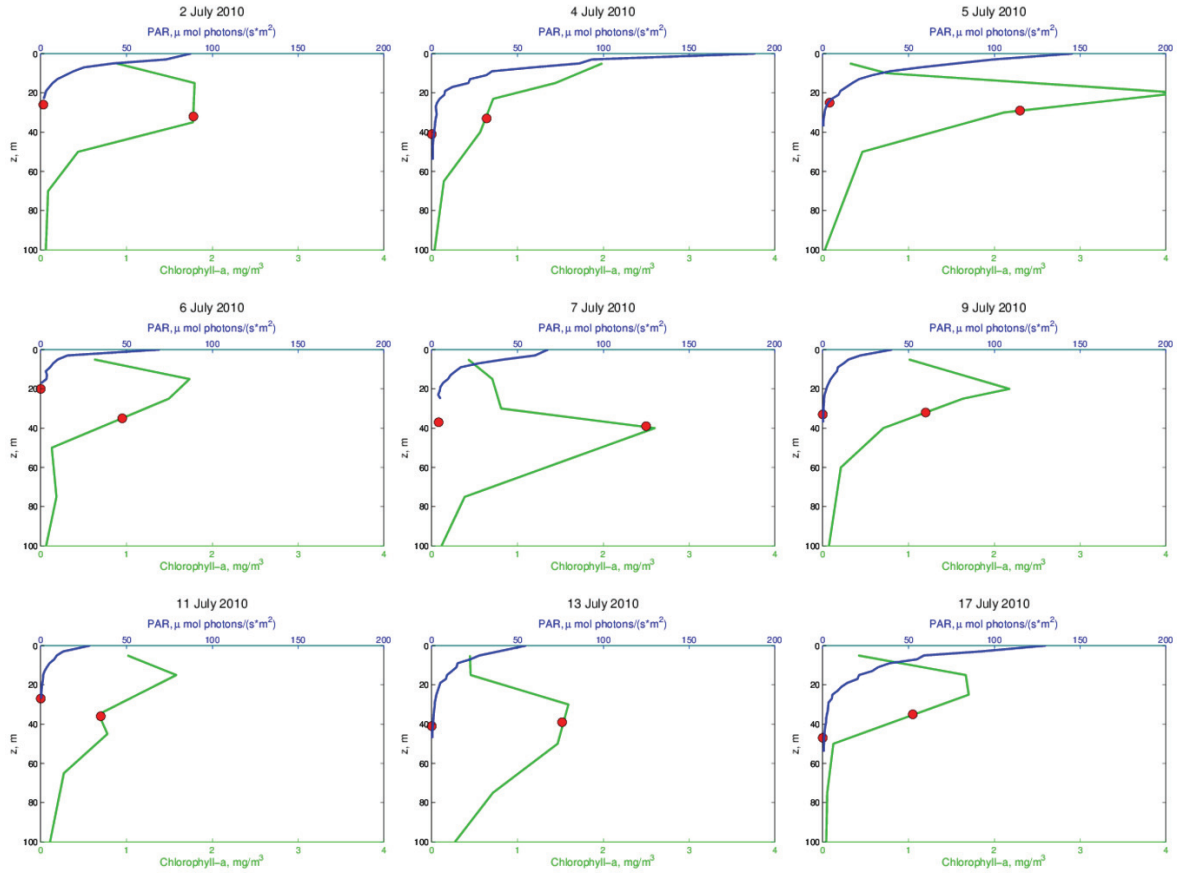

Figure 6.1 Vertical profiles of PAR and CHL simultaneously taken in Greenland Sea in July 2010. Euphotic layer depths inferred from CHL profiles following Morel (1988) and calculated from PAR profile are marked as red circles on the corresponding profiles. The average error for Morel (1988) euphotic layer depth is 23% (section 6.2.3). Data of R/V Polarastern cruise.

We calculated the penetration depth (Z_{pd}), where 90% of the optical remote sensing information comes from, as was defined in section 4.2.2.1. Using Z_{pd}, we calculated the CHL value to be seen by the satellite sensor – the mean CHL concentration for the penetration depth layer (C_{pd}). Mean CHL for Z_{eu} layer (C_{zeu}) was computed as well.

The dimensionless profiles (obtained to compare our results to those of Morel and Berthon (1989)) were computed as follows: the dimensionless depth as the actual depth value divided by Z_{eu} and the dimensionless CHL as the actual CHL values divided by C_{zeu}. Thus the shape of the vertical profiles

(for different stations) could be compared regardless of their absolute magnitude (Morel and Berthon, 1989).

6.2.4 Selection of the representative surface layer chlorophyll-a categories and statistics

According to the method of Morel and Berthon (1989) and based on a histogram analysis of C_{pd}, we divided all data into six categories containing an equal number of profiles. Thereafter, we organized the data within each category into monthly bins and calculated the median profiles inside each bin. The median profiles were used in the further analysis as the representative profiles for the certain C_{pd} in a certain month, because as opposed to the mean profiles, the median gives less weight to outliers. To have an idea on the spread of the initial data, we plotted half of the interquartile range together with the median.

We additionally calculated the mean, standard deviation, depth of the CHL maximum and its value for each category as they provided a more detailed view on the variation of the data within each category. The C_{tot} and the ratio of CHL maximum value to C_{pd} were included to Table 6.1 to have a further insight to the amount of CHL that is not detected by a satellite sensor. The variability of C_{tot} vs C_{pd} was explored using the White (1980) heteroscedasticity test. With a subset of the data (R/Vs *Polarstern* and *Maria S Merian* 2000-2009 data only) we also investigated the different ways to categorize the profiles (e.g. by latitude, longitude, temperature or salinity of the surface layer). However, the selection of categories based on the CHL in the surface layer and month showed the least variability within a category.

Keeping in mind that we planned to use the results of this study as representative CHL profiles of the Greenland Sea for a certain month and surface concentration which involved the least computational effort, we were interested in having equations to describe the profiles. Thus, we took the processed median profiles and fitted a Gaussian to each of the median profiles in the least squares sense (see equation (5)). Median profiles were linearly interpolated for surface CHL values from 0 to 5 mgCHL/m^3 with 0.1 mgCHL/m^3 steps. The Gaussian shape was chosen for fitting as the vertical profiles of bio-optical profiles such as the CHL maximum layer are shown to be well defined using this shape (Arnone et al., 2007).

6.2.5 Analysis of the seasonal variability and reference to uncertainties in primary production estimates

Monthly CHL profiles of separate C_{pd} categories can occur in different regions of the Greenland Sea with different nutrient or physical conditions and thus not always correspond to the seasonal cycle of CHL. In order to account for the contribution of the monthly profiles from the different areas of the Greenland Sea, we firstly averaged all the profiles that were available in our data base for each month. Besides, we calculated the monthly profiles for a smaller region to minimize the inhomogeneity of physical conditions. A monthly profile was considered to be valid if it was an average of more than 20 profiles. As a smaller (case study) region, based on a latitude-longitude density analysis of all samples, the area within 77°N to 82°N and 5°W and 10°E was chosen. This is the "Hausgarten" area, the long-term underwater observatory of AWI (Soltwedel et al., 2005).

In order to roughly assess the effect of the SCM (Subsurface CHL Maximum) on PP estimates and the errors associated with that in PP models based on remote sensing data, we determined monthly PP in the Greenland Sea according to Eppley et al. (1985), where PP is assumed to be proportional to the square root of CHL. We firstly calculated PP based on the C_{tot} values from in-situ profiles and used these as a reference. These reference calculations were compared to those obtained from: 1) Gaussians fitted to monthly in-situ profiles with 0.1 mgCHL/m^3 step of C_{pd} (this study); 2) uniform profiles by keeping the surface value constant; 3) profiles of Morel and Berthon (1989). Morel and Berthon (1989) profiles were used for C_{pd}>0.05 mgCHL/m^3 only to exclude the negative values which occured for C_{pd}<0.05 mgCHL/m^3. For calculations of Z_{eu} we used the Morel and Berthon (1989) method described in the beginning of section 6.2.3. The errors of single profiles were calculated first and then the monthly medians of the errors were calculated.

6.3 Results

6.3.1 Data quality control and preprocessing

Our initial CHL database for the Greenland Sea consisted of 1676 profiles, with 548 profiles derived from the data of R/V *Polarstern* and R/V *Maria S Merian* cruises and the rest from the ARCSS-PP database. After applying quality control procedures (section 6.2.2), 1472 profiles were left.

In addition, nearly 300 profiles did not reach the euphotic depth and thus were excluded. After such preprocessing our database consisted of 1199 profiles.

Figure 6.2 shows a clear relationship between C_{pd} (mean CHL within the penetration depth) and C_{tot} (total CHL in the water column) for the Greenland Sea from our database (left) and for the global database from Morel and Berthon (1989), which is based on the analysis of 3497 profiles (right).

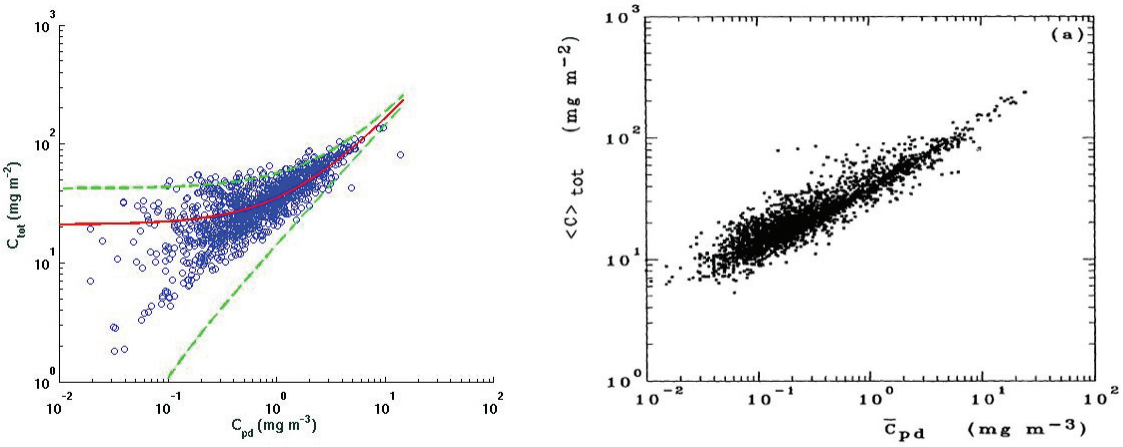

Figure 6.2 Total CHL content within the euphotic layer (C_{tot}) versus mean CHL within the surface layer (C_{pd}). Left: for the Greenland Sea, this study, R=0.84, N=1199, significant correlation (p<0.0001). The red line is the linear regression line, green lines are the 95% confidence intervals. Right: from the global study by Morel and Berthon (1989)

Equations [6.3] and [6.4] correspond to the fitted regression lines of our dataset and that of Morel and Berthon (1989), respectively.

$$C_{tot} = 39.0\, C_{pd}^{0.48} \qquad [6.3]$$

$$C_{tot} = 40.6\, C_{pd}^{0.46} \qquad [6.4]$$

The slopes of the regression lines in the double-logarithmic plots are close: 0.48 for the Greenland

Sea and 0.46 for the global dataset. Scatter plots show nearly no difference in the high C_{pd} values related to C_{tot}. The differences between the two datasets occur at low C_{pd} values which for the Greenland Sea correspond to a wider range of C_{tot} as compared to the global relationship. We attribute this difference to the various magnitudes of SCM in our data. Specifically, very low values of C_{tot} (in the range of 1-5 mgCHL/m^2) are present in our dataset only. We've further explored the change in C_{tot} with respect to C_{pd} variability using the heteroscedasticity test (White, 1980). The only parameter showed to be causing the change in C_{tot} with respect to C_{pd} variability was the month (with p=0.05), supporting the choice of the categorization method by season. The other predictors tested were latitude, longitude, year, euphotic layer depth and penetration depth. For all of them the null hypothesis of heteroscedasticity was accepted at the confidence level of 0.05. To sum up, the clear relationship between C_{pd} and C_{tot} for the Greenland Sea proved that a mathematical dependency between these two parameters is to be expected, though it has to be regarded carefully for the low C_{pd} values.

6.3.2 Selection of the representative surface layer chlorophyll-a categories and fitting of Gaussians

Based on the histogram of C_{pd} (Figure 6.3) we defined six ranges of C_{pd} with roughly 200 profiles per range. The histogram showed that most of the profiles have low values in the upper ocean layer (C_{pd} lower than 1 mgCHL/m^3). The obtained C_{pd} (mgCHL/m^3) ranges were: 1) <0.3; 2) 0.3-0.45; 3) 0.45-0.7; 4) 0.7-1; 5) 1-1.5; 6) >1.5. The median of the profiles for each range (see sections 2.3-2.4) showed that the shape of the profiles for the ranges 4 to 6 are nearly identical. Therefore we combined those into one range (> 0.7mgCHL/m^3) that covers about 600 profiles.

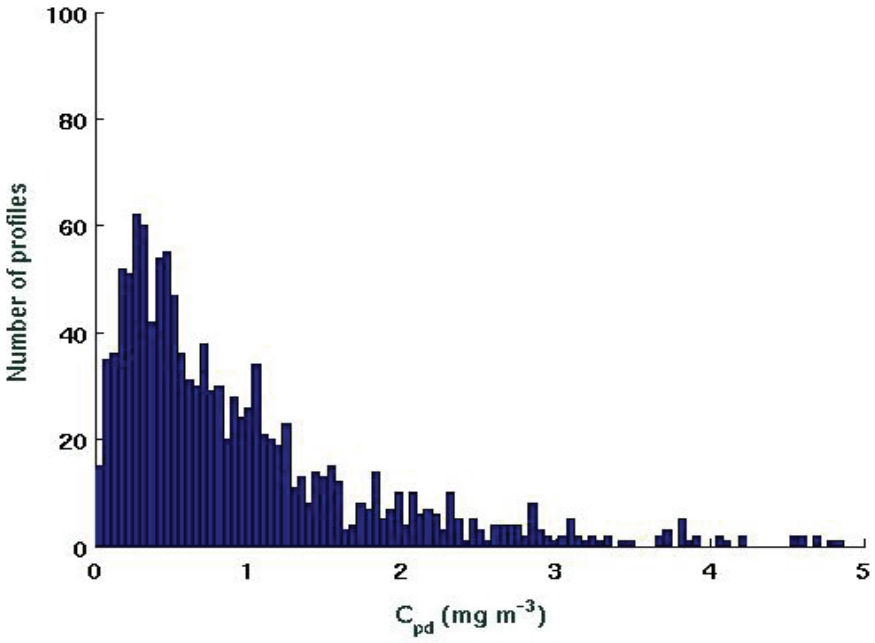

Figure 6.3 Histogram describing the distribution of the mean CHL within the surface layer (C_{pd}) over the 1199 CHL profiles.

Figure 6.4 illustrates the spatial distribution of the final four categories assigned (left), and shows the months when the samples were taken (right). South of 74°N, in the area of the warm Atlantic waters, the category with highest surface CHL (C_{pd}>0.7 mgCHL/m^3) was prevalent. In contrast, in the north-west part of the basin, which is the sea ice affected area of the Greenland shelf, the category with the lowest surface CHL (C_{pd}<0.3 mgCHL/m^3) occured more often than the other ones. Both these categories, however, appeared throughout the basin as well. The two other intermediate C_{pd} categories were spatially more evenly distributed. Generally, the sampling was concentrated along the two transects at 75°N and at 78°N-79°N. Each of the two transects included samples for all the months analysed, with August being the least sampled month and April samples being more concentrated in the area north of 78°N.

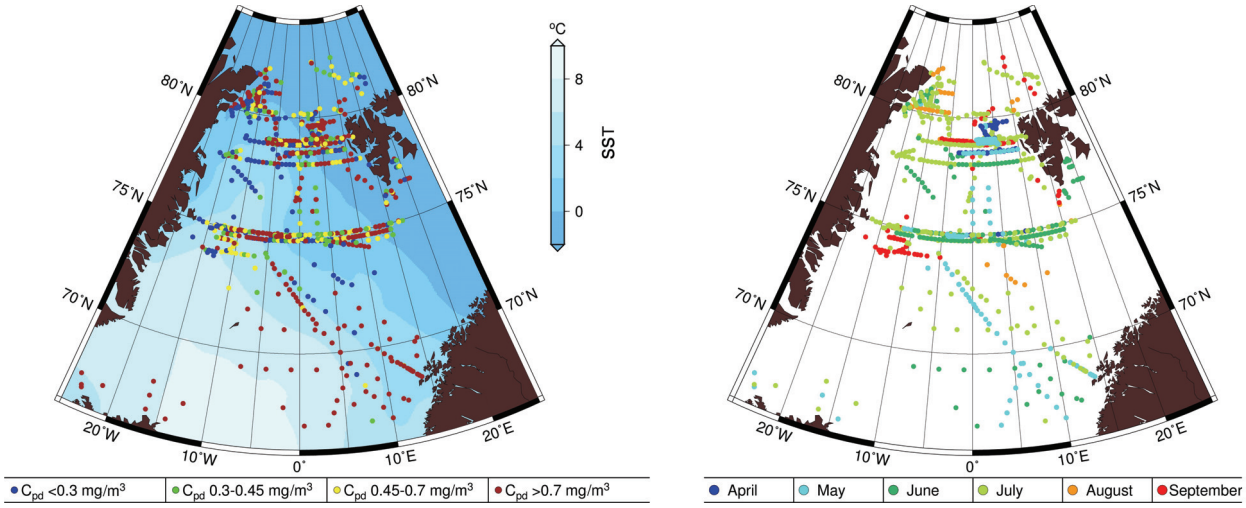

Figure 6.4 Left: Locations of CHL profiles, colour of the circle indicates the C_{pd} category assigned. In the background is the sea surface temperature climatology map for 2002-2012 (data of Physical Sciences Division, Earth System Research Laboratory, NOAA, Boulder, Colorado, http://www.esrl.noaa.gov/psd/). Right: Locations of CHL profiles, colour of the circle indicates the month of sampling.

Figure 6.5 shows the median profiles for the four C_{pd} ranges. For all C_{pd} ranges the CHL maximum shallows towards the end of the season. The SCM for the majority of the months is most pronounced in the lowest C_{pd} range (plot I), where it is also deeper than in other ranges. Within this range, the magnitude of the April-May SCM is equal to or greater than in September. May to July, having no clear SCM, represent a transitional state between the two seasons. The relative spread of the maxima is highest in this range (Figure 6.6). In the second and third C_{pd} ranges (plots II and III) the SCM is more difficult to distinguish (except for the August profiles), and there is a rather gradual shift of the maximum towards the surface from April to September. In the fourth and highest C_{pd} range (plot IV) the maxima mostly occur exactly at the surface. This is the only range with most months reaching maximum values at the surface. The fourth range shows a clear decrease of the surface CHL values from April to September.

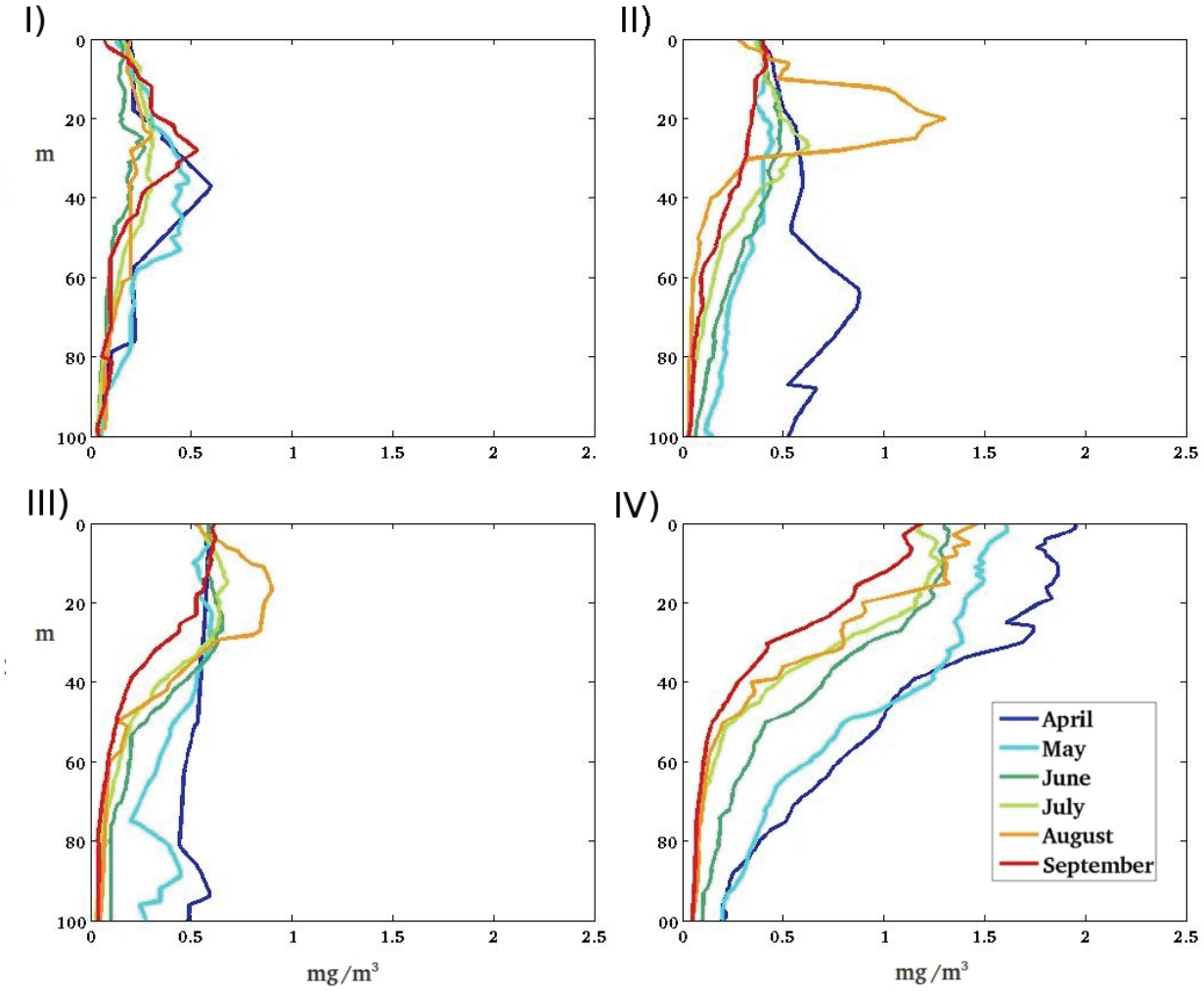

Figure 6.5 Median monthly CHL profiles obtained for the four ranges of mean CHL within the surface layer (C_{pd}, mgCHL/m^3). Ranges: I) <0.3; II) 0.3-0.45; III) 0.45-0.7; IV) >0.7. Data of R/V Polarstern and Maria S Merian cruises, and from ARCSS-PP database, 1957-2010.

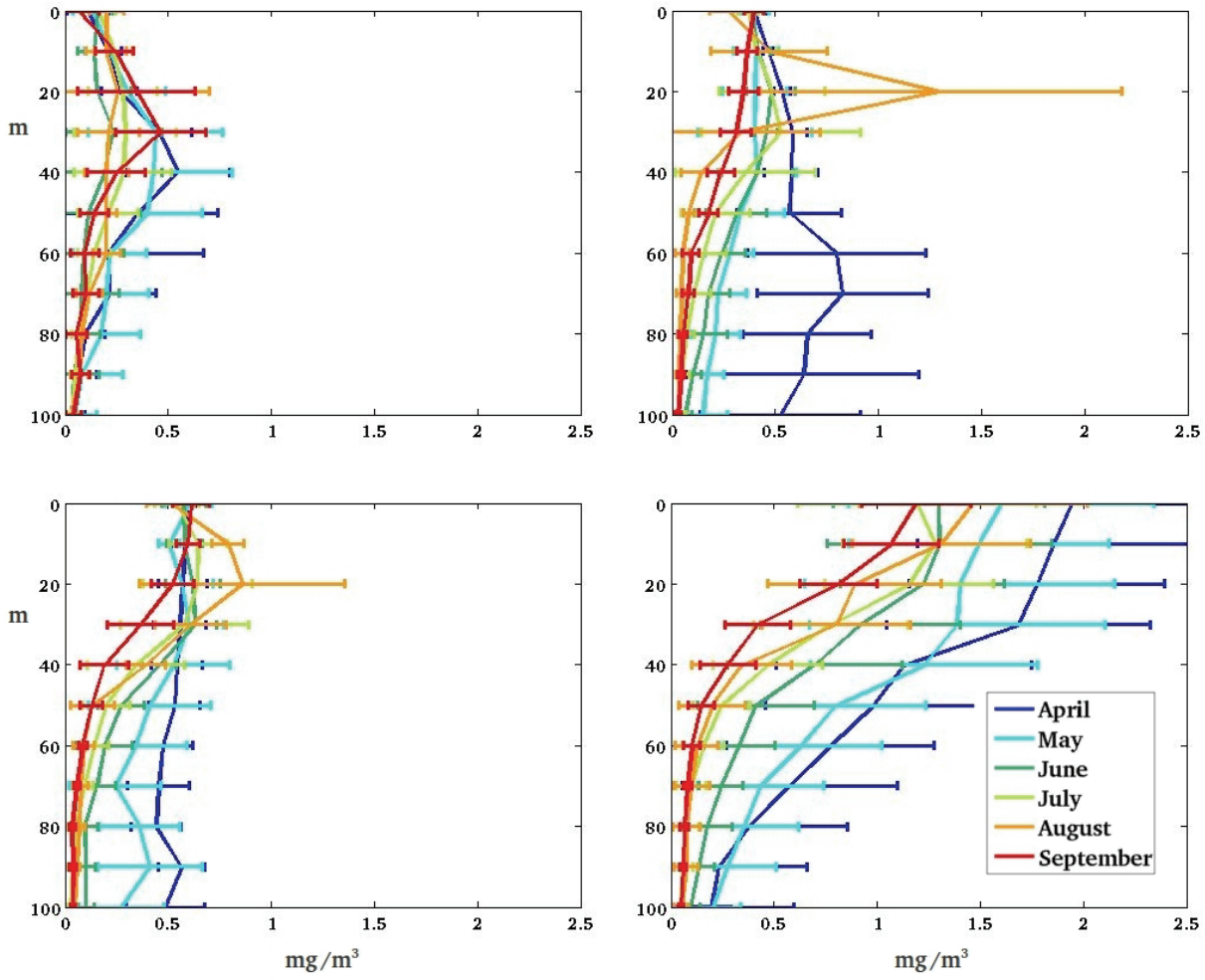

Figure 6.6 Interquartile ranges for the monthly CHL profiles in the four ranges of mean CHL within the surface layer (C_{pd}, mgCHL/m^3) binned into 10 m depth intervals. Ranges: I) <0.3; II) 0.3-0.45; III) 0.45-0.7; IV) >0.7. Data of R/Vs Polarstern and Maria S Merian cruises, and from ARCSS-PP database, 1957-2010.

Fitting Gaussian functions to the median profiles resulted in much smoother curves which have a single pronounced maximum (see Figure 6.7). Some of the original median profiles (Figure 6.5) that are quite different from each other, appear nearly identical in the fitted Gaussians (such as April-May of the lowest C_{pd} range). However, the main features of the median profiles (such as the propagation of the maximum towards the surface as the season goes by in September) are also present in the fitted curves.

A table with the coefficients A, σ and μ for the Eq [6.5] of the Gaussians fitted with 0.1 mgCHL/m^3 surface CHL resolution was derived and is available on request.

[6.5]
$$CHL = Ae^{-\frac{(z-\mu)^2}{2\sigma^2}}$$

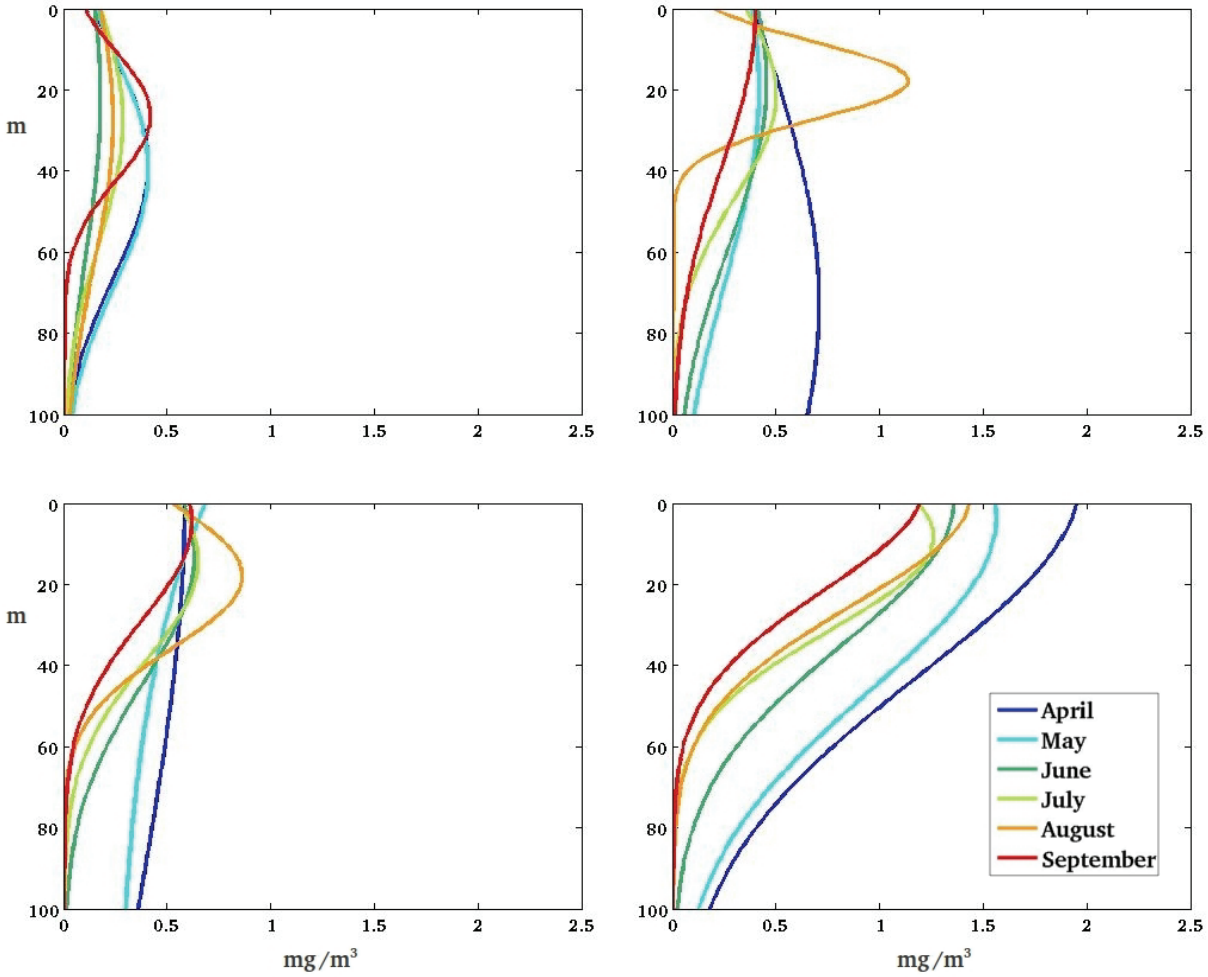

Figure 6.7 Gaussians fitted to the median monthly CHL profiles obtained for the four ranges of mean CHL within the surface layer (C_{pd}, mgCHL/m^3). Ranges: I)<0.3; II) 0.3-0.45; III) 0.45-0.7; IV)>0.7. Data of R/V Polarstern and Maria S Merian cruises, and from ARCSS-PP database, 1957-2010.

6.3.3 Statistical analysis

In addition to the figures presented above, Table 6.1 gives more details on the basic statistics and CHL maximum characteristics of the dataset and enables the comparison of the features of the different C_{pd} ranges (vertically) and of the different months (horizontally). The median, mean, inter-quartile range and standard deviation are averaged for the whole water column.

The profiles with low CHL concentration in the surface layer, the lower C_{pd} ranges, always show a SCM (see the depth of the CHL maximum for the first two ranges). Median values rise towards the maximum C_{pd}, pointing out that the SCM does not critically influence the median CHL in the water column. In case of low surface concentration, however, the relative contribution of SCM to the total CHL is important, with its magnitude exceeding the surface value by up to a factor of three (see e.g. April for the lowest C_{pd} range). The latter is additionally supported by the months with highest CHL maximum to C_{pd} ratio being also those with highest C_{tot} values within the range (April, May of the first range, and April, August of the second range). Median and mean for all the C_{pd} ranges show the bloom weakening from April till September (see also Figure 6.5, for the highest range only). The CHL maximum does not show the same clear trend, e.g. the third C_{pd} range with all months except August having about the same CHL maximum. Generally, the mean is higher than the median, signifying that most of the outliers are higher than the median. The percentage spread of the data (interquartile range) is usually highest in the lowest C_{pd} range. September is the month with the least spread. The penetration depth (Z_{pd}) did not vary much seasonally, but showed the expected variability between the C_{pd} ranges: maximum Z_{pd} was observed in April in the lowest C_{pd} range and minimum Z_{pd} was observed in April-May in the highest C_{pd} range. The relationship between Z_{pd} and C_{pd} (Figure 6.8) has large scatter in the low C_{pd} area, but overall a shows significant correlation as was also the case for C_{tot} (Fig. 6.2).

Table 6.1 Characteristics of the CHL profiles categorized according to the mean CHL in the surface layer (C_{pd}), and then binned into monthly bins. Roman numbers indicate the four ranges of C_{pd} (mgCHL/m^3): I) <0.3; II) 0.3-0.45; III) 0.45-0.7; IV) >0.7. C_{tot} is the total CHL content in the water column, Z_{pd} is the penetration depth (also known as the first optical depth). The median, mean, inter-quartile range, and standard deviation are averaged for the whole water column.

		April	May	June	July	August	September
Median (mgCHL/m^3)	**I**	0.25	0.26	0.12	0.18	0.16	0.19
	II	0.61	0.31	0.30	0.26	0.30	0.19
	III	0.52	0.44	0.34	0.30	0.35	0.24
	IV	1.04	0.89	0.61	0.49	0.48	0.37
Interquartile range (%)	**I**	75	81	134	62	64	56
	II	39	47	31	60	54	22
	III	23	46	25	41	30	24
	IV	53	52	46	45	46	27
Depth of CHL max (m)	**I**	38	37	28	26	25	29
	II	65	27	23	28	21	8
	III	1	1	25	16	17	5
	IV	2	2	3	11	1	1
Value of CHL max (mgCHL/m^3)	**I**	0.60	0.49	0.27	0.31	0.30	0.53
	II	0.88	0.45	0.48	0.63	1.30	0.41
	III	0.59	0.60	0.65	0.68	0.90	0.62
	IV	1.95	1.61	1.32	1.28	1.47	1.19
Mean (mgCHL/m^3)	**I**	0.43	0.46	0.33	0.30	0.23	0.25
	II	0.68	0.42	0.41	0.42	0.35	0.20
	III	0.52	0.60	0.41	0.38	0.37	0.26
	IV	1.18	1.17	0.78	0.66	0.60	0.40
Standard deviation (%)	**I**	102	131	145	116	92	93
	II	41	80	87	113	58	34
	III	34	79	68	70	44	33
	IV	66	79	72	88	65	42
CHL max/Cpd (%)	**I**	324	270	176	157	155	292
	II	207	118	127	169	346	109
	III	108	108	117	121	157	108
	IV	108	92	87	91	89	108
Ctot (mgCHL/m^2)	**I**	22.89	22.4	16.45	20.98	19.18	19.54
	II	27.01	25.41	24.25	26.01	30.62	17.65
	III	25.89	29.32	28.51	28.16	30.59	22.71
	IV	51.88	51.34	45.16	43.06	42.92	32.26
Zpd (m)	**I**	19	14	18	15	16	15
	II	11	12	12	12	11	15
	III	11	10	10	11	10	12
	IV	7	7	8	8	8	10

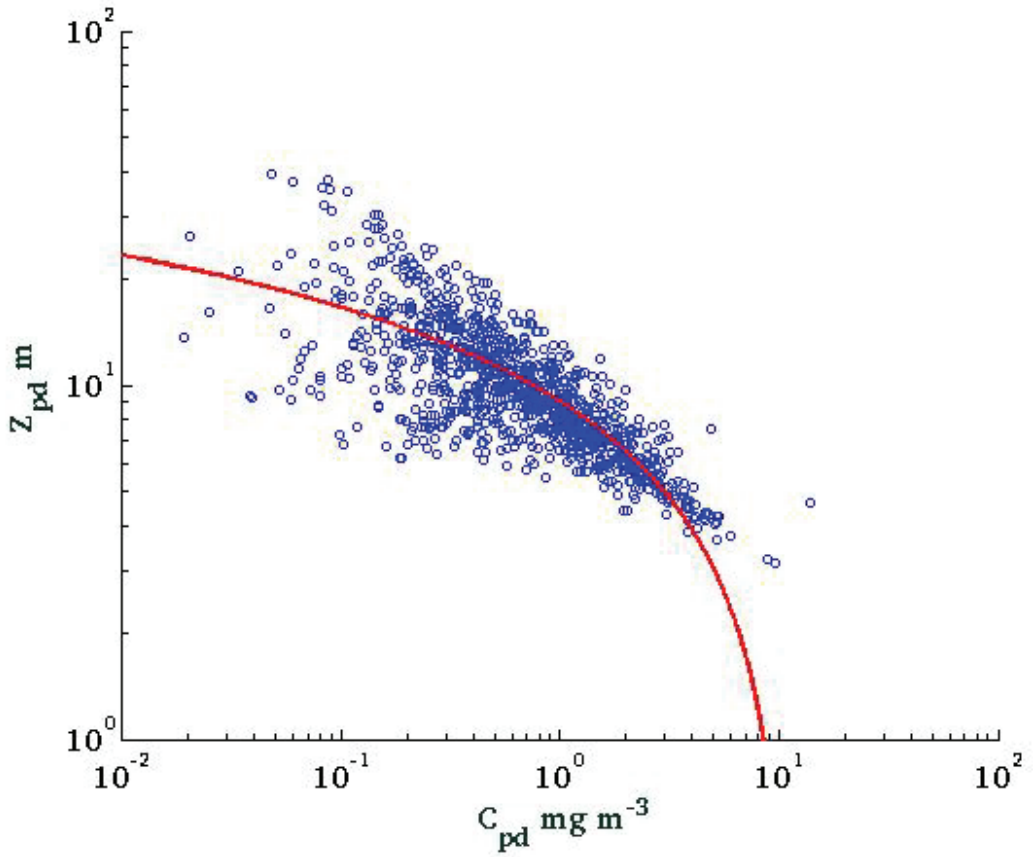

Figure 6.8 Penetration depth, also called first optical depth (Z_{pd}) versus mean CHL within the surface layer (C_{pd}). R=0.71, N=1199, significant correlation (p<0.0001). Red line is the regression line.

6.3.4 Analysis of the seasonal variability

Overall monthly CHL profiles of the Greenland Sea phytoplankton computed regardless of surface concentration categorization (Fig. 6.9, left) show a pattern similar to the median profiles of the C_{pd} > 0.7 mgCHL/m^3 category (Fig. 6.5, plot IV), which contribute to more than 50% of all profiles. Surface CHL values are highest in April, lower in May-June, and the lowest in July-August. July and August are the months with localized and clear SCM. We do not observe here the SCM in the other months as it had a variable depth and was smoothed out when averaging all categories of profiles. The depth, down to which CHL stays close to or higher than the surface value, shallows as the season goes by. As

it was also seen earlier in Figure 6.5, the significant CHL values at depth are usually a continuation of a surface bloom in case of high surface CHL, or are a SCM in case of low surface CHL. For the smaller highly sampled "Hausgarten" region the stepwise decrease of surface CHL from April to September is less clear (Fig 6.9, right). The peak of surface CHL occurs in April as for the whole Greenland Sea, but later in the season, the surface CHL values are alike for all the months. A SCM is seen in May-July. In August too few profiles (less than 20) were available and therefore are not compared with other months. For this small region, even though it is the most sampled region in our data set, the spread between years in the samples of certain months is bigger than in the case of averages for the whole Greenland Sea, making the seasonal patterns observed in the small region less reliable. Hence for the further discussion, we assume the averages for the whole region as the Greenland Sea phytoplankton seasonal cycle.

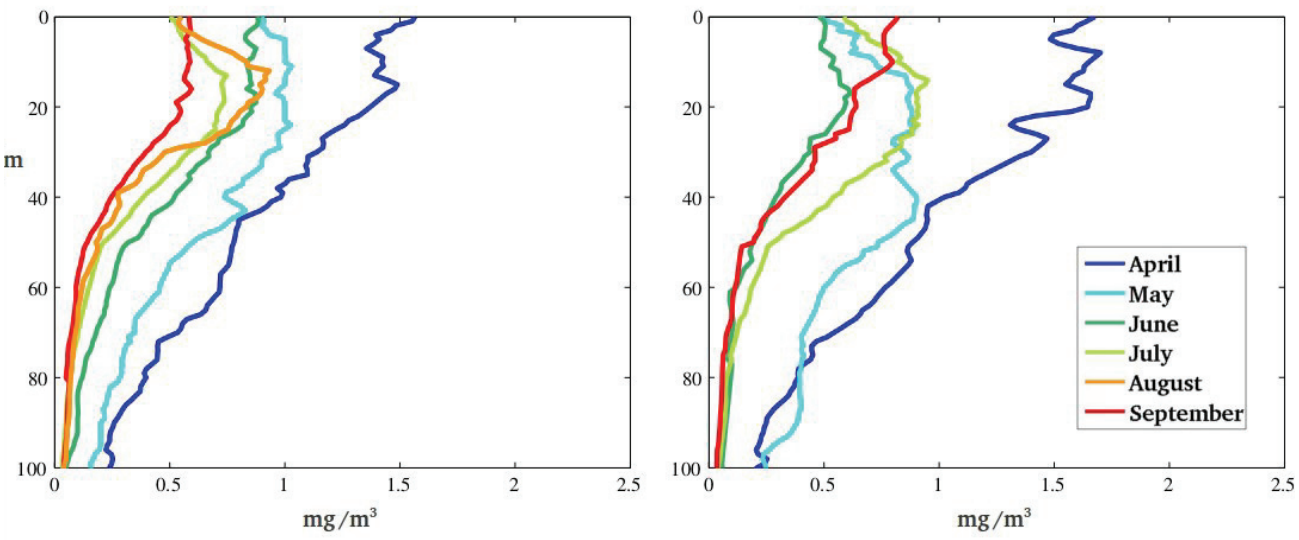

Figure 6.9 Monthly CHL profiles averaged over all the C_{pd} categories. Left: for the Greenland Sea (north of 66°33'39''N, 45°W-20°E). Right: for the smaller highly sampled region at Fram Strait only (77°N-82°N, 5°W-10°E). At Fram Strait in August only too few profiles (less than 20) were available and therefore are not compared with other months. Data of R/V Polarstern and Maria S Merian cruises, and from ARCSS-PP database, 1957-2010.

6.3.5 Error analysis and reference to uncertainties in primary production estimates

The error analysis, performed for the Gaussian curves retrieved here, and alternatively for the uniform profiles and those of Morel and Berthon (1989), revealed the following patterns. Compared to the uniform profiles or profiles calculated by Morel and Berthon (1989), the errors in C_{tot} and PP_{tot} (PP integrated for the water column) are smallest or comparable for most months at all C_{pd} ranges when it is the Gaussian profile that is used (see Table 6.2). Generally Gaussian profiles tend to underestimate the C_{tot} by 0%-7% (with a relative error range from -17% to +6% for C_{tot}, and -9% to +3% for PP_{tot}). Morel & Berthon (1989) profiles, on the contrary, always overestimate the in-situ values by 8%-21% in the case of the averages for all the months. The monthly errors for Morel and Berthon (1989) range from -21% to +48% for C_{tot}, and -11 to +21% for PP_{tot}. This overestimation increases with increasing surface CHL. For Morel & Berthon (1989) profiles, months April-June are usually the months with the lowest errors. Errors for using uniform profiles were relatively large and ranged from -37% to +27% for C_{tot}, and -21% to +13% for PP_{tot}.

Table 6.2 Relative errors in the total PP and CHL content in the water column (PP_{tot} and C_{tot} respectively). PP_{tot} and C_{tot} inferred from in-situ CHL profiles are used as a reference, and are compared to C_{tot} and PP_{tot} inferred using 1) mathematical Gaussian fits of this study; 2) uniform CHL profiles; 3) Morel and Berthon (1989) profiles. C_{tot} and PP_{tot} are integrated until the euphotic depth estimated following Morel (1988). PP is proportional to square root of CHL following Eppley et al. (1985). Overestimations of the in-situ values are in red and underestimations are in blue. Roman numbers indicate the four ranges of C_{pd} (mgCHL/m^3): I) <0.3; II) 0.3-0.45; III) 0.45-0.7; IV) >0.7.

Range	Error (%) in	CHL profile used	April	May	June	July	August	September	Average
I	PP_{tot}	Gaussian	-1	-5	-7	-1	1	-6	-3
		uniform	-12	-21	-1	-9	-11	-9	-10
		M&B 1989	-3	-5	7	10	11	3	4
	C_{tot}	Gaussian	-2	-9	-13	-2	1	-13	-6
		uniform	-22	-37	-3	-16	-21	-17	-19
		M&B 1989	-6	-10	17	20	22	7	8
II	PP_{tot}	Gaussian	-3	3	-1	0	-9	-1	-2
		uniform	-6	-1	-3	-4	-19	9	-4
		M&B 1989	2	8	5	5	-11	18	4
	C_{tot}	Gaussian	-5	6	-2	-1	-17	-2	-3
		uniform	-11	-1	-6	-7	-34	20	-7
		M&B 1989	4	16	10	9	-21	39	10
III	PP_{tot}	Gaussian	2	-1	-3	1	-1	1	0
		uniform	0	-1	0	2	-4	12	1
		M&B 1989	8	7	9	10	3	21	10
	C_{tot}	Gaussian	4	-2	-5	3	-2	1	0
		uniform	0	-3	0	4	-8	24	3
		M&B 1989	17	15	18	20	7	48	21
IV	PP_{tot}	Gaussian	-3	-2	-3	-2	-5	-4	-3
		uniform	-1	-1	0	2	7	13	3
		M&B 1989	2	1	4	5	9	15	6
	C_{tot}	Gaussian	-6	-5	-7	-4	-9	-8	-7
		uniform	-1	-3	1	4	14	27	7
		M&B 1989	4	3	8	11	19	33	13

In the following we discuss C_{tot} and PP_{tot} estimates of the C_{pd} category with the maximum ratio of SCM relative to surface CHL (C_{pd}<0.3 mgCHL/m^3), because these are the cases of C_{tot} being mostly influenced by the shape of the profile. For this range with most pronounced SCM, monthly C_{tot} values from uniform CHL profiles underestimated on average by 19% the C_{tot} values obtained from in-situ CHL profiles. Such underestimation decreased to 6% when the Gaussian fits were used. The use of Morel and Berthon (1989) approximation resulted in an average error of 8%, which is small as well, but one has to keep in mind that this is because the positive (up to 22%) and negative (down to -10%)

monthly errors cancel out each other. As expected, the errors were lower for the rough proxy of PP, which had a monthly average underestimation of 10% when the uniform CHL profile was compared to the in-situ CHL profile. The error was largest in May (-19%) and smallest in June (-1%). Using Gaussian profiles reduced the average error to -3%, with a small range of monthly errors (from -7% till 1%).

Our interpretation of the differences observed is as follows. Uniform profiles are not able to represent the vertical changes of the profile and therefore result in both average underestimations (-19%, lowest C_{pd} range) and overestimations (7%, highest C_{pd} range) of C_{tot}. The Morel and Berthon (1989) maximum covers a larger part of the water column than that of the in-situ profiles, which results in a higher value than the localized maximum of the in-situ profiles, thus the in-situ C_{tot} is overestimated (on average 14%). The derived Gaussian approximations have a lower magnitude of the CHL maximum than the in-situ profiles, and do not reproduce the small scale changes of the in-situ CHL profile, thus typically slightly underestimate C_{tot} (on average 4%).

6.3.6 Summary of the results

In summary, the general patterns of the median profiles are: 1) low surface values are usually an indication of SCM; 2) the relative contribution of SCM to the total CHL in case of low surface concentration can be important, with maximum values exceeding surface CHL by up to a factor of three; 3) for the low surface CHL, total CHL is the highest in cases of pronounced SCM; 4) the relative spread of the data (interquartile range) is highest for the lowest surface concentration; 5) maxima of the profiles gradually moved from greater depths in spring towards the surface in September; 6) median values averaged for the whole water column show a weakening of the bloom from April to September; the CHL maximum values do not show such a trend; 7) when all the surface CHL concentrations are averaged for each month only, surface CHL values decrease from April to September; 8) Gaussians fitted to the median profiles generally reproduce the magnitude and position of the CHL maximum, resulting in 4% average underestimation of C_{tot}; 9) omission of SCM in PP models (i.e., when the uniform CHL profile is used) results in an average of about 10% underestimation for the Greenland Sea PP_{tot} at lowest surface CHL concentrations; use of Gaussian profiles reduces the underestimation to 3%.

6.4 Discussion

In the following, the specifics of Greenland Sea CHL profiles and C_{tot} and their comparison to the global approximation by Morel and Berthon (1989) are further discussed with respect to the specific hydrographic conditions and other studies focusing on phytoplankton dynamics in the Arctic region (sections 6.4.1 and 6.4.2, respectively).

6.4.1 Special features of the Greenland Sea chlorophyll-a profiles

For the surface CHL lower than 1 mgCHL/m^3, total phytoplankton varies much more in the Greenland Sea than for the global case. The prediction of Greenland Sea C_{tot} values corresponding to low C_{pd} is thus more challenging than that of the lower latitudes. Such a big range of the C_{tot} values is attributed to the variable depth and magnitude of the CHL maximum associated with the complex hydrographic conditions.

We observed two different scenarios of phytoplankton distribution in the water column and through the season, depending on whether the CHL of the surface layer is higher or lower than 0.7 mgCHL/m^3. At low surface concentration a SCM was always observed (its magnitude, however, for some profiles is quite small). This case could be typical for regions of sea ice melting in the Greenland Sea characterized by strong stratification and therefore lack of nutrients in the surface layer. We observed indeed that samples of low C_{pd} (<0.3 mgCHL/m^3) are concentrated in the sea ice affected region, the shelf of Greenland, though they appear in other parts of the basin as well. Surface layer concentrations higher than 0.7 mgCHL/m^3 have a maximum CHL in the surface layer, with a gradual decrease of this maximum from April towards September. This category was prevalent in the area south to 74°N, which is the warm Atlantic waters area. When all the database was categorized only by month, the seasonal cycle showed a similar pattern with a gradual decrease of surface CHL from April onwards. The water column layer where high CHL concentrations occur got thinner from month-to-month. Such a decrease of the bloom could be caused by either the phytoplankton using up the nutrients or the grazing pressure getting stronger. We do not observe a bloom limitation by light, keeping in mind that the daylight at

these latitudes is increasing from April to June (while we observed a bloom decrease for these months). As mentioned earlier, the Greenland Sea is an inhomogeneous region in terms of water masses properties. It has parts with cold and fresh waters as well as warmer and salty ones, and the sea ice drift adds to the complexity of the region. As a result, here at the same month in the top layer, both small phytoplankton concentrations and blooms are observed.

Considering the seasonal cycle, both previous satellite (Arrigo et al., 2011) and in-situ (Rey et al., 2000) data analyses show that blooms start with the increase of daylight in spring and peak in May-June, with a rapid decrease afterwards. Compared to that, blooms in our analysis appear earlier, in April. The sampling period of Rey et al. (2000) however, is quite different to that of our database. Rey et al. (2000) sampled in the months May-July only in 1993-1995, while most of data used here were sampled after 1995 and for all months between April and September. Satellite-based work by Arrigo et al. (2011) also showing the May-June peak, dealt with NPP only. This can be quite different from the CHL values, because the higher contribution of light in May as opposed to April affects PP more than CHL. There is yet another point of view on the North Atlantic phytoplankton seasonal cycle. Recent work by Behrenfeld (2010) shows that the bloom initiation occurs in winter when the Mixed Layer Depth is at maximum. This is in line with what we observed in April, being the maximum of the bloom which starts to decrease afterwards. However, note that the majority of our April profiles are concentrated in the Fram Strait area (78°N-80°N), significantly farther north than Behrenfeld (2010) study area (40°N-65°N).

Within our study, the SCM only contributes significantly to C_{tot} within the lowest surface CHL range (<0.3 mgCHL/m^3). The relative spread of the data is greatest for this range, showing a highly variable position and magnitude of SCM, which is most probably caused by differences in the nutrient conditions. This variability, leading to significant relative errors in C_{tot} when the modeled CHL profiles are validated by in-situ CHL profiles (on average -19% to 8% depending on the parametrization method, see section 6.3.5 and Table 6.2), results in small absolute errors as compared to other ranges. Nevertheless, for the areas of the Arctic where the low C_{pd} profiles are prevalent, such errors associated with SCM could have a strong effect on the regional estimates of C_{tot} and PP_{tot}. In accordance with a study by Tremblay et al. (2012) based on in-situ data of the Canadian Arctic, we observed that the SCM is a long-lived (present from April till September) and wide-spread biological structure, which needs to be monitored carefully. In the future, freshening of the Arctic waters caused by the increasing sea ice melt due to climate change, coupled with the atmospheric circulation patterns that favour

advection of the sea ice out of the Arctic Ocean (Liu et al., 2007; Maslanik et al., 2007; Rigor and Wallace, 2004) should lead to stronger water stratification. Thus the cases of low surface CHL with SCM may become even more frequent, because the nutrients will not reach the top layer.

6.4.2 Comparison of the Greenland Sea chlorophyll-a profiles with those of the global ocean

To compare our results to the global relationship by Morel and Berthon (1989), we derived dimensionless profiles from the data. The mean profiles for the selected low ($0.15<C_{pd}<0.3$) and high ($1.5<C_{pd}<5$) ranges introduced by Morel and Berthon (1989) are presented in Figure 6.10. The examples for these two ranges are shown as they clearly present two different trophic situations. The other ranges are variations of the two mentioned above, for the Greenland Sea generally showing two different patterns of the CHL profile for April-June and August-September, and the spread of both, depth and value of CHL maxima, decreasing as the C_{pd} range rises. July is the 'deviating' profile, in some ranges behaving like April-June, and in others like August-September.

One has to keep in mind that dimensionless profiles magnify the shape of the actual profile, giving the largest values to the steepest changes of the profile. (Therefore, the CHL maximum values on Figure 6.10 are not comparable with those of the median profiles on Figures 6.5-6.7). In the low range, the Greenland Sea April-June CHL maxima correspond to the global annual maximum. Later in the season, in July-August, the SCM value almost matches that of the global relationship, but the location is much shallower. In the high range as well, the April-June CHL maxima are like the global maximum, while in the later months both values and the depth of the Greenland Sea CHL maxima are not represented by the global relationship. This is in line with the results of the error analysis (section 3.5). To sum up, although the Morel and Berthon (1989) relationships are global and exclude all the high latitudes (thus did not account for any data of the Greenland Sea) and in addition did not account for the seasonality, they agree well with the Greenland Sea CHL maxima early in the season, whereas the months after June are not correctly represented. Our results show that for the correct parametrization of CHL content in the water column at high latitudes we need both the monthly- and surface CHL-resolved relationship. A remarkable feature of our dimensionless profiles is the intersection at one depth of all the monthly profiles. It is especially visible around depths 0.5 in the high C_{pd} range (Figure 6.10, bottom left), but was observed for all the ranges. As mentioned above the dimensionless profiles

give the attention to the shape of the CHL maxima, but do not reproduce the magnitude of the CHL maxima correctly, which made us decide for the profiles having “natural” dimensions as the output of the current effort.

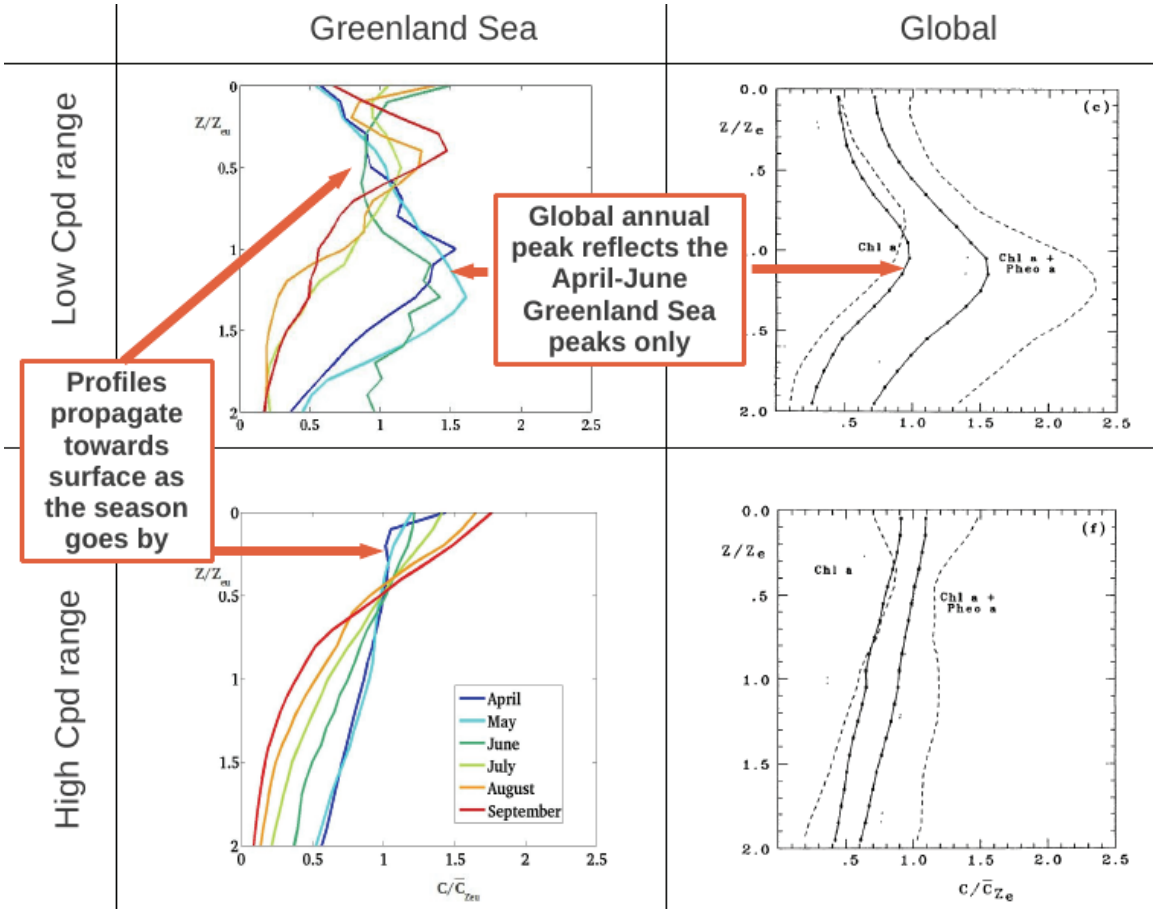

Figure 6.10 Dimensionless CHL profiles categorized according to their CHL within the surface layer (C_{pd}). Two C_{pd} ranges out of seven computed are shown. Vertical axis shows depth divided by the euphotic layer depth (Z_{eu}). Horizontal axis shows CHL divided by the mean CHL for Z_{eu}. Left: Greenland Sea monthly mean profiles computed in this study. Right: from global relationship (Morel and Berthon (1989), we are interested in the solid line marked CHLa (mean CHL profile). Top is low C_{pd} range ($0.15<C_{pd}<0.30$), bottom is high C_{pd} range ($1.5<C_{pd}<5$).

Comiso (2010) found small inter-annual variability of the CHL in the Greenland Sea and Pabi et al. (2008) observed that the Greenland Sector (geographically the same as our area of investigation) had the lowest inter-annual variability of PP of all the Arctic Ocean. Small inter-annual variability implies that the relationship we observed may be used for any year with a minimum risk of year-to-year change.

6.5 Conclusions

In this chapter we derived the relationship between CHL in the surface layer and its vertical profile for the Greenland Sea. Median profiles and the Gaussian fits to the median profiles which reduce the computational effort were obtained. The relationship is resolved in terms of CHL content in the surface layer as well as in terms of seasonal cycle. The mathematical fits of this study are used in Chapter 7 to obtain the CHL profile based on the satellite CHL value (which well coincides with the Cpd value). This CHL profile is in turn used as an input to a PP model for improving the PP estimates in the Greenland Sea.

Chapter 7

Greenland Sea primary production estimated using in-situ and satellite observations

7.1 Motivation

The in-situ measurements of PP are time-consuming, and the most common in-situ method (^{14}C) involves the use of radioactive isotopes (see section 2.6). Therefore, in-situ measurements of PP are conducted very rarely as compared to measurements of phytoplankton biomass. To our knowledge, no measured PP exists in the Greenland Sea for the period over which the current thesis is focused (1998-2012. Period for which satellite ocean color data were continuously available). Therefore a model was used to estimate the PP from the existing in-situ data. For the in-situ PP calculations, the Morel (1991) model was used. For the satellite PP calculations, the Antoine and Morel (1996) model, which is the Morel (1991) model adapted to the input of satellite data, was used.

The choice of the PP model is not a straightforward task as it was shown that no best model exists for all conditions (Saba et al., 2011). However, during the latest Primary Production Algorithm Round Robin (PPARR), which was the test used to compare PP models, the model chosen to be used in this study performed among the best models (in terms of lowest root mean square difference between the in-situ and modeled data) in eight out of ten regions that were studied (Saba et al., 2011). The conclusive recommendation of Saba et al. was that “in deeper waters, Antoine and Morel (1996) model might be an excellent choice” and this encouraged our decision to use this particular PP model.

7.2 Model description

7.2.1 Estimation of in-situ primary production following Morel (1991)

In the classification of PP models, Morel (1991) is a wavelength-resolved-depth-resolved (WRDR)

model. The core of the parameterization of the production-irradiance relationship is the local (depth, z) and instantaneous (time, t) growth rate equation (Bannister, 1974; Kiefer and Mitchell, 1983) written for a monochromatic radiation. Morel (1991) modified this core parameterization in such a way that daily wavelength-intergrated PP for the water column could be computed. The equation accounted for two sequential processes of photosynthesis, namely, for the absorption of radiant energy and then for the transformation of this harvested energy into chemical energy stored in algae biomass. Such a computation was developed to capture the current PP for the period of input data provided, and was not a predictive model for the evolution of phytoplankton. It dealt with the increase in phytoplankton carbon pool, regardless of its degradation and consumption (decay, sinking, grazing). Morel (1991) base equation reads:

$$PP = 12\, a^{*}_{max}\, \varphi_{\mu,max} \int_{0}^{L} \int_{0}^{D} \int_{400}^{700} CHL(z)\, PUR(z,t,\lambda)\, f(x(z,t))\, d\lambda\, dz\, dt \qquad [7.1]$$

During a given day, the PP within the productive column, is, a priori, proportional to the radiant energy available in the visible range of the spectrum (here expressed as PUR, μmol quanta/m^2 s, see details below) and to the phytoplankton biomass in the water column (here expressed using a proxy of biomass, Chl(z), gCHL/m^3). The interaction between radiant energy and phytoplankton biomass was described by the terms f(x), $\varphi_{\mu,max}$ (gCHL/mol usable quanta m^{-2}), and a^{*}_{max} (m^2/gCHL), in such a way that term f(x) parameterizes this interaction (shape of Photosynthesis versus Irradiance curve, see section 2.5.1) with no dimensions, and $\varphi_{\mu,max}$ and a^{*}_{max} assign the actual scales to it. $\varphi_{\mu,max}$ is a physiological parameter describing the transformation of light energy into carbohydrates, while a^{*}_{max} is the optical parameter describing the maximum CHL-specific phytoplankton absorption (more information see below).

The term CHL(z) was directly obtained from the measured CHL profiles, while the other terms required further calculations. PUR(z,t,λ) is the fraction of PAR (z,t,λ) (Photosynthetically Available Radiation) which can be potentially used by the phytoplankton. It was calculated as PAR multiplied by the dimensionless function describing the shape of CHL-specific absorption spectrum, $A^{*}(z,\lambda)$ and integrated over the whole photosynthetic spectral range (400-700 nm):

$$PUR(z,t)=\int_{400}^{700} PUR(z,t,\lambda)A^{*}(z,\lambda)d\lambda \quad [7.2]$$

The shape of $A^{*}(z, \lambda)$ was calculated using Particulate ABsorption in-situ measurements (PABs), which provide the values of CHL-specific absorption spectrum, $a^{*}(z, \lambda)$. a^{*}_{max}, the maximum value of $a^{*}(\lambda)$, generally occuring at λ about 440 nm, was directly estimated from $a^{*}(z, \lambda)$. Having the values of $a^{*}(z, \lambda)$ and a^{*}_{max}, $A^{*}(z, \lambda)$ expressed as:

$$A^{*}(\lambda,z)=a^{*}(\lambda,z)/a^{*}_{\max} \quad [7.3]$$

In the underwater environment, the light field is spatially rearranged by scattering processes and internal reflection. Randomly oriented phytoplankton cells can collect radiations from all possible directions. Therefore, according to Morel (1991), PAR must be definitely defined as scalar (or spherical) irradiance, $\overset{o}{E}$. The measurements of the downwelling radiant energy we have collected were the downwelling irradiance profiles (E_d). It was, therefore, necessary to transform the E_d values into $\overset{o}{E}$ values in order to properly estimate the available radiation at all levels within the productive column and to compute the energy actually absorbed by phytoplankton.

This was achieved by introducing a geometrical correction term g, equal to the ratio of $\overset{o}{E}$ to E_d:

$$g(z,\lambda)=\overset{o}{E}(z,\lambda)/E_d(z,\lambda) \quad [7.4.1]$$

Morel (1991) showed that g can be approximated by calculating the ratio of diffuse attenuation coefficient to a*:

$$g(z,\lambda)=K_d(z,\lambda)/a^{*}(z,\lambda) \quad [7.4.2]$$

, where K_d is the diffuse attenuation coefficient, the parameter that controls the propagation of light through water. K_d was defined as the reciprocal of E_d, with the depth interval dependent on the thickness of the medium (Mobley, 1994).

Though we have calculated K_d/a^* from our own measurements, the results of Morel (1991) appeared to be more plausible and were used. The Kd/a* values used are shown in Figure 7.1. Refer to the end of the next section for the description of how the Morel (1991) method was used for obtaining Kd/a* data.

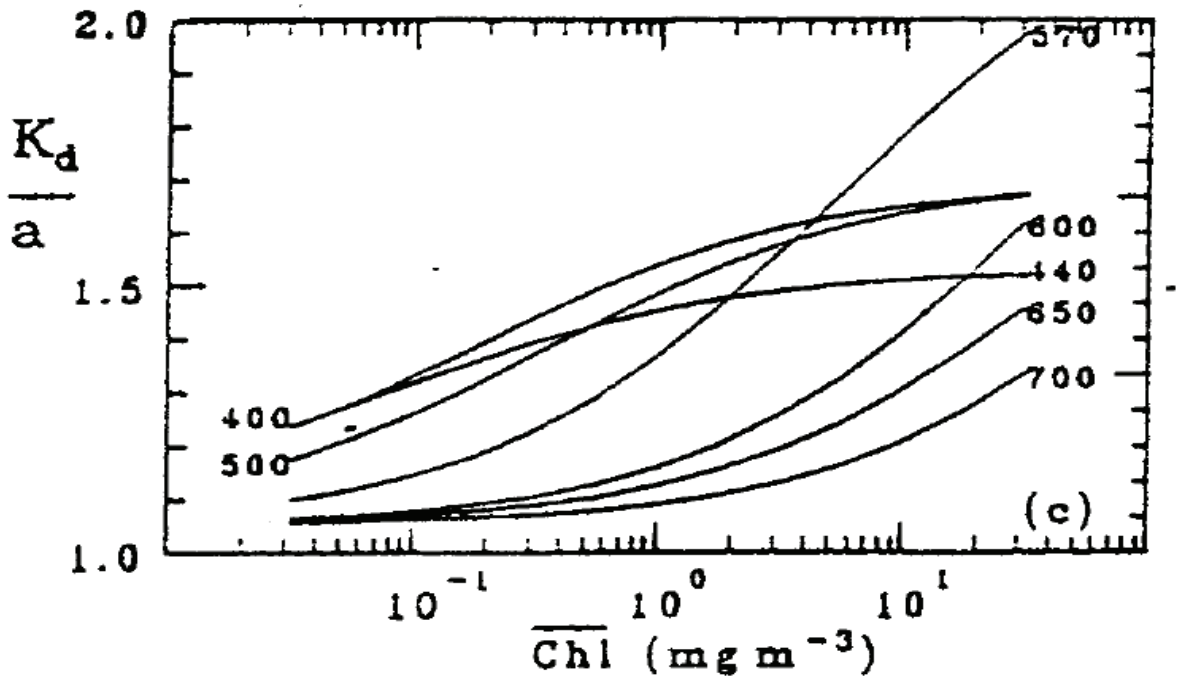

Figure 7.1 Variations of the ratio Kd/a for selected wavelength (nm) as a function of CHL concentration. Figure 4c in Morel (1991)

After the geometrical correction term was calculated, E_d was converted into scalar irradiance as

$$PAR(z,t,\lambda) = E_d(z,t,\lambda)\, g(z,\lambda) \quad [7.5]$$

Please keep in mind that as opposed to the theoretical model of Morel (1991), the dependency of g on the time was neglected, since we did not have a continuous hourly time series of data at a certain point.

Once PUR(z,t) was obtained from equation [7.2], the time evolution of PUR(z,t) on the current date

was accounted using the factor computed based on the Global Radiation (GR) measurements of the ship meteorological station. GR_{point} corresponded to the time when an E_d measurement was taken. $GR_{day}(t)$ were the GR measured during the current date.

$$PUR(z) = \int_0^L PUR(z) GR_{day}(t) / GR_{point}\, dt \qquad [7.6]$$

In the parameter f(x(z,t)), the shape of the photosynthesis versus irradiance curve, Platt et al. (1980) type of the curve with the ß constant for light inhibition at high irradiance equal to 0.01 was adopted, allowing f(x) to be calculated through:

$$f(x) = x^{-1}\left(1 - e^{-x}\right) e^{-\beta x} \qquad [7.7]$$

, where x(z,t) is a dimensionless descriptor of usable irradiance, defined as

$$x(z,t) = PUR(z,t)\, GR_{day}(t) / GR_{point}\, KPUR(z) \qquad [7.8]$$

KPUR is the normalizing value of PUR, and is the saturation onset parameter defined by Talling (1957), provided that PP is considered to be the function of PUR and not (as usual) as a function of PAR. KPUR is one of the two equation terms which accounts for the temperature effect upon phytoplankton growth, dependent on the temperature with a Q_{10} (increase in growth rate per $10^{O}C$) equal to 1.88 as suggested by Eppley (1972):

$$KPUR(T) = KPUR(20°)\, 1.065^{(T-20°)} \qquad [7.9]$$

The equation below provided the maximum value of the photosynthesis versus irradiance curve, $P^{B}_{max}(z)$, once the initial slope of the curve was fixed (through the product $a^{*}_{max}(z)\ \varphi_{\mu,max}(z)$), the saturation onset parameter was fixed (through KPUR(z)), as well as was the shape of the curve (the f(x) function). The factor 12 (gC/molC) of conversion to mol was introduced since $\varphi_{\mu,max}(z)$ was expressed as mol C per mol of (absorbed) quanta. The $[xf(x)]_{max}$ was constant for the equation [7.7], equal to 0.945.

$$P^{B}_{max} = 12\, a^{*}_{max}\, \varphi_{\mu,max}\, [x f(x)]_{max}\, KPUR \qquad [7.10]$$

At the same time, following Eppley (1972), P^{B}_{max} equaled

$$P^{B}_{max}(T,z) = P^{B}_{max}(20°)\, 1.065^{(T(z)-20°)} \qquad [7.11]$$

P^{b}_{max} (at 20^{O}C) equals 4.6 gC(gChl)$^{-1}$ h^{-1} as computed from equation [7.10] using standard values of KPUR (at 20^{O}C) of 80 µmol quanta m^{-2} s^{-1}, $a^{*}_{max}(z)$ $\varphi_{\mu,max}(z)$=16 gC (gChl)$^{-1}$ (mol usable quanta m^{-2})$^{-1}$ (Antoine and Morel, 1996). The last missing parameter in equation [7.1], $\varphi_{\mu,max}(z)$, is the maximum yield for net growth, which expresses the efficiency in the transformation of the captured energy added to, and ultimately retained within the initial carbon pool, was obtained by transforming equation [7.10]:

$$\varphi_{\mu,max} = P^{B}_{max} / 12\, a_{max} [xf(x)]_{max}\, KPUR \qquad [7.12]$$

Once all the input parameters for equation [7.1] were derived, PP was computed. The depth integrals of PP and CHL were computed for an "extended" productive layer D which corresponds to 0.1% of PAR at the sea surface, because the somewhat arbitrary definition of Z_{eu} (1% of PAR at the surface) led us to presume that carbon fixation does not necessarily cease below this level (Morel, 1991). Increments for all the integrations were: Δλ=10 nm, Δt=1/30 Daylength, Δz=1/75D.

7.2.2 Estimation of satellite primary production following Antoine and Morel (1996)

The base difference in calculation of PP using satellite data from the calculation of PP using in-situ data were that the remote sensing data has more limitations in terms of the depth until which data are obtained, and the types of input data available.

Firstly, the remotely sensed information originates only from the surface layer of the ocean (which is, for CHL data rarely greater than 25 m in extremely clear waters (Antoine, 2006). The photosynthesis occurs until much deeper sunlit portions of the water column (which can reach up to 150-200 m

(Antoine, 2006)). Secondly, some of the in-situ data types, such as the CHL-specific absorption spectrum, E_d spectrum and daily PAR evolution cannot obtained from space (at least in the high-latitude region of our study). They, thus, have to be either assumed constant or modeled. In the following, the models of the vertical profiles are described first, and then the parameters to be modeled when using satellite data are presented.

Originally, Antoine and Morel (1996) model determined CHL profile to be well-mixed or stratified according to the ratio of MLD and Z_{eu}, and if stratified, assigned a profile as in Morel and Berthon (1989). Here, the mathematical equations of CHL profiles derived specifically for the Greenland Sea, which proved to reproduce the Greenland Sea total CHL in the water column better than Morel and Berthon (1989) profiles (Chapter 6), were used. The separation of waters into well-mixed and stratified waters was not made as the stratification regime of Greenland Sea is very different from that of global waters.

PAR was propagated through the water column following the bio-optical model proposed by Morel (1988) for case 1 waters, where nothing besides phytoplankton influences the ocean properties. According to this model, downwelling irradiance was computed from the surface as:

$$E_d(\lambda, z_n + dz, t_0) = E_d(\lambda, z_n, t_0)\, e^{-K_n(\lambda) dz} \qquad [7.13]$$

, where the first z_n value is zero. The spectral attenuation coefficient for downwelling irradiance, $K_n(\lambda)$, which depends on the CHL concentration $(CHL)_n$ within the layer extending from z_n to z_n+dz, was obtained from:

$$K_n(\lambda) = K_w(\lambda) + \chi(\lambda)(CHL)_n^{e(\lambda)} \qquad [7.14]$$

$K_w(\lambda)$ stands for the influence of pure water; the factors $\chi(\lambda)$ and the exponents $e(\lambda)$ were obtained through regression analysis (Morel, 1988: the tabulated values of $K_w(\lambda)$, $\chi(\lambda)$ and $e(\lambda)$ are given in this reference). At each level, the wavelength-integrated irradiance was compared to the existing value just above the surface. Depth of the productive layer D was determined and the computations were stopped resulting in the E_d profile used, once the downwelling irradiance fell to 1/1000 of the initial value.

As for the vertical temperature profiles, they were assumed to be uniform as originally thought of in Antoine and Morel (1996). Please note that the temperature-dependent variables KPUR and P^B_{max} have

therefore uniform vertical profiles as well.

The parameters that could not be obtained from satellite data, i.e. the normalized CHL-specific absorption spectrum $A^*(\lambda)$ (Figure 7.2) and the maximum of CHL-specific absorption spectrum a^*_{max} were adopted from Morel (1991). The a^*_{max} value used is 0.033 $m^2(mgCHLa)^{-1}$ and occurs at λ=435 nm. It was obtained from an average CHL-specific absorption spectrum computed from measurements of 14 phytoplankton species, grown in culture, and cyanobacteria were disregarded (Morel, 1991).

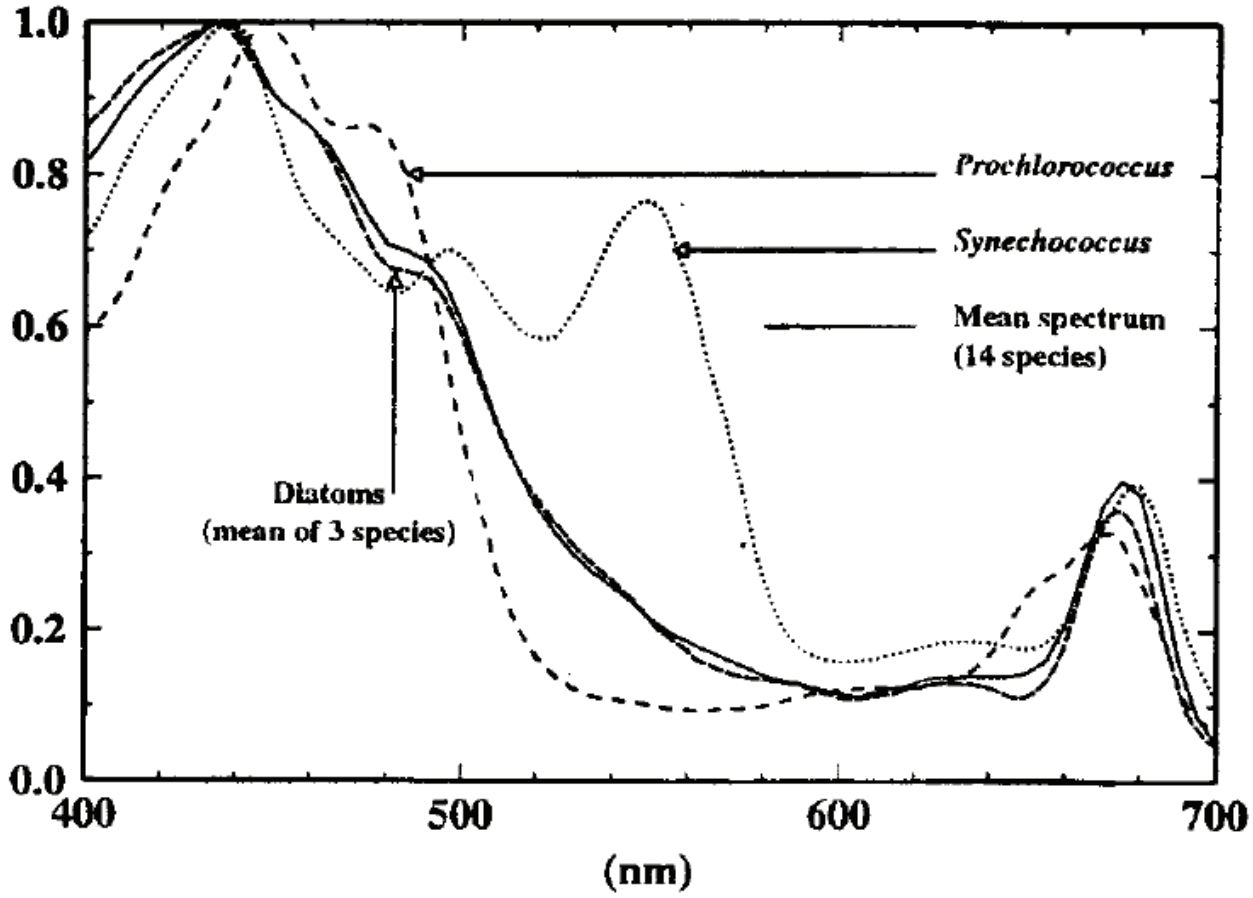

Figure 7.2 The dimensionless function $A^*(\lambda)$, describing the shape of algal absorption spectra of various photosynthesizing species or groups (Figure 3 in Antoine and Morel, 1996)

The maximum value of the quantum yield for growth, $\varphi_{\mu,max}$, instead of being estimated through other parameters, as it was in the in-situ version (equation [7.12]), was taken equal to 0.06 molC (mol

quanta absorbed)$^{-1}$ according to converging analyses (Bannister and Weidemann, 1984; Berman and Schanz, 1984; Dubinsky, Welshmeyer and Lorenzen, 1981).

The spectral distribution of PAR was computed using the diffuse and direct components of irradiance from "5S model" (Tantre et al., 1979) together with standard atmospheric conditions of the clear atmosphere (barometric pressure 1013 hPa, total ozone content 350 DU, precipitable water 2 cm, maritime aerosol 23 km visibility). To account for the temporal evolution of PAR, for each particular day the declination of the sun was computed (Spencer, 1971) and then combined with the latitude of the selected location in order to obtain the daylength and the solar elevation as a function of time.

The geometrical correction (equation [7.5]) was performed as described in Morel (1991). Morel (1991) took the relationship that links radiance and irradiance from Preisendorfer (1976):

$$a\overset{o}{E} = K_d E_d [1 - R(K_u / K_d)] \qquad [7.15]$$

, where K_d and K_u are the attenuation coefficients for the downwelling and the upwelling irradiances, respectively, and R is the reflectance, defined as E_u/E_d, the ratio of upwelling to downwelling irradiance. In general, K_u does not widely differ from K_d, .Moreover, R is only of the order of a few percent. Therefore:

$$a\overset{o}{E} \approx K_d E_d \qquad [7.16]$$

or

$$\overset{o}{E} / E_d \approx K_d / a \qquad [7.17]$$

In essence, K_d/a is a non-explicit function of the radiance distribution above the surface, of the depth and of the inherent optical properties of the medium, namely its absorption and scattering coefficients, a and b, and its volume scattering function. Kirk (1984) showed that the average value of K_d throughout the euphotic zone can be expressed as

$$K_d = a\mu_0^{-1}\left[1 + \left(0.425\,\mu_0 - 0.19\right) b/a\right]^{1/2} \qquad [7.18]$$

, where μ_o is the average cosine for downwelling radiation just below the surface which is computed along with the PAR spectral distribution using the "5S model" by Tantre et al. (1979). To obtain the K_d value, b(λ) was modeled as a function of CHL according to Gordon and Morel (1983):

$$b(\lambda)=b_w(\lambda)+(550/\lambda)0.3(CHL)^{0.62} \quad [7.19]$$

a(λ) was modeled according to Prieur and Sathyendranath (1981)

$$a(\lambda)=\left[a_w(\lambda)+0.06\,A_{CHL}(\lambda)(CHL)^{0.65}\right]\left[1+0.2y(\lambda)\right] \quad [7.20]$$

with y(λ) adopted from Bricaud, Morel and Prieur (1981)

$$y(\lambda)=\exp\left[-0.014(\lambda-440)\right] \quad [7.21]$$

For the discussion on variations of the K_d/a ratio and the K_d modeling refer to Morel (1991).

7.3 Input data description

7.3.1 In-situ measurements

The in situ measurements were performed during the ARK-25 RV "Polarstern" cruises (leg 1 and 2) in June-July 2010. The data used here covers twenty sampling stations, where simultaneous measurements of irradiance, radiance and sea temperature were made and samples for absorption and CHL analysis were taken. Below, the sampling and processing method of each data type is described in detail.

7.3.1.1 Irradiance and radiance measurements

Underwater optical light fields were measured using two types of RAMSES hyperspectral

radiometers (TriOS GmbH, Germany), which measured the profiles of radiance and irradiance in a wavelength range from 350 nm to 950 nm with a spectral resolution of approximately 3.3 nm and a spectral accuracy of 0.3 nm. Irradiance data were already described and used in Chapter 6. The radiance sensor had a field of view of 7º. All of the measurements were obtained with an automated integration time of the respective sensor between 4 ms and 8 s. A reference irradiance device was placed above the water surface to monitor the downwelling incident sunlight and allowed the normalization of the in-water measurements according to Stramski et al. (2008). For the selected stations of the irradiance, integrated for the wavelength range from 400 to 700 nm (PAR), see section 6.2.3.

7.3.1.2 Water sampling for absorption and chlorophyll-a measurements

Water sampling was conducted with Niskin bottles attached to a CTD sensor (SBE 9 plus, Sea-Bird Electronics Inc, Washington D.C., USA) mounted on a stainless frame. Samples for the absorption of particulates were taken from four to six sampling depths, and for the CHL from six to ten sampling depths. The sampling depths were chosen according to the fluorescence profile provided by a CTD sensor to obtain a better resolution at the depth of the CHL maximum. From 0.25 to 3 L of seawater were filtered onto Whatman GF/F filters of 25 mm for CHL and of 48 mm for absorption of particulates, with a pressure of less than 120 mbar. After the filtration, the filters were folded, immediately frozen in liquid nitrogen and stored at −80ºC. The collected samples were all analyzed in the laboratory within 8 months.

The samples for CHL were taken for the further analysis using two methods: fluorometric and High Performance Liquid Chromatography (HPLC). On some stations, the samples for the two analyses were taken simultaneously and on the other stations the samples for only one analysis were taken. As for PP validation we needed the maximum number of stations where the absorption, irradiance and CHL were measured (or sampled) simultaneously, and hence, we considered both the stations with only HPLC CHL sampling and the stations with only fluorometric CHL sampling for the further analysis. The fluorometric CHL values were then converted into HPLC CHL values by multiplying the fluorometric CHL by 1.0245 (average value for the data of the cruise, personal communication I.Peeken). Below we describe the procedures of sample processing on land in the laboratory of the AWI.

7.3.1.3 Absorption measurements

Measurements of the particulate absorption were carried out according to Taylor et al. (2011) on a dual-beam UV/VIS spectrophotometer (Cary 4000, Varian Inc.) equipped with a 150 mm integrating sphere (external DRA-900, Varian, Inc. and Labsphere Inc., made from Spectralon (TM)) using a quantitative filterpad technique modified as follows (see e.g. Simis et al., 2005). The filters were placed in the center of the integrating sphere using a center-mount filter holder perpendicular to the light beam.

A wavelength scan from 300 to 850 nm with a resolution of 1 nm (slit width 2 nm, scan rate 150 nm min^{-1}) was performed, when the reflectance ports were covered with Spectralon (TM) reflectance standards. The baseline was recorded beforehand with a clean, dry filter, and a filter which was soaked for more than 30 min in purified water served as a reference. The absorption coefficient was calculated from optical density (OD) measurements using a path length amplification factor of 4.5 (β=1/4.5, Röttgers, personal communication) as a [m^{-1}]=-ln($T \cdot A \cdot \beta / V$), where the transmittance T=exp(-OD), V is the filtrated sample volume in m^3 and A the filter clearance area in m^2. Results from the original filter gave total particulate absorption, a_p. To determine the absorption by non-algal particles (a_{NAP}), the algal pigments were bleached with NaOCl as described in Tassan and Ferrari (1995) and Ferrari and Tassan (1999). The bleached filters were measured as described above. To obtain the parameter of interest, particulate absorption of phytoplankton ($a_{ph}(\lambda)$) which was used to model PP in the current study, a_{NAP} was subtracted from a_p. The above description is from Taylor et al. (2011).

7.3.1.4 High Performance Liquid Chromatography measurements of chlorophyll-a

The HPLC CHL data of this cruise have already been published in Tran et al. (2013). In detail, the samples were measured using a Waters HPLC system (Waters Corporation, Milford MA, USA) equipped with an autosampler (model 717 plus autosampler), an HPLC pump (model 600 HPLC LCD pump), a photodiode array detector (model PDA 2996), a fluorescence detector (model 2475 fluorescence detector) and the Empower software. For analytical preparation, 50 µL of an internal

standard (canthaxanthin) and 2 mL of acetone were added to each filter sample and homogenized for 20 s. After centrifugation, the supernatant liquid was filtered through a 0.2 µm filter and placed in Eppendorf cups from which aliquots (100 µL) were transferred in the autosampler vials (4ºC). Just prior to analysis, the sample was premixed with a 1 M ammonium acetate solution in a 1 : 1 (v/v) ratio in the autosampler and injected onto the HPLC system. The pigments were analyzed using reverse-phase HPLC with a VARIAN Microsorb MV3 C8 column (4.6 × 100 mm) and HPLC-grade solvents (Merck KGaA, Darmstadt, Germany). Solvent A consisted of 70 % methanol and 30 % 1 M ammonium acetate, and solvent B contained 100 % methanol. The gradient was modified following Barlow et al. (1997). The eluting pigments were detected by absorbance (440 nm) and fluorescence (Ex: 410 nm, Em: > 600 nm). The pigments were identified by comparing their retention times with those of pure standards and algal extracts. Additional confirmation for each pigment was completed using on-line diode array absorbance spectra from 390–750 nm. The pigment concentrations were quantified based on the peak areas of external standards, which were spectrophotometrically calibrated using extinction coefficients published by Bidigare (1991) and Jeffrey and Vesk (1997). For correction of experimental losses and volume changes, the concentrations of the pigments were normalized to the internal standard canthaxanthin. The taxonomic structure of the phytoplankton communities was derived from photosynthetic pigment ratios using the CHEMTAX® program (Mackey et al., 1996). The above description is from Tran et al. (2013).

7.3.1.5 Fluorometric measurements of chlorophyll-a

The fluorometric measurements of CHL were processed using the same method as those used in Chapters 4 and 6.

7.3.1.6 Temperature profiles and meteorological data

Temperature profiles were determined using a temperature sensor of Seabird 911 Plus CTD. Standard meteorological information (global radiation) was obtained from the ship’s weather station equipped with a pyranometer measuring solar irradiance (http://www.awi.de/de/infrastruktur/schiffe/polarstern/bordwetterwarte/continuousmeasurements/sensor

information/). For PP computations, we used the ratio of a value of global radiation at the current station to the values of global radiation for the current day (24 hours).

7.3.1.7 Preprocessing of the in-situ data

Most of the sampled profiles of all the data types, except temperature, did not reach either the surface or the depth of the productive layer (interval in which the PP calculations are to be made), and thus needed extrapolation. The first step was to extrapolate the PAR profile (see equation [7.5] above) until the 0.001 of the surface PAR value and obtain the depth of the productive layer. PAR profiles were first binned into 1 m depth resolution increments. Then the last two measurements which showed the change in values were linearly extrapolated until the depth of the productive layer was reached. After the depth of the productive layer was estimated, CHL and absorption profiles were linearly extrapolated to it and to the surface. In case negative values appeared as the result of extrapolation, they were substituted to zero. As all of the data except irradiance/radiance profiles were acquired for the discrete depths, they were linearly interpolated between the sampling depths.

The conversion of the irradiance profiles from W/m^2 to μmol quanta/m^2 s (the input units of the model) was performed wavelength-dependent following Mobley (1994). Examples of the PAR, CHL and absorption profiles along with their extrapolation and interpolation are given in Figure 7.3.

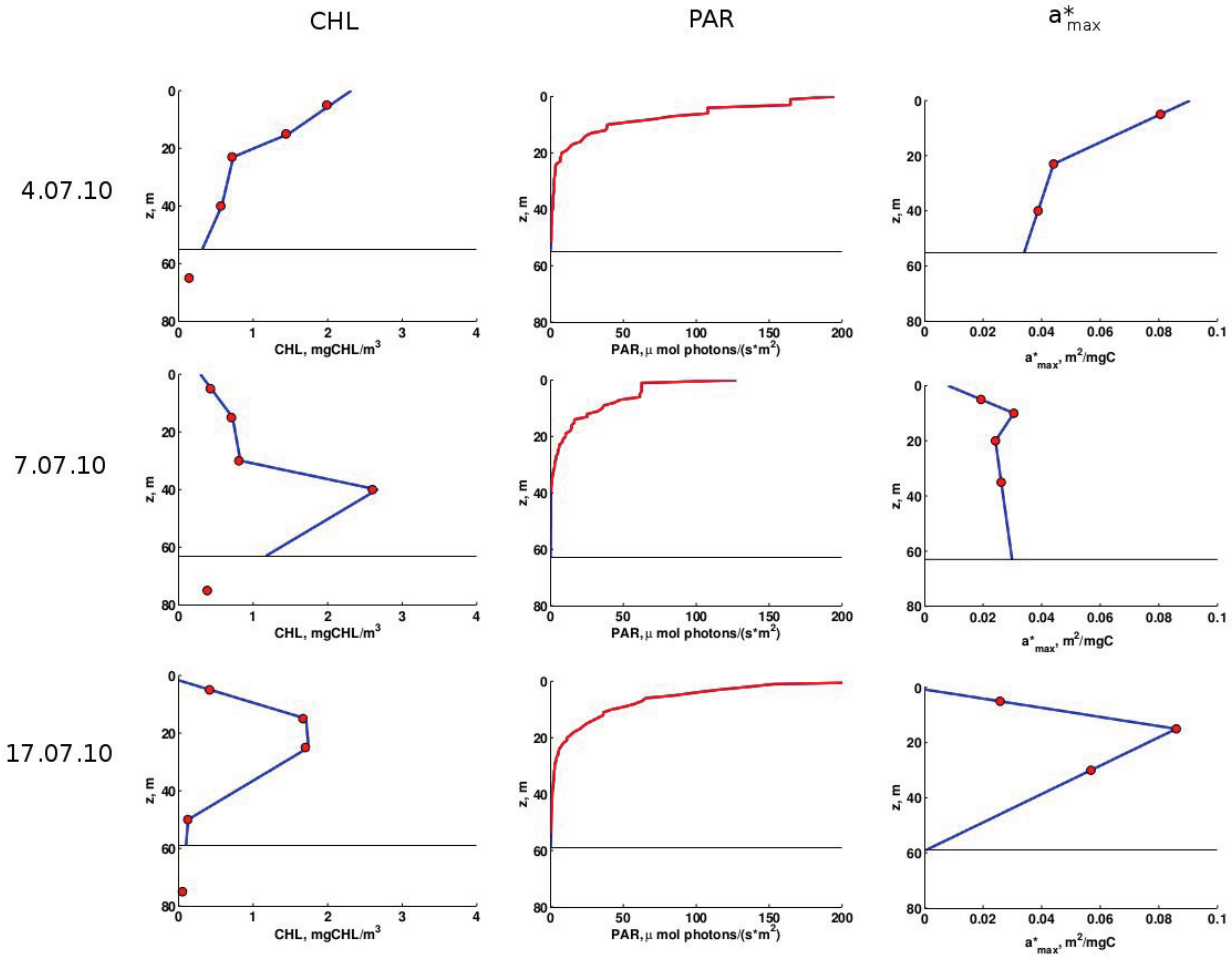

Figure 7.3. CHL, PAR and a^*_{max} measurements collected on 4, 7 and 17 July 2010 during RV 'Polarstern' ARK-25 cruise (in red) and corresponding interpolated/extrapolated profiles (in blue, section 7.3.1.7). Dates of sampling is indicated on the left side. Locations of the measurements: 4 July (78°8337 N, 5°9828 E), 7 July (79°0287 N, 11°0853 E), 17 July (78°834 N, 0°3935 E). PAR measurements are converted into scalar irradiance (Eq. [7.5]).

7.3.2 Satellite measurements: description and processing

The PP data calculated using Antoine and Morel (1996) with Cherkasheva et al. (2013a) CHL profile parametrization were provided by Bernard Gentili and David Antoine from the Laboratoire d'Océanographie de Villefranche/Mer. In addition to that, for the validation process of PP data, we

computed the output of Behrenfeld and Falkowski (1997a) Vertically Generalized Primary production Model (VGPM), for the points where in-situ data was available.

The input data used are monthly GlobColour CHL with 4.6 km spatial resolution, SeaWiFS PAR and MODIS Sea Surface Temperature with 1/12° spatial resolution. For comparison with the in-situ data, the computed satellite PP values were averaged within a 3x3 pixel box. See further section 7.6.1 for the results of the comparison.

7.4 Statistics assessing model performance

The parameter computed first was bias which is commonly used to assess the quality of any model performance:

$$BIAS = \overline{NPP_m} - \overline{NPP_d} \quad [7.21]$$

, where $NPP_m(i)$ is modeled PP and $NPP_d(i)$ represents PP modeled from in-situ data for each sample *i*.

Additionally, the log normalized bias and log normalized RMSD, parameters used to asses specifically the quality of PP models in Primary Production Round Robin Activities (Carr et al., 2006; Friedrichs et al., 2009; Saba et al., 2011), were computed as in Saba et al. (2011):

$$BIAS_{log} = \left(\overline{\log\left(NPP_m\right)} - \overline{\log\left(NPP_d\right)}\right)/\sigma_d \quad [7.22]$$

, where σ_d is the normalized standard deviation of in-situ data.

$$RMSD_{log} = \sqrt{\frac{1}{N}\sum_{i=1}^{N}\left(\log\left(NPP_m(i)\right) - \log\left(NPP_d(i)\right)\right)^2} \quad [7.23]$$

The predictive skill of a given model is inversely related to the RMSD statistics (lower RMSD=higher skill).

Coefficient of variation, which is commonly used instead of standard deviation to compare the data

with widely different means, was computed to assess the performance of the model.

$$CV = \frac{\sqrt{\frac{1}{N}\sum_{i=1}^{N}\left(NPP_m(i) - NPP_d(i)\right)^2}}{\overline{NPP_d}} \quad [7.24]$$

7.5 Integrated basin estimates and temporal trends

Total PP (gC month^{-1}) for the region was calculated for each month as the product of the average daily integrated production, the number of days in the month, and the Greenland Sea open water area adopted from the same region as in Pabi et al. (2008), $1.634*10^6$ km^2. Annual PP was then calculated by summing up all months. The PP value for September (required for comparison purposes) was assigned to the value of average monthly PP.

The analysis of PP temporal variability was designed in such a way that it is comparable with the results of CHL temporal variability obtained in previous chapters. We have studied the temporal trends: 1) at the ten sites in the ice-free Fram Strait as in Chapter 4; 2) in the western and eastern Fram Strait as in Chapter 5, and 3) at the whole Greenland Sea sector of the Arctic as in Chapter 6. There are, however, also differences in the approaches. First, we have focused on the analysis of trends using the anomalies of the data only. The spatial patterns of the trends obtained using the original time series or the time series smoothed with a moving average of five months were similar to those that resulted from anomaly data and are not shown. Second, the time intervals for which the trends were calculated differ in all three chapters. Chapter 4 studies the time interval of 1998-2009, since the analysis was restricted to the time when NAOSIM model data was available. In Chapter 5 the time interval is 1998-2012. The current chapter studies the temporal trends for 1998-2010 (till the time when PAR data was provided by SeaWiFS sensor). The final difference is that the CHL time series of Chapters 4 and 5 are complete, while in the PP time series of the current chapter, June 2007, July 2008, and May 2009 are missing because of the lack of SeaWiFS PAR data.

7.6 Results and discussion

7.6.1 Validation of PP modeled from satellite data by PP modeled from in-situ data

The validation of the of the input parameters along with the comparison between the validation statistics for the PP calculated using the Antoine and Morel (1996) model with the Cherkasheva et al. (2013a) parametrization (further on referred to as 'A&M 1996 & Che 2013'), Antoine and Morel (1996) (further on referred to as 'A&M 1996 standard'), and Behrenfeld and Falkowski (1997a) (further on referred to as 'B&F 1997') is described below.

We first studied the spatial distribution of the PP data and the input parameters. Figures 7.4 and 7.5 show the PP maps of A&M 1996 & Che 2013 (upper left), and the input data for June 2010 and July 2010, respectively. The in-situ data points are situated in the eastern Fram Strait in July and to the south-west in the open part of the Greenland Sea in June. Satellite CHL data show that the maximum of the phytoplankton bloom happens in June, and in July the decrease of the bloom starts (top right of Figures 7.4, 7.5, and Figures 4.3, 4.4a). Different oceanographic and biologic conditions are therefore considered in our limited validation dataset (N=20).

Table 7.1 Validation statistics for the satellite data used as an input for PP model. Validation data were collected in the Greenland Sea during June-July 2010 R/V 'Polarstern' ARK25-1/-2 cruises. Data are for 20 points used in the PP model

	CHL	PAR	SST
BIAS_abs	0.08	2.7	-1.49
BIAS_log	0	0.04	-0.98
RMSD_log	0.72	0.54	0.97
CV(RMSD)	0.67	0.51	0.55

Out of the three input data fields of the satellite PP model, CHL corresponds best to the in-situ data, PAR is quite well-matched as well and SST has the worst agreement (Figures 7.4 and 7.5, Table 7.1). The SST though has a rather minor effect on the output PP values as it is very slightly affecting the saturation parameters, P^B_{max} and KPUR (equations [7.9, 7.11]). Errors in SST thus will result in minor errors in PP. The CHL and PAR are on the other hand the input profiles, which are the base of the PP calculations, thus the errors in these parameters will have a critical effect on PP values.

When looking at PP data only (Figure 7.6), one can see that about half of the points are well-matched. Mind that PAR is a temporarily more varying parameter than CHL and SST, and the comparison is made between the monthly satellite data with daily values.

The statistical analysis shows that overall the CHL and PAR data are nearly not biased. The differences at single data points are, however, large as reflected in RMSD values (Table 7.1). Thus we may expect that for our dataset, the highest errors will be associated to the discrepancy between satellite and in-situ PAR data as well as CHL data. In some cases though the errors in PAR and CHL cancel each other out (see for example June 2010, points around 75°N, 3°W-0°).

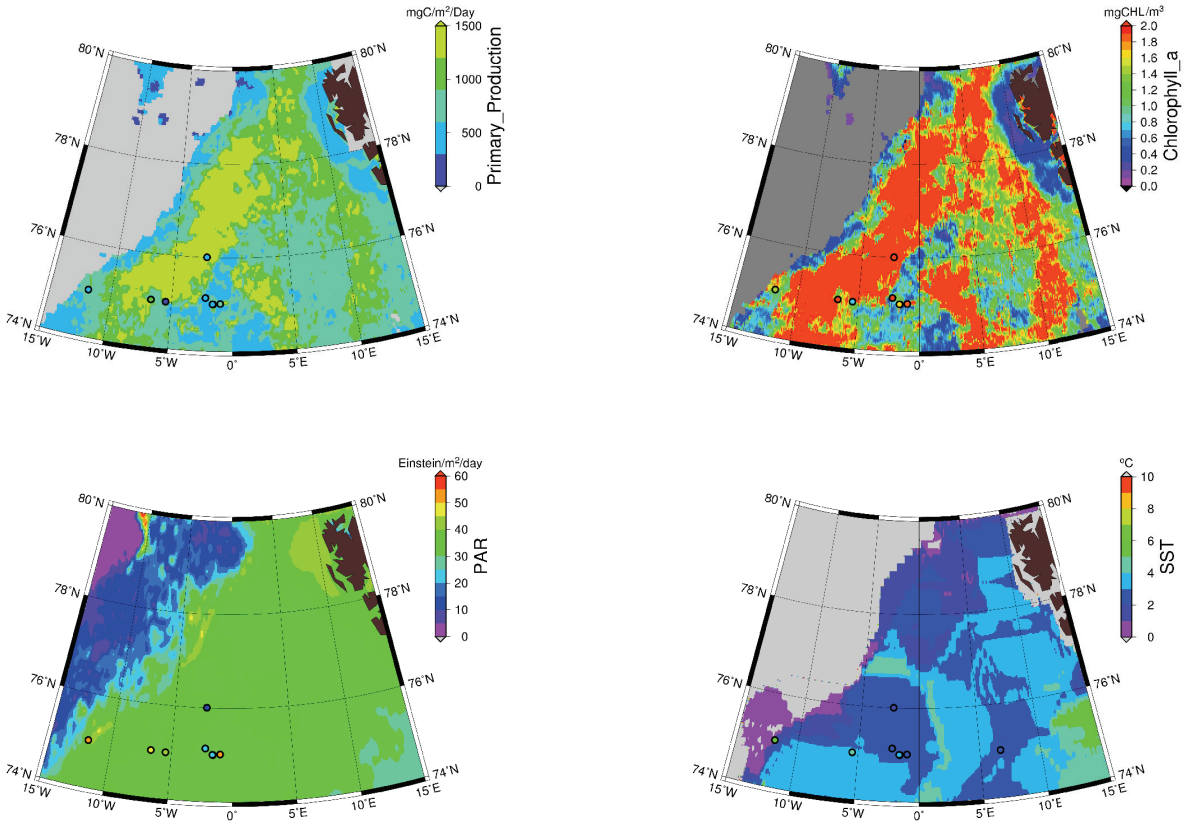

Figure 7.4 Satellite PP in June 2010 modeled following A&M 1996 & Che 2013 and the input satellite data. Top left: satellite PP, logarithmic scale; top right: GlobColour CHL; bottom left: SeaWiFS PAR; bottom right: MODIS SST. In-situ data used for validation were collected in the Greenland Sea during June-July 2010 R/V 'Polarstern' ARK25-1/-2 cruises and are overlayed as colored circles. The color of the circle corresponds to the in-situ value of the parameter at the current location. In-situ PP is modeled following Morel (1991).

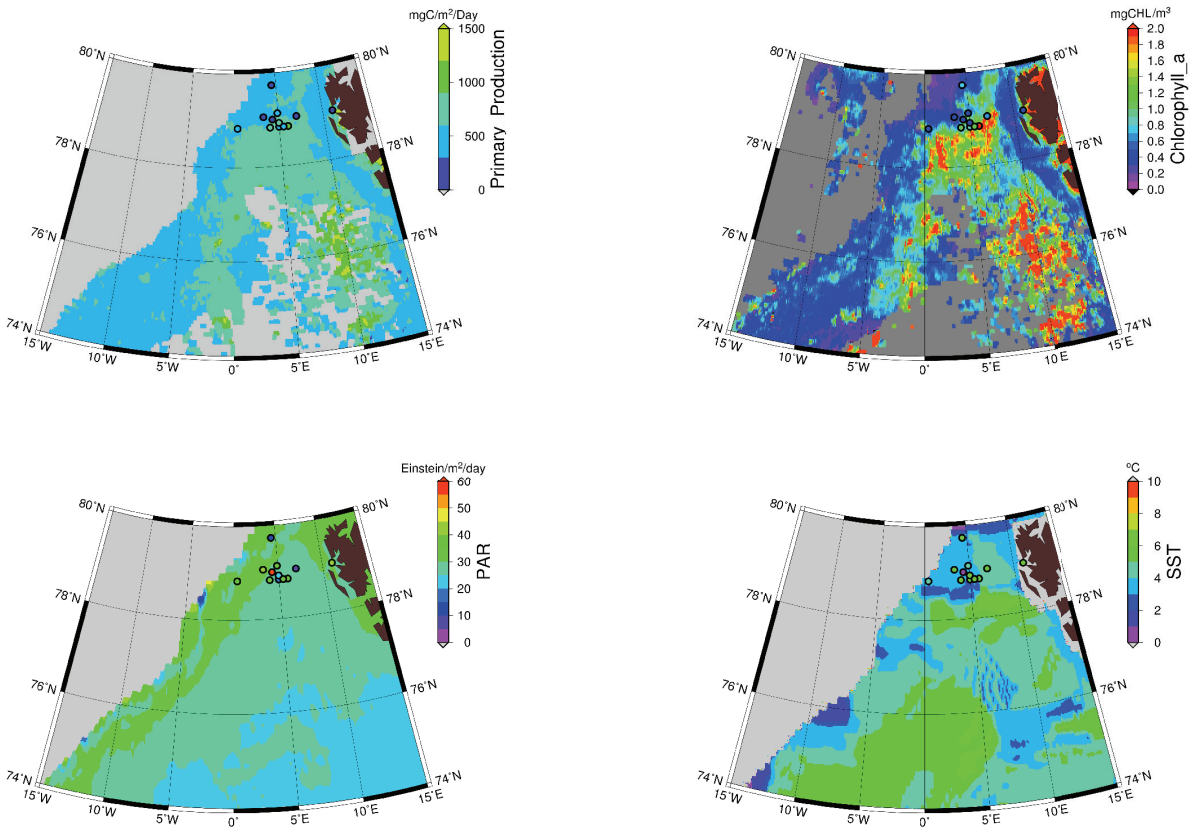

Figure 7.5 Satellite PP in July 2010 modeled following A&M 1996 & Che 2013, and the input satellite data. Top left: satellite PP, logarithmic scale; top right: GlobColour CHL; bottom left: SeaWiFS PAR; bottom right: MODIS SST. In-situ data used for validation were collected in the Greenland Sea during June-July 2010 R/V 'Polarstern' ARK25-1/-2 cruises and are overlayed as colored circles. The color of the circle corresponds to the in-situ value of the parameter at the current location. In-situ PP is modeled following Morel (1991)

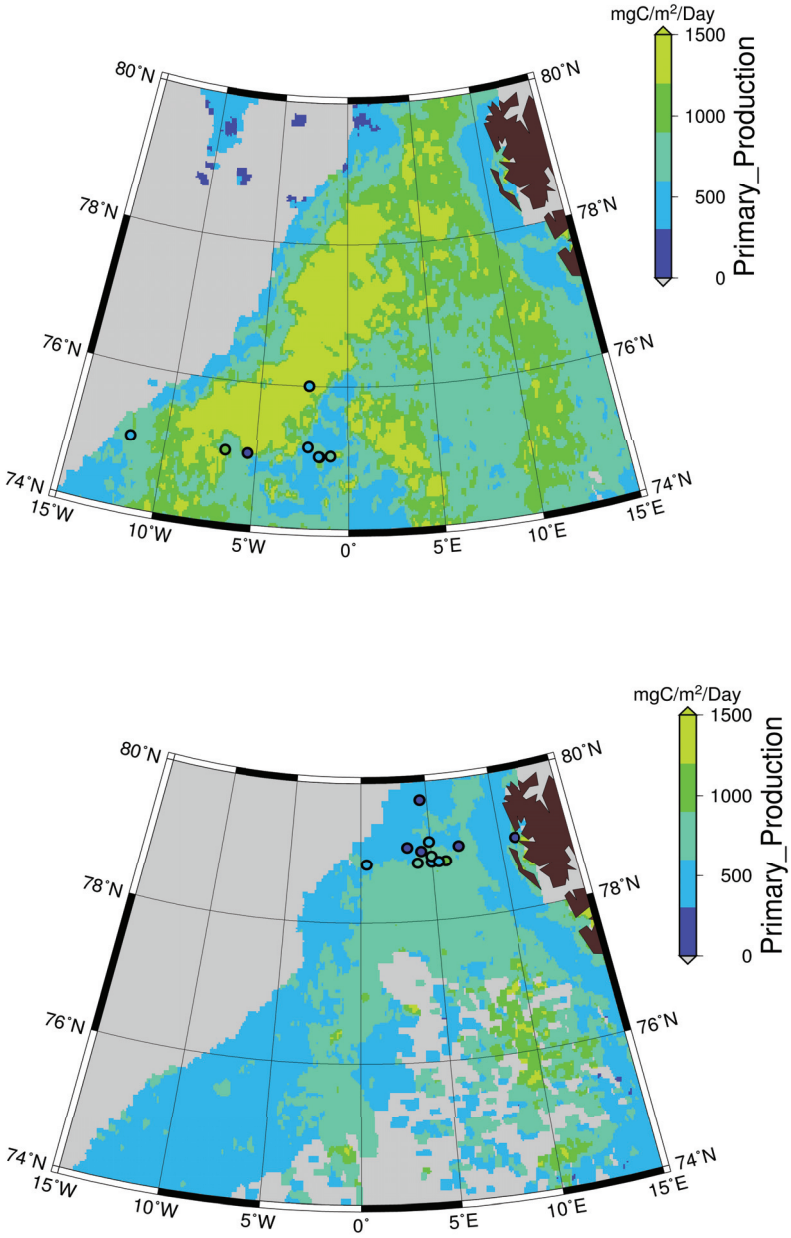

Figure 7.6 Satellite PP in June 2010 (top) and July 2010 (bottom) modeled following A&M 1996 & Che 2013 (zoomed in top right plots of Figures 7.4 and 7.5). Validation in-situ data were collected in the Greenland Sea during June-July 2010 R/V 'Polarstern' ARK25-1/-2 cruises and are overlayed as coloured circles.

The comparison of validation statistics between the three PP models used is presented in Table 7.2. All the statistical characteristics studied show that A&M 1996 & Che 2013 reproduce the in-situ PP data better than A&M 1996. The statistical characteristics are also consistent in showing that the B&F 1997 model (=VGPM) performs the worst.

Table 7.2 Comparison of validation statistics for PP modeled from satellite data using the A&M 1996 & Che 2013, A&M 1996 standard and B&F 1997. Validation data are the Greenland Sea in-situ PP modeled following Morel (1991) for 20 data points collected during June-July 2010 R/V 'Polarstern' ARK25-1/-2 cruises

	A&M 1996 & Che 2013	A&M 1996_standard	VGPM
BIAS_abs	189.72	263.91	438.47
BIAS_log	0.82	0.99	1.37
RMSD_log	0.70	0.75	0.89
CV(RMSD)	0.65	0.78	1.16

However, all the three models capture the range of Greenland Sea in-situ PP values quite well, on average overestimating the in-situ PP on 190 mgC/m^2/day for A&M 1996 & Che 2013, on 264 mgC/m^2/day for A&M 1996 standard and on 439 mgC/m^2/day for B&F 1997. The normalized logarithmic representation of bias varies from 0.82 to 1.36. These values show that these models perform better (for both versions of Antoine and Morel (1996) model) in the Greenland Sea than those shown by Saba et al. (2011) for the Northeast Atlantic (41°N-55°N), where (on average for six WRDR PP models) in-situ PP was overestimated by 1.2. The higher bias observed in Saba et al. (2011) for A&M 1996 standard is most likely to be caused by the higher concentrations of Colored Dissolved Organic Matter in the North Sea than in the Greenland Sea.

RMSD in logarithmic representation is consistent with other statistics and is lowest for A&M 1996 & Che 2013 (0.7), higher for A&M standard (0.75), and highest for B&F 1997 (0.89). The RMSD of 0.7 is still quite high as compared to 0.3, observed by Saba et al. (2011) for A&M 1996 standard in the Northeast Atlantic. In the whole Arctic, RMSD values around 0.5 were observed for the Wavelegth-Integrated-Depth-Resolved PP model (Hill et al., 2013). Our high RMSD values seem to be caused by the high RMSD of the two main input parameters, which is 0.72 for CHL and 0.54 for PAR. The same

is true for the coefficient of variation (CV). High RMSD and CV indicate that the local variability of the single data points is not reproduced well enough by the satellite data. Considering that due to a small number of co-locations the comparison in this study was made between the monthly satellite PP and daily in-situ PP, the daily variability indeed can not be reflected in satellite data correctly. The conventional comparisons with the RMSD and bias values cited above are based on daily data. Another point which needs to be addressed is the reliability of the in-situ PP data used here. Since no in-situ PP measurements were made in Greenland Sea in 2010 (as well as for the whole period of current study, since the launch of SeaWiFS in 1998), we had no possibility to compare the PP modeled from in-situ data with the measured PP. The comparison with in-situ PP was also not made either in Morel (1991) or in Antoine and Morel (1996). And even if the comparison would have been made for the global waters, this would not have meant that it remains the same for the Greenland Sea, as the discrepancy if existed, is expected to be region-dependent. This issue of the validity of the PP modeled from in-situ data could be an additional source of error.

7.6.2 Integrated basin estimates and temporal trends

According to our satellite-based calculations, Greenland Sea PP per unit area is 98.6 gC/m^2/year. Arrigo and van Dijken (2011) previously reported a lower value (86 gC/m^2/year) for exactly the same region. When using a more conventional method of basin estimate (multiplied by the area), our calculations resulted in 161.1 TgC/year, which is also larger than 148 TgC/year (Arrigo and van Dijken, 2011) and coincides with 162 TgC/year reported by Hill et al. (2011) for about the same region, but excluding the Greenland Shelf. Mind that as opposed to Hill et al. (2011) and Arrigo and van Dijken (2011), we did not include September PP in the annual estimate. The reason for this is that satellite data for September covered the southern Greenland Sea only and would not have been consistent with the satellite coverage of other months. If we assume that PP in September is the average of April-August PP, then our annual value would rise to 194 TgC/yr^{-1}, and be larger than any of the previously mentioned estimates. Both, Arrigo and van Dijken (2011) and Hill et al. (2011), estimates did not account for SCM, which seems to be the reason for their lower PP values. The more temporally resolved (i.e. monthly) comparison is given in the Table 7.3. Interestingly, the range of monthly values is smaller for our calculations (18-42 TgC/yr^{-1}) than the range of values obtained by Hill et al. (2011) (8-70 TgC/yr^{-1}).

Table 7.3 Satellite PP integrated for the Greenland Sea sector of Arctic (north to the Arctic circle, 45°W-15°E), in TgC/yr^{-1}. The calculations of this study are described in section 7.3.2. Hill et al. (2011) used SeaWiFS CHL data and the PP model developed for the Chukchi Sea by Hill and Zimmerman (2010). ND stands for no calculations made

	April	May	June	July	August	September	annual
This study	18.23	34.74	42.12	35.81	30.20	ND	161.1
Hill et al (2011)	19.1	70	24.2	15.7	7.68	25.4	162

The temporal trends for 1998-2010 (Table 7.4) were significant only if a detailed temporal resolution was chosen. For the whole Greenland Sea or western and eastern parts of Fram Strait, no trends were detected. Out of the ten 20x20 km sites, which were also analysed in Chapter 4 (see Table 4.3 for locations), two open ocean sites D and H have shown a significant increase in PP for the period studied (+117 and +122 mgC/m^2/day respectively). When in previous chapters we were studying the temporal evolution in CHL, these two points also showed an increase. Generally, the increase in CHL was more spatially consistent than in PP: four sites out of ten and the whole eastern part of the Fram Strait. Why does PP show a more occasional increase as compared to CHL? This is most likely due to the fact that PP is a more stable quantity than CHL. Some PP models simply calculate it as proportional to the square root of CHL, hence a large increase in CHL corresponds to low increase in PP, which is not detectable for some areas of the Greenland Sea. The observed increase in PP corresponds to warming of the sea surface temperatures in the area and decrease in coastal ice of Svalbard (see Chapter 4). Previously, in the Greenland Sea, the opposite of what we found, i.e. a significant negative trend in PP from 1998 till 2009 was observed by Arrigo and van Dijken (2011). The results of Arrigo and van Dijken (2011) are even more interesting as the CHL data, which is the main input parameter to both PP models was shown in our study to have the increasing tendency for the period from 1998 till 2009 in the Greenland Sea. It is not clear to us what are the reasons for the difference between Arrigo and van Dijken (2011) and our results. It might be that the different input CHL data (single sensor CHL used by Arrigo and van Dijken (2011) versus merged three-sensor CHL used in our study) and the different PP model used (WIDR model used by Arrigo and van Dijken (2011) versus WRDR model used in this study) could have profoundly affected the results.

Table 7.4 Mean values and trends for 1998-2010 April-August satellite PP, in mgC/m^2/day (section 7.2.2). Trends are calculated based on the anomalies of the data. Significant trends ($p<0.05$) are marked in bold. Letters A-J correspond to the 20x20 km sites, which were studied in Chapter 4. For the locations see Table 4.3. WF stands for Western Fram Strait (76°N-84°N, 15°W-0°), and EF for Eastern Fram Strait (76°N-84°N , 0°-15°E), which were studied in Chapter 4. GS_all stands for the average for the Greenland Sea sector of the Arctic (north to the Arctic circle at 66°33'39''N, 45°W-15°E)

	A	B	C	D	E	F	G	H	I	J	WF	EF	GS_all
mean	658	674	644	621	671	670	661	554	599	627	561	624	594
trend	65	20	83	**117**	-17	65	106	**122**	-5	24	-36	-24	-34

The changes in the Arctic Ocean PP need to be documented in order to understand and predict the impact of PP on the carbon cycle. Another crucial point is the monitoring of the effect of these changes on the food webs (e.g of the links between primary and secondary producers). In this chapter it was demonstrated that the Antoine and Morel (1996) PP model tuned for the Greenland Sea by Cherkasheva et al. (2013b) results in more accurate PP estimates than those obtained from the global PP models, thus the development of regional PP models for the Arctic Ocean is recommended. As for the continuation of current work, future efforts should be concentrated on adopting the parameterizations in the model to the absorption properties of the Greenland Sea phytoplankton and tests of the model in the neighboring regions such as Barents Sea.

Chapter 8

Conclusions and outlook

In this monograph remote sensing, modeled and field data were used to investigate the seasonal cycle, variability and productivity of phytoplankton in the Greenland Sea during the years 1998-2012. The modeled and remote sensing data were used to study the long-term variability in phytoplankton blooms and the causes for such variability. The field data were used for the development and validation of a regional satellite algorithm which estimated the rate of phytoplankton growth, i.e. PP, in the Greenland Sea. The current chapter summarizes the conclusions in Chapters 4 to 7 and presents an outlook to where future research could be carried out.

Chapter 4 studied the differences between the biological regimes within the Fram Strait or the northern Greenland Sea and the physical drivers responsible for these differences. In the western Fram Strait, at the marginal sea ice zone, stratification induced by sea-ice melt is most likely to have promoted phytoplankton growth, which resulted in enhanced biomass observed in May. In the eastern Fram Strait, stratification due to solar warming proved to act as a guiding factor for the open ocean phytoplankton blooms, while the declining shelf ice was seen to promote the phytoplankton blooms along the coast of Svalbard.

A significant increase in phytoplankton biomass for the period of observation i.e 1998-2009, albeit only in the south-eastern part of the Fram Strait, which is mostly influenced by the Atlantic waters, was reported in this chapter. In the south-eastern Fram Strait we also observed a significant increase in sea surface temperature and coastal ice concentration, but not in sea surface salinity. We thus concluded that the observed increase in CHL, is most likely to have resulted from an increase in sea surface temperatures and from a better light availability for the phytoplankton.

The maxima of phytoplankton blooms, defined as the maximum monthly average in a year, were observed to occur later in the summer after 2002. The same was found for the subarctic waters by Harrison et al. (2013) and for the Fram Strait area by Kahru et al. (2011). The reason for this delay is still unknown, but may be attributed to the increasing ice transport through the Fram Strait. While growth of phytoplankton can respond quickly to changes in light (caused by changes in ice), the higher trophic levels are not as flexible. Therefore such delay in phytoplankton bloom could lead to a

mismatch between primary and secondary producers and a re-organisation of the benthic food web (Hill et al., 2011). Chapter 4 is based on Cherkasheva et al. (2013b).

Chapter 5 further explored the regional differences of the phytoplankton bloom variability in the Fram Strait. The mean time-series of CHL, along with onset and duration of the phytoplankton bloom were comparatively studied in: 1) a region roughly corresponding to that studied in Chapter 4, and 2) an equally-sized region westward to that. In accordance to observations made in Chapter 4, phytoplankton bloom showed a tendency to begin later in the westward direction in the Fram Strait. Ice-covered part of Fram Strait along the coast of Greenland in the western Fram Strait proved to have short, late (middle May) and time varying phytoplankton blooms. The eastern part, dominated by warm and salty Atlantic waters, experienced earlier (end of April) and longer blooms with a significantly increasing trend in bloom intensity for the period of study, similar to that observed earlier in Chapter 4. In addition, the link between oceanographic conditions, phytoplankton bloom and the export of organic material to the seafloor has been reported in this chapter. In 2006, when warm Atlantic waters dominated the Fram Strait, we found an early and intense increase of phytoplankton biomass, which most likely resulted in an increased carbon export and was observed in the deviation of benthic community data. Chapter 5 is based on author's contribution made to Nöthig et al. (in review).

Chapter 6 reported a first step to transform the satellite data concerning surface phytoplankton biomass into information regarding the amount of carbon going through the phytoplankton biomass in the water column (i.e. Net PP), by analysing the vertical distribution of the available in-situ phytoplankton biomass data for the years 1957-2010. We tested the hypothesis that the Greenland Sea data deviates from the standard global parametrization of vertical phytoplankton profiles (Morel and Berthon, 1989) due to the unique optical properties of the Arctic waters and due to the presence of a variable SCM (Arrigo et al., 2011; Matsuoka et. al., 2007, 2011; Weston et al., 2005). Once the hypothesis was tested, we proceeded to develop a relationship for the Greenland Sea specifically. First, consistent with the global study by Morel and Berthon (1989), we observed in principal different patterns of the CHL profile for low and high CHL concentration in the surface layer. This showed the need to account for the surface CHL value when calculating the shape of the profile. However, since the Morel and Berthon (1989) relationship was seasonally averaged, it captured only the early months of the Greenland Sea season, which suggested the need to use a monthly resolved relationship for the region, which we then developed.

The majority of profiles used had low CHL values in the surface layer, and corresponded to a larger

range of total CHL than globally, which means that in the oligotrophic parts of Greenland Sea, the estimation of total CHL from surface data is less reliable. The reason for this may be due to the variable values and position of the SCM, which is significant for the profiles with low surface CHL. An error analysis for the profiles with low surface CHL (< 0.3 mgCHL m^{-3}) showed that the use of our parameterization of the CHL profile using our Gaussian approximation instead of the uniform profile, reduced the underestimation of total CHL from 19 % to 6 % on average. At the same time, errors in rough estimates of PP were reduced, on average, from 10 % to 3 %. The simple PP model used in our error analysis (Eppley et al., 1985) has a number of limitations, but proved to estimate consistent global and regional average production (Carr et al., 2006).

A general conclusion of the error analysis was that for all the surface CHL concentrations, Gaussian approximations that we derived underestimated the in situ total CHL value by 4 %, which is an improvement as compared to the values obtained from the Morel and Berthon (1989) profiles (14 % overestimation), or the uniform profiles (which varied from 19 % underestimation to 7 % overestimation depending on the surface CHL value). Chapter 6 is based on Cherkasheva et al. (2013a).

In Chapter 7, the relationship between the surface CHL and its vertical profile derived in Chapter 6 was combined with the satellite model of Antoine and Morel (1996), to estimate Greenland Sea PP. The validation of these satellite estimates showed that the range of PP values, modeled from in-situ data, was captured well by both, our Greenland Sea (i.e. containing the functions reported in Chapter 6) as well as the global, versions of the Antoine and Morel (1996) model. Both versions were less biased in the Greenland Sea when compared to the Saba et al. (2011) work where the results were obtained using a global version of Antoine and Morel (1996) in the Atlantic region ten degrees south (41°N-55°N) to our area of analysis. Generally, as it was seen in all the statistics studied, our Greenland Sea-adapted version of Antoine and Morel (1996) model reproduces the in-situ data with better accuracy than the global Antoine and Morel (1996) model or the more commonly used satellite PP model, VGPM (Behrenfeld and Falkowski, 1997a). The best performing model overestimated the in-situ PP by 190 $mgC/m^2/day$ on average. This relatively small bias could be corrected by calibrating the model parameters. However, for such a step we would require that PP that we modeled from in-situ data first is validated by in-situ PP measured by, for example, the ^{14}C assimilation method, which is beyond the scope of this study as such simultaneous measurements were not performed in the Greenland Sea. They, however, were done for the central Arctic basin in 2011 and shall be used for future validation activities.

The good performance we observed for Antoine and Morel (1996) with Cherkasheva et al. (2013a) Greenland Sea parametrization is an expected outcome, because the work reported in Cherkasheva et al. (2013a) and described in Chapter 6 is focused on the correct representation of the variability of CHL profiles, accomplished by assigning a unique CHL profile for a certain month as well as a certain surface CHL. The local variability expressed through root mean square difference is poorly reflected in satellite PP data, which we considered a feature of monthly satellite and daily in-situ data co-location rather than of the model parametrization. This is supported by the large deviation between satellite and in-situ input data (CHL and photosynthetically active radiation have the largest impact). The capture of local and instantaneous variability should improve if larger number of co-locations are made available, which would then allow daily inter-comparisons. The main problem that needs to be addressed is the availability of spectrally resolved irradiance data. The annual Greenland Sea PP was estimated as 161-194 TgC/yr^{-1}, which is slightly higher than previously reported estimates. Time series of monthly PP showed an increase in the northern open ocean area of the Greenland Sea, on about 120 $mgC/m^2/day$ for the thirteen years of observations.

What are the potential lessons learned for the bigger picture?

Firstly, even though an effect of the Arctic sea ice decrease may not be directly seen in the time series of the Greenland phytoplankton, it nevertheless appears through the stabilization of water column. In the summer months, the phytoplankton are concentrated in the upper ocean layer and are not limited by the light availability. The concentration of nutrients in the upper ocean layer of these polar latitudes will determine the threshold until which PP will increase in the future, given that the environmental changes in the Arctic Ocean will continue. A detailed picture of the nutrient estimates in the Arctic are still fragmented, and on a large scale relies on climatologies composed of episodic data from different years, which hinders the forecast of the future PP estimates.

Secondly, we have showed that for the Arctic region it is recommended to use a regional PP model, with the regional model corresponding better to in-situ data than the most commonly used global models.

Finally, the method of modeling PP from available in-situ irradiance, biomass and absorption data proved to have a great potential. These measurements, which are often acquired for other purposes such as validation of satellite reflectances, absorption and biomass, could increase the number of data points for our understanding of the ocean productivity. When combined with direct measurements of PP, a more complete and accurate estimation of basin-wide PP could be provided.

The Greenland Sea PP estimates we derived can be used for validation of PP obtained from biogeochemical models (such as Losch et al., 2008), which are based on the climatology of nutrients. On a local scale, it would be interesting for marine biologists to thoroughly compare our estimates with the benthic data to study the part of the carbon cycle which links PP and the carbon stored in sediments.

References

ACRI-STLOV et al., 2006. GlobCOLOUR: An EO based service supporting global ocean carbon cycle research: Full Validation Report. GC-PL-NIVA-FVR-01. Available from: http://www.globcolour.info/validation/report/GlobCOLOUR_FVR_v1.1.pdf.

André, J. M. and A. Morel, 1991. Atmospheric corrections and interpretation of marine radiances in CZCS imagery, revisited. Oceanologica Acta, 14, 3–22

Antoine, D. and A. Morel, 1996. Oceanic primary production : I. Adaptation of a spectral light-photosynthesis model in view of application to satellite chlorophyll observations, Global Biogeochemical Cycles, 10, 43-55

Antoine D., André J.M. and A. Morel. 1996. Oceanic primary production: II. Estimation at global scale from satellite (Coastal Zone Color Scanner) chlorophyll, Global Biogeochemical Cycles, 10, 57-69

Antoine, D. and A. Morel. 1998. Relative importance of multiple scattering by air molecules and aerosols in forming the atmospheric path radiance in the visible and near infrared parts of the spectrum. Applied Optics, 37, 2245–2259

Antoine, D. and A. Morel. 1999. A multiple scattering algorithm for atmospheric correction of remotely-sensed ocean color (MERIS instrument): Principle and implementation for atmospheres carrying various aerosols including absorbing ones. International Journal of Remote Sensing, 20, 9, 1875– 1916

Antoine D., 2006. Global- and Ocean-scale primary production from satellite observations, In "Manual of Remote Sensing, 3rd edition, volume 6, Remote Sensing of the Marine environment", J.F.R. Gower Ed., ASPRS pub., Bethesda, MD, 85-147.

Ardyna, M., Babin, M., Gosselin, M., Devred, E., Bélanger, S., Matsuoka, A., and Tremblay, J.-É. 2013. Parameterization of vertical chlorophyll *a* in the Arctic Ocean: impact of the subsurface chlorophyll maximum on regional, seasonal, and annual primary production estimates, Biogeosciences, 10, 4383-4404, doi:10.5194/bg-10-4383-2013

Armstrong, R. A., 2006. Optimality-based modeling of nitrogen allocation and photo-acclimation in photosynthesis, Deep-Sea Research. Part. II, 53, 513–531

Arnone, R. A., Casey, B., Ko, D., Flynn, P., Carrolo, L., and S. Ladner. 2007. Forecasting Coastal

Optical Properties using Ocean Color and Coastal Circulation Models. Proc. Of SPIE, 6680, 66800S, doi: 10.1117/12.737201

Arrigo, K. R. and G. L. van Dijken, 2011. Secular trends in Arctic Ocean net primary production. Journal of Geophysical Research, 16, C09011, doi:10.1029/2011JC7273

Arrigo, K. R., Matrai, P. A., and van Dijken, G. L., 2011. Primary productivity in the Arctic Ocean: Impacts of complex optical properties and subsurface chlorophyll maxima on large scale annual estimates. Journal of Geophysical Research, 116, C11022. doi:10.1029/2011JC007273

Arrigo, K. R., Perovich, D. K., Pickart, R. S., Brown, Z. W., van Dijken, G. L., Lowry, K. E., Mills, M. M., Palmer, M. A., Balch, W. M., Bahr, F., Bates, N.R., Benitez-Nelson, C., Bowler, B., Brownlee, E., Ehn, J. K., Frey, K. E., Garley, R., Laney, S. R., Lubelczyk, L., Mathis, J., Matsuoka, A., Mitchell, B. G., Moore, G. W., Ortega-Retuerta, E., Pal, S., Polashenski, C. M., Reynolds, R. A., Schieber, B., Sosik, H. M., Stephens, M., Swift, J. H. 2012. Massive phytoplankton blooms under sea ice. Science, 336(6087), 1408. doi: 10.1126/science.1215065

Asanuma, I., Nieke, J., Matsumoto, K., Kawano, T., 2003. Optical properties control primary productivity model on the East China Sea. In: Frouin, J.R. (Ed.), Ocean Remote Sensing and Applications, 4892. SPIE, pp. 312–319

Astoreca, R., Rousseau, V., and Lancelot, C. 2006. Specific phytoplankton absorption variability and implication for chlorophyll-a retrieval in Belgian waters (Southern North Sea). Proceedings of the Second meeting on MERIS and AATSR Calibration and Geophysical Validation (MAVT-2006), European Space Agency, SP-615

Balch, W. M., Eppley, R. W., and M. R. Abbott, 1989. Remote sensing of primary production, II, A semi-analytical algorithm based on pigments, temperature, and light. Deep Sea Research, 36, 1201–1217

Balch, W. M., Evans, R., Brown, J., Feldman, G., McClain, C., and W. Esaias, 1992. The remote sensing of ocean primary productivity: Use of a new data compilation to test satellite algorithms, Journal of Geophysical Research, 97(C2), 2279–2293

Bannister, T. 1974. Production equations in terms of chlorophyll concentration, quantum. Limnology and Oceanography, 19, 1–12

Bannister, T. and Weidemann, A., 1984. The maximum quantum yield of phytoplankton photosynthesis *in situ.* Journal of Plankton Research, 2, 275–294

Banse, K. 1992. Grazing, temporal changes of phytoplankton concentrations, and the microbial loop in

the open sea. In: Primary productivity and biogeochemical cycles in the sea, 409-440. Ed. by P.G. Falkowski and A.P. Woodhead. Plenum press, New York, New York, USA.

Banse, K. 2002. Steeman Nielsen and the zooplankton. Hydrobiology, 480, 15–28.

Barlow, R. G., Cummings, D. G., and S. W. Gibb. 1997. Improved resolution of mono- and divinyl chlorophylls a and b and zeaxanthin and lutein in phytoplankton extracts using reverse C-8 HPLC, Marine Ecology - Progress Series, 161, 303–307

Behrenfeld, M. J., and P. G. Falkowski, 1997a. Photosynthetic rates derived from satellite-based chlorophyll concentration, Limnology and Oceanography, 42, 1–20

Behrenfeld, M. J., and P. G. Falkowski, 1997b. A consumer's guide to phytoplankton primary productivity models, Limnology and Oceanography, 42, 1479–1491

Behrenfeld, M. J. 2010. Abandoning Sverdrup's Critical Depth Hypothesis on phytoplankton blooms. Ecology, 91, 977–989

Ben Mustapha, S., Bélanger, S., Larouche, P.. 2012. Evaluation of ocean color algorithms in the southeastern Beaufort Sea, Canadian Arctic: new parameterization using SeaWiFS, MODIS, and MERIS spectral bands. Canadian Journal of Remote Sensing, 38, 535-566

Berger, W. H., 1989. Global maps of ocean productivity, Productivity of the Ocean: Present and Past. W. H. Berger, V. S. Stemacek, G. Wefer, 429–455, John Wiley, New-York.

Beszczynska-Möller, A., Woodgate, R. A., Lee, C., Melling, H., Karcher, M. 2011. A synthesis of exchanges through the main oceanic gateways to the Arctic Ocean. Oceanography 24(3), 82- 99

Bidigare, R. R., 1991. Analysis of algal chlorophylls and carotenoids, in: Marine particles: Analysis and characterisation. Edited by: Hurd, D. C. and Spencer, D. W., American Geophysical Union, 119– 123

Bidle, K.D. and P.G. Falkowski. 2004. Cell death in planktonic, photosynthetic microorganisms. Nature Reviews: Microbiology, 2, 643–655. doi:10.1038/nrmicro956

Boetius, A., Albrecht, S., Bakker, K., Bienhold, C., Feldenm J., Fernández-Méndez, M., Hendricks, S., Katlein, C., Lalande, C., Krumpen, T., Nicolaus, M., Peeken, I., Rabe, B., Rogacheva, A., Rybakova, E., Somavilla, R., Wenzhöfer, F. 2013. RV Polarstern ARK27-3-Shipboard Science Party. Science 339(6126), 1430-2. doi: 10.1126/science.1231346.

Box, G. E. P., and Jenkins, G. M. 1976. Time series analysis: Forecasting and control. San Francisco: Holden-Day

Boyce D.G., Lewis, M.R., Worm, B. 2010. Global phytoplankton decline over the past century. Nature, 466, 591–596

Bracher, A. 1999. Photoacclimation of phytoplankton in different biogeochemical provinces of the Southern Ocean and its significance for estimating primary production. Berichte zur Polarforschung, Alfred-Wegener-Institute for Polar and Marine Research, Bremerhaven, 341. ISSN0176-5027

Bracher, A.U., and M.M. Tilzer. 2001. Underwater light field and phytoplankton absorbance in different surface water masses of the Atlantic sector of the Southern Ocean. Polar Biology, 24, 687-696

Bricaud, A., and A. Morel. 1987. Atmospheric corrections and interpretation of marine radiances in CZCS imagery: Use of a reflectance model. Oceanologica Acta SP, 33–50

Bricaud, A., Morel, A., Prieur, L. 1981. Absorption by dissolved organic matter of the sea (yellow substance) in the U.V. and visible domains. Limnology and Oceanography, 26, 43–53

Brockwell, P. J., and Davis, R. A. 2002. Introduction to Time Series and Forecasting. Springer-Verlag, New York. 421pp, ISBN 0-387-95351-5

Brown, C. 2008. Response to a skeptic on satellite ocean color. Limnology and Oceanography Bulletin, 17(4)

Brownlee, C., and A.R. Taylor. 2002. Algal calcification and silification. In: Encyclopedia of life sciences. Macmillan Publishers Ltd, Nature Publishing Group, 1-6

Budéus, G., and S. Ronski. 2009. An integral view of the hydrographic development in the Greenland Sea over a decade. The Open Oceanography Journal, 3, 8-39

Campbell, J. W., and J. E. O'Reilly. 1988. Role of satellites in estimating primary productivity on the northwest Atlantic continental shelf, Continental Shelf Research, 8(2), 179–204

Cannizzaro, J.P., and K.L. Canler. 2006. Estimating chlorophyll a concentrations from remote-sensing reflectance in optically shallow waters. Remote Sensing of Environment, 101, 13-24

Carr, M.-E., Friedrichs, M. A. M., Schmeltz, M., Aita, M. N., Antoine, D., Arrigo, K. R., Asanuma, I., Aumont, Barber, R., Behrenfeld, M., Bidigare, R., Bustenhuis, E., Campbell, J., Ciotti, A., Dierssen, H., Dowell, M., Dunne, J., Esaias, W., Gentili, B., Gregg, W.,, Groom, Hoepffner, N., Ishizaka, J., Kameda, T., LeQuere, C., Lohrenz, S., Marra, J., Melin, F., Moore, K., Morel, A., Reddy, T. E., Ryan, J., Scardi, M., Smyth, T., Turpie, K., Tilstone, G., Waters, K., and Yamanaka, Y. 2006. A comparison of global estimates of marine primary production from ocean color, Deep Sea Research II, 53, 741–770. doi:10.1016/j.dsr2.2006.01.028

Carroll, M. L., Ambrose Jr., W. G., Levin, B. S., Locke, V. W. L., Henkes, G. A., Hop, H., Renaud, P. E. 2011a. Pan-Svalbard growth rate variability and environmental regulation in the Arctic bivalve *Serripes groenlandicus*. Journal of Marine Systems, 88, 239-251

Carroll, M. L., Ambrose Jr., W. G., Levin, B. S., Ryan, S. K., Ratner, A. R., Henkes, G. A., Greenacre, M. J. 2011b. Climatic regulation of *Clinocardium ciliatum (bivalvia)* growth in the northwestern Barents Sea . Paleogeography, Paleoclimatology, Paleoecology, 302, 10-20

Cavalieri, D. J., and Parkinson, C. J. 2012. Arctic sea ice variability and trends, 1979–2010. The Cryosphere, 6, 881–889

Chamberlin, W. S., Booth, C. R., Kieffer, D. A., Morrow, J. H., Murphy, R. C. 1990. Evidence for a simple relationship between natural fluorescence, photosynthesis and chlorophyll in the sea. Deep Sea Research Part A. Oceanographic Research Papers, 37, 6, 951-973, ISSN 0198-0149, http://dx.doi.org/10.1016/0198-0149(90)90105-5.

Chamberlin, W. S., and T. D. Dickey, 2008, Exploring the World Ocean, McGraw-Hill, New York. ISBN: 0073016543

Chavez, F. P., Messié, M., and J. T. Pennington. 2011. Marine Primary Production in Relation to Climate Variability and Change. Annual Review of Marine Science, 3, 227 -260

Chen, C. T. A., 2007. Nutrient cycling in the oceans; in: "Oceanography," ed. by J.C.J. Nihoul and C.T.A. Chen, in Encyclopedia of Life Support Systems (EOLSS), Developed under the Auspices of the UNESCO, Eolss Publishers, Oxford, UK, ISBN: 978-1-905839-62-9 e-Book, 1, 331-343

Cherkasheva, A., Nöthig, E. M., Bauerfeind, E., Melsheimer, C., and A. Bracher. 2013a. From the chlorophyll-a in the surface layer to its vertical profile: a Greenland Sea relationship for satellite applications. Ocean Science, 9 (2), 431-445. doi:10.5194/os-9-431-2013

Cherkasheva, A., Bracher, A., Melsheimer, C., Köberle, C., Gerdes, R., Nöthig, E.-M., Bauerfeind, E., and A. Boetius. 2013b. Influence of the physical environment on polar phytoplankton blooms: a case study in the Fram Strait. Journal of Marine Systems. doi: 10.1016/j.jmarsys.2013.11.008

Comiso, J. C. 2010. Polar oceans from space. New York: Springer, 741-770

Comiso, J. C., Parkinson, C. L., Gersten, R., and Stock, L. 2008. Accelerated decline in the Arctic sea ice cover. Geophysical Res Lett, 35: L01703

Cooper, L. H. X. 1938. Phosphate in the English Channel. Journal of Marine Biological Association of the United Kingdom, 23 181-195

Cota, G. F., Harrison, W. G., Platt, T., Sathyendranath, S., and V. Stuart. 2003. Bio-optical properties of the Labrador sea. Journal of Geophysical Research , 108, c7, 3228, doi:10.1029/2000jc000597

Cota, G. F., Wang, H., and J. C. Comiso. 2004. Transformation of global satellite chlorophyll retrievals with a regionally tuned algorithm. Remote Sensing of Environment 90: 373-377

Davis, C. C. 1963. On questions of production and productivity in ecology. Archiv für Hydrobiologie, 59, 145-161

De Steur, L., Hansen, E., Gerdes, R., Karcher, M., Fahrbach, E., and J. Holfort. 2009. Freshwater Fluxes in the East Greenland Current: A decade of observations. Geophysical Research Letters, 36, L23611. doi: 10.1029/2009GL041278

Dickson, R.R., Kelly, P.M., Colebrook, J.M., Wooster, W.S., Cushing, D.H. 1988. Northwinds and production in the eastern North Atlantic. Journal of Plankton Research, 10, 151–169

Doney, S. C. 2006. Plankton in a warmer world. Nature, 444: 695–696.

Dubinsky, Z. 1992. The functional and optical absorption cross sections of phytoplankton photosynthesis, p. 31-45. In P.G. Falkowski and A.D: Woodhead (eds.), Primary productivity and biogeochemical cycles in the sea, Environmental Science Research, 43. Plenum.

Dubinsky, Z., Berman, T., Schanz, F. 1984. Field experiments for in situ measurement of photosynthetic efficiency and quantum yield. Journal of Plankton Research, 6, 339–349

Dugdale, R. C. and J. J. Goering. 1967. Uptake of new and regenerated forms of nitrogen in primary productivity. Limnology and Oceanography 12:196–206.

Edler, L. 1979. Recommendations on methods for marine biological studies in the Baltic Sea. Phytoplankton and chlorophyll. BMB Publishing, 5: 1-38.

Eppley, R.W. 1972. Temperature and phytoplankton growth in the sea. Fisheries Bulletin, 70, 1063–1085

Eppley, R. W. and B. J. Peterson. 1979. Particulate organic matter flux and planktonic new production in the deep ocean. Nature 282: 677–680.

Eppley, R., Steward, E., Abbott, M., Heyman, U. 1985. Estimating ocean primary production from satellite chlorophyll: introduction to regional differences and statistics for the Southern California Bight. Journal of Plankton Research, 7, pp. 57–70

Evans, G. T. and J. S. Parslow. 1985. A model of annual plankton cycles. Biological Oceanography 3:327–347

Evans, C. A., and J. E. O'Reily. 1987. A handbook for the measurement of chlorophyll a in net plankton and nanoplankton. BIOMASS Handbook, 9: 1-14

Falkowski, P. G. 1981. Light-shade adaptation and assimilation numbers. Journal of Plankton Research 3: 203-216

Feistel, R. 2010. TEOS-10: A New International Oceanographic Standard for Seawater, Ice, Fluid

Water, and Humid Air , International Journal of Thermophysics: 1-17

Ferrari, G. M. and S. Tassan. 1999. A method using chemical oxidation to remove light absorption by phytoplankton pigments. Journal of Phycology, 35, 1090–1098

Fieg, K., Gerdes, R., Fahrbach, E., Beszczynska-Möller, A., and U. Schauer. 2010. Simulation of oceanic volume transports through Fram Strait 1995–2005. Ocean Dynamics, 12: 491-502.

Field, C. B., Behrenfeld, M. J., Randerson, J. T., and Falkowski, P. 1998. Primary Production of the Biosphere: Integrating Terrestrial and Oceanic Components, Science, 281 (5374): 237-240

Fitzwater, S. E., Knauer, G. A., and J. H. Martin. 1982. Metal contamination and its effects on primary production. Limnology and Oceanography, 27: 544-551

Flynn, K. J. 1988. The concept of 'primary production' in aquatic ecology. Limnology and Oceanography, 33, 1215-1216

Forest, A., Wassmann, P., Slagstad, D., Bauerfeind, E., Nöthig, E. M., and M. Klages. 2010. Relationships between primary production and vertical particle export at the Atlantic-Arctic boundary (Fram Strait, HAUSGARTEN). Polar Biology, 33: 1733–1746.

Fraser, R. S., Mattoo, S., Yeh, E., and C. R. McClain. 1997. Algorithm for atmospheric and glint corrections of satellite measurements of ocean pigment. Journal of Geophysical Research 102:17107–17118.

Friedrichs, M. A. M., et al. 2009. Assessing the uncertainties of model estimates of primary productivity in the tropical Pacific Ocean, Journal of Marine Systems, Vol. 76, Iss. 1–2, 20, Pp. 113-133, ISSN 0924-7963, doi: 10.1016/j.jmarsys.2008.05.010.

Frouin, R., Schwindling, M., and Deschamps, P.-Y. 1996. Spectral reflectance of sea foam in the visible and near-infrared: In-situ measurements and remote sensing implications. Journal of Geophysical Research, 101, 14361-14471

Gerdes, R., Karcher, M., Kauker, F., and U. Schauer. 2003. Causes and development of repeated Arctic Ocean warming events, Geophysical research letters, 30 (19). doi: 10.1029/2003GL018080

Gilbert, P. M., Biggs, D. C., and McCarthy, J. J. 1982. Deep-Sea Research, 29, 837-850

Giles, K. A., Laxon, S. W., and Ridout, A. L. 2008. Circumpolar thinning of Arctic sea ice following the 2007 record ice extent minimum. Geophysical Research Letters, 35: L22502

Gordon, H. R. 1997. Atmospheric correction of ocean color imagery in the Earth observing system era. Journal of Geophysical Research 102: 17081–17106.

Gordon, H. R. 1978. Removal of atmospheric effects from satellite imagery of the oceans. Applied Optics 17:1631–1636.

Gordon, H. R., Brown, J. W., and R. H. Evans. 1988. Exact Rayleigh scattering calculations for use with the Nimbus-7 coastal zone color scanner. Applied Optics 27: 862–871.

Gordon, H. R., and D. K. Clark. 1980. Remote sensing optical properties of a stratified ocean: an improved interpretation. Applied Optics 19: 3428-3430.

Gordon, H. R., and W. R. McCluney. 1975. Estimation of the depth of sunlight penetration in the sea for remote sensing. Applied Optics 14: 413–416.

Gordon, H. R., and A. Y. Morel. 1983. Remote Assessment of Ocean Color for Interpretation of Satellite Visible Imagery: A review. Springer-Verlag. Berlin, Pp. 114

Gordon, H. R. and M. Wang. 1992a. Surface-roughness considerations for atmospheric correction of ocean color sensors. I: The rayleigh-scattering component. Applied Optics 31:4247–4260

Gordon, H. R. and M. Wang. 1992b. Surface-roughness considerations for atmospheric correction of ocean color sensors. II: Error in the retrieved water-leaving radiance. Applied Optics 31: 4261–4267

Gordon, H. R. and M. Wang. 1994. Retrieval of water-leaving radiance and aerosol optical thickness over the oceans with SeaWIFS: A preliminary algorithm. Applied Optics 33: 443–452

Gradinger, R. R. and M. E. M. Baumann. 1991. Distribution of phytoplankton communities in relation to the large-scale hydrographical regime in the Fram Strait. Marine Biology 111, S. 311-321

Gruber, N. and J. L. Sarmiento. 2002. Biogeochemical/Physical Interactions in Elemental Cycles, in: THE SEA: Biological-Physical Interactions in the Oceans, Vol. 12, edited by: Robinson, A. R., McCarthy, J. J., and Rothschild, B. J., John Wiley and Sons, New York, 337–399

Harrison, W. G., Børsheim, K. Y., Li, W. K. W., Maillet, G. L., Pepin, P., Sakshaug, E., Skogen, M. D., Yeats, P. A. 2013. Phytoplankton production and growth regulation in the Subarctic North Atlantic: A comparative study of the Labrador Sea-Labrador/Newfoundland shelves and Barents/Norwegian/Greenland seas and shelves, Progress in Oceanography, 114, 26-45, ISSN 0079-6611, doi: 10.1016/j.pocean.2013.05.003.

Hibler, W. D. 1979. A Dynamic Thermodynamic Sea Ice Model. Journal of Physical Oceanography, 9, 815–846. doi: 10.1175/1520-0485(1979)009<0815:ADTSIM>2.0.CO;2

Hill, V. J., and Zimmerman, R. C. 2010. Estimates of primary production by remote sensing in the Arctic Ocean: Assessment of accuracy with passive and active sensors, Deep Sea Research Part I,

57, 1243–1254, doi: 10.1016/j.dsr.2010.06.011

Hill V. J., Matrai, P. A., Olson, E., Suttles, S., Steele, M., Codispoti, L. A., and Zimmerman, R. C. 2013. Synthesis of integrated primary production in the Arctic Ocean: II. In situ and remotely sensed estimates, Progress of Oceanography, 110, 107–125, doi:10.1016/j.pocean.2012.11.005

Hop, H., Falk-Petersen, S., Svendsen, H., Kwasniewski, S., Pavlov, V., Pavlova, O., Søreide, J. E. 2006. Physical and biological characteristics of the pelagic system across Fram Strait to Kongsfjorden, Progress in Oceanography, 71 (2–4), 182-231, ISSN 0079-6611, doi: 10.1016/j.pocean.2006.09.007.

Howard, K. L. 1995. Estimating global ocean primary production using satellite-derived data, M.S. thesis, 98 pp., Univ. of R. I., Kingston.

Hunt Jr, G. L., Stabeno, P., Walters, G., Sinclair, E., Brodeur, R. D., Napp, J. M., Bond, N. A. 2002. Climate change and control of the southeastern Bering Sea pelagic ecosystem, Deep Sea Research Part II: Topical Studies in Oceanography, 49 (26), 5821-5853, ISSN 0967-0645, doi: 10.1016/S0967-0645(02)00321-1

Hunt Jr., G. L., Stabeno, P. J., Strom, S., Napp, J. M. 2008. Patterns of spatial and temporal variation in the marine ecosystem of the southeastern Bering Sea, with special reference to the Pribilof Domain, Deep Sea Research Part II: Topical Studies in Oceanography, 55 (16–17), 1919-1944, ISSN 0967-0645, doi: 10.1016/j.dsr2.2008.04.032

Iverson, R. L., Esaias, W. E., and K. Turpie. 2000. Ocean annual phytoplankton carbon and new production, and annual export production estimated with empirical equations and CZCS data, Global Change Biology, 6, 57–72.

Jeffrey, S. W. and Vesk, M. 1997. Introduction to marine phytoplankton and their pigment signatures, in: Phytoplankton pigments in oceanography: Guideline to modern methods., edited by: Jeffrey, S. W., Mantoura, R. F. C., and Wright, S. W., 10, UNESCO Publishing, Paris, 37–84.

Jennings Jr, J.C., Gordon, L.I., and Nelson D.M., 1984. Nutrient depletion indicates high primary productivity in the Weddell Sea. Nature, 309, 51-54

Johannessen, J. A., Johannessen, O. M., Svendsen, E., Schuchman, R., Manley, T., Cambell, W. J., Josberger, E. G., Sandven, S., Gascard, J. C., Olaussen, T., Davidson, K., Vanleer, J. 1987. Mesoscale eddies in the Fram Strait marginal ice zone the 1983 and 1984 Marginal Ice Zone Experiments. Journal of Geophysical Research, 92, 6754–6772

Kahru, M., Brotas, V., Manzano-Sarabia, M., and B.G. Mitchell. 2011. Are phytoplankton blooms occurring earlier in the Arctic? Global Change Biology, 17: 1733-1739.

Karcher, M., Gerdes, R., Kauker, F., and C. Köberle. 2003. Arctic warming - Evolution and Spreading of the 1990s warm event in the Nordic Seas and the Arctic Ocean, Journal of Geophysical Research, 108(C2). doi: 10.1029/2001JC001265

Karcher, M., Gerdes, R., Kauker, F., Köberle, C., and I. Yashayev. 2005. Arctic Ocean change heralds North Atlantic freshening, Geophysical research letters, 32(21), L21606. doi: 10.1029/2005GL023861

Karcher, M., Smith, J. N., Kauker, F., Gerdes, R., and W. Smethie Jr. 2012. Recent changes in Arctic Ocean circulation revealed by 129-Iodine observations and modelling, Journal of Geophysical Research - Oceans, AGU. doi: 10.1029/2011JC007513

Karl, D. M., Christian, J. R., Dore, J. R., Hebel, D. V., Letelier, R. M., Tupas, L. M., and C. D. Winn. 1996. Seasonal and interannual variability in primary production and particle flux at Station ALOHA. Deep-Sea Research Part II 43: 539-568

Karstensen, J., Visbeck, M., Müller, T., Send, U., and H. Valdimarson. 2011. On the role of freshwater forcing on the convection intensity in the central Irminger Sea between 2002 and 2011. Oral presentation at ICES/NAFO Decadal Symposium 2011: Ref.107.

Kauker, F., Gerdes, R., Karcher, M., Köberle, C., and J. L. Lieser. 2003. Variability of Arctic and North Atlantic sea ice: A combined analysis of model results and observations from 1978 to 2001, Journal of Geophysical Research, C6, 108. doi: 10.1029/2002JC001573

Kiefer D. A., and B. G. Mitchell. 1983. A simple steady state description of phytoplankton growth based on absorption cross section and quantum efficiency. Limnology and Oceanography, 28, 770–775

Kirk, J. T. 1984. Dependence of relationship between inherent and apparent optical properties of water on solar altitude. Limnology and Oceanography, 29, 350–356

Kirk J. T., 1994. Light and Photosynthesis in Aquatic Ecosystems, Cambridge University Press, 509 pp., ISBN 0521459664

Koblentz-Mishke, O. I., Volkovinsky, V. V., Kabanova, J. G. 1970. Plankton primary production of the world ocean. In: Scientific exploration of the South Pacific, National Academy of Sciences, 183–193

Köberle, C. and R. Gerdes. 2003. Mechanisms determining the variability of Arctic sea ice conditions and export, Journal of Climate, 16, 2843-2858

Köberle, C. and R. Gerdes. 2007. Simulated variability of the Arctic Ocean fresh water balance 1948-2001, Journal of Physical Oceanography, 37 (6), 1628-1644 . doi: 10.1175/JPO3063.1

Kraft, A. 2013. Arctic pelagic amphipods - community patterns and life-cycle history in a warming Arctic Ocean. PhD Thesis, FB2, University of Bremen, Germany.

Kraft, A., Bauerfeind, E., Nöthig E.-M., Klages, M., Beszczynska-Möller, A., Bathmann, U. V. 2013. Amphipods in sediment traps of the eastern Fram Strait with focus on the life-history of the lysianassoid *Cyclocaris guilelmi*. Deep-Sea Research Part I, 73, 62-72

Lancelot, C., Mathot, S., Veth, C., and Baar, H. de. 1993. Factors controlling phytoplankton ice-edge blooms in the marginal ice-zone of the north-western Weddell Sea during sea ice retreat 1988: field observations and mathematical modeling. Polar Biology, 13, 377-387

Lee, Z., A. Weidemann, J. Kindle, R. Arnone, K. L. Carder, and C. Davis. 2007. Euphotic zone depth: Its derivation and implication to ocean-color remote sensing, Journal of Geophysical Research, 112, C03009, doi:10.1029/2006JC003802

Levitus, S. 1982. Climatological Atlas of the World Ocean, NOAA/ERL GFDL Professional Paper 13, NTIS PB83-184093. Princeton, New Jersey, USA. 173 pp.

Levitus, S., Antonov, J.I., Boyer, T.P., and Stephens, C. 2000. Warming of the world ocean. Science, 287, 2225-2229

Little, W., Fowler, H. W., and Coulson, J. 1983. The shorter Oxford dictionary, 2672 pp, Oxford University Press, Oxford

Liu, J., Curry, J. A., Dai, R., and R. Horton. 2007. Causes of the northern high-latitude land surface winter climate change, Geophysical Research Letters, 34(14), L14702, doi:10.1029/2007GL030196.

Longhurst, A., Sathyendranath, S., Platt, T., Caverhill, C. 1995. An estimate of global primary production in the ocean from satellite radiometer data. Journal of Plankton Research, 17, 1245–1271

Losch, M., Schröter, M., Hohn, S., and C. Völker. 2008. High-resolution modelling of phytoplankton distribution and adaptation, NIC Symposium 20-21 February 2008, Forschungszentrum Jülich; proceedings (NIC series 39)/ organized by John von Neumann Institute for Computing. Ed. by Gernot Münster, Forschungszentrum Jülich, 289-296

Lubac, B., Loisel, H., Guiselin, N., Astoreca, R., Artigas, L-F., and X. Meriaux. 2008. Hyperspectral and multispectral ocean color inversions to detect Phaeocystis globosa blooms in coastal waters. Journal of Geophysical Research, 113, C06026, doi:10.1029/2007JC004451

Mackey, M. D., Mackey, D. J., Higgings, H. W., and S. W. Wright. 1996. “CHEMTAX” – a program for estimating class abundances from chemical markers: Application to HPLC measurements of phytoplankton. Marine Ecology - Progress Series, 144, 265–283, doi:10.3354/meps144265

Maier-Reimer, E., Mikolajewicz, U., and A. Winguth. 1996. Future ocean uptake of CO2: interaction between ocean circulation and biology. Climate Dynamics, 12, 711-721

Maritorena, S. and D.A. Siegel. 2005. Consistent Merging of Satellite Ocean Color Data Sets Using a Bio-Optical Model. Remote Sensing of Environment, 94(4), 429-440

Maritorena, S., D.A. Siegel, and A. Peterson. 2002. Optimization of a Semi-Analytical Ocean Color Model for Global Scale Applications. Applied Optics, 41(15), 2705-2714.

Marra J., 2002. Approaches to the Measurement of Plankton Production. Phytoplankton Productivity: Carbon Assimilation in Marine and Freshwater Ecosystems. Eds. P.J. le B. Williams, D.N. Thomas and C.S. Reynolds. Cambridge, U.K.: Blackwell Science, 78-108.

Marra, J., Ho, C., Trees, C. 2003. An alternative algorithm for the calculation of primary productivity from remote sensing data. LDEO Technical Report #LDEO-2003-1.

Marra, J. and R. T. Barber. 2005. Primary productivity in the Arabian Sea: a synthesis of JGOFS data. Progress in Oceanography, 65, 159–175.

Marra, J. 2009. Net and Gross: Weighing in With 14C. Aquatic Microbial Ecology, 56, 123-31.

Martin, S. 2004. An introduction to ocean remote sensing. Cambridge University Press, Cambridge, UK. ISBN 978-0-521-80280

Martin, J., Tremblay, J. E, Gagnon, J., Tremblay, G., Lapoussiere, A., Jose, C., Poulin, M., Gosselin, M., Gratton, Y., and C. Michel. 2010. Prevalence, structure and properties of subsurface chlorophyll maxima in Canadian Arctic waters. Marine Ecology - Progress Series, 412, 69-84

Martiny, A. C., Pham, C. T. A., Primeau, F. W., Vrugt, J. A., Moore, J. K., Levin, S. A., and Lomas, M. W. 2013. Strong latitudinal patterns in the elemental ratios of marine plankton and organic matter. Nature Geoscience, 6, 279–283, doi:10.1038/ngeo1757

Maslanik, J., Drobot, S., Fowler, C., Emery, W., and R. Barry. 2007. On the Arctic climate paradox and the continuing role of atmospheric circulation in affecting sea ice conditions, Geophysical Research Letters, 34, L03711, doi:10.1029/2006GL028269.

Matrai, P. A., Olson, E., Suttles, S., Hill, V. J., Codispoti, L. A., Light, B., and M. Steele. 2013. Synthesis of primary production in the Arctic Ocean: I. Surface waters, 1954–2007. Progress in Oceanography, 110, 93–106, doi:10.1016/j.pocean.2012.11.004

Matsuoka, A., Huot, Y., Shimada, K., Saitoh, S.I., and M. Babin. 2007. Bio-optical characteristics of the western Arctic Ocean: implications for ocean color algorithms. Canadian Journal of Remote Sensing, 33, 503-518.

Matsuoka, A., Hill, V., Huot, Y., Bricaud, A., and M. Babin. 2011. Seasonal variability in the light absorption properties of western Arctic waters: parameterization of the individual components of absorption for ocean color applications, Journal of Geophysical Research, 116, C02007, doi:10.1029/2009JC005594

Milke, A., and Heygster, G. 2009. Trend der Meereisausdehnung von 1972-2009. Technical Report, Institut for Environmental Physics, University of Bremen, Bremen. http://www.iup.uni-bremen.de/iuppage/psa/documents/Technischer_Bericht_Milke_2009.pdf

Milutinovic, S. 2011. Uncertainty in a model for estimating euphotic depth from satellite observations of chlorophyll. NERSC Special Report, No 88, Nansen Environmental and Remote Sensing Center, Bergen, Norway

Mitchell, B. G., and O. Holm-Hansen 1991. Bio-optical properties of Antarctic Peninsula waters: differentiation from temperate ocean models. Deep Sea Research, 38: 1009-1028

MIZEX'87 Group. 1989. MIZEX East 1987 Winter Marginal Ice Zone Program in the Fram Strait and Greenland Sea. Eos, 70 (17), 545-555

Mobley C. D. 1994. Light and water: radiative transfer in natural waters. Academic Press, 592 pp

Moeller, E. F., Nielsen, T. G., and K. Richardson. 2005. The zooplankton community in the Greenland Sea: Composition and role in carbon turnover. Deep Sea Research Part I, 53, 76-93

Moore, K. D., Voss, K. J., and Gordon, H. R. 2000. Spectral reflectance of whitecaps: their contribution to the water-leaving radiance. Journal of Geophysical Research, 105, 6493-6499

Morel, A. 1988. Optical modeling of the upper ocean in relation to its biogenous matter content (case 1 waters). Journal of Geophysical Research, 93(C9), 10749 – 10768

Morel, A. 1991. Light and marine photosynthesis: A spectral model with geochemical and climatological implications, Progress in Oceanography, 26, 263-306

Morel A. and J.F. Berthon. 1989. Surface Pigments, Algal Biomass Profiles, and Potential Production of the Euphotic Layer: Relationships Reinvestigated in View of Remote-Sensing Applications. Limnology and Oceanography, 34, 8, Hydrologic Optics, 1545-1562

Morel, A. and B. Gentili. 1991. Diffuse reflectance of oceanic waters: Its dependence on sun angle as influenced by the molecular scattering contribution. Applied Optics, 30, 4427– 4438.

Morel, A. and B. Gentili. 1993. Diffuse reflectance of oceanic waters. II. Bidirectional aspects. Applied Optics, 32, 6864–6879.

Morel, A., Voss, K. J., and B. Gentili. 1995. Bidirectional reflectances of oceanic waters: A comparison

of modeled and measured upward radiance fields. Journal of Geophysical Research, 100, 13143–13150

Morel, A. and B. Gentili. 1996. Diffuse reflectance of oceanic waters. III. Implication of the bidirectionality for the remote sensing problem. Applied Optics, 35, 4850–4862.

Morel, A., Antoine, D., Babin, M., and Y. Dandonneau. 1996. Measured and modeled primary production in the Northeast Atlantic (EUMELI JGOFS program): The impact of natural variations in photosynthetic parameters on model predictive skill. Deep-Sea Research Part I, 43, 1273–1304

Morel, A. and S. Maritorena. 2001. Bio-optical properties of oceanic waters: A reappraisal. Journal of Geophysical Research, 106, 7763–7780

NSIDC, 2012. National Snow and Ice Data Center Press Release: Arctic sea ice reaches lowest extent for the year and the satellite record. 19 Sep 2012. http://nsidc.org/news/press/2012_seaiceminimum.html

Olson, R. J., 1980. Limnology and Oceanography, 25, 1064-1074

Ondrusek, M. E., Bidigare, R. R., Waters, K., and D. M. Karl. 2001. A predictive model for estimating rates of primary production in the subtropical North Pacific Ocean, Deep Sea Research Part II, 48, 1837–1863

O'Reilly, J. E., Maritorena, S., Mitchell, B. G., Siegel, D. A., Carder, K. L., Garver, S. A., Kahru, N., and McClain, C. 1998. Ocean color chlorophyll algorithms for SeaWiFS. Journal of Geophysical Research, 103, 24937-24953

Pabi, S., van Dijken, G.L., and K. R. Arrigo. 2008. Primary production in the Arctic Ocean, 1998 – 2006. Journal of Geophysical Research, 113, C08005.

Pacanowski, R.C. 1995. MOM2 Documentation, User's Guide and Reference Manual. NOAA/Geophysical Fluid Dynamics Laboratory

Peterson, B. J., Holmes, R. M., McClelland, J. W., Vörösmarty, C. J., Lammers, R. B., Shiklomanov, A. I., Shiklomanov, I. A., and S. Rahmstorf. 2002. Increasing River Discharge to the Arctic Ocean, Science, 298(5601), 2171 – 2173, doi:10.1126/science.1077445.

Platt, T., Gallegos, C., Harrison, W. 1980. Photoinhibition of photosynthesis in natural assemblages of marine phytoplankton. Journal of Marine Research, 38, 687–701

Platt, T. 1986. Primary production of the ocean water column as a function of surface light intensity: Models for remote sensing. Deep-Sea Research, 33, 149-163

Platt, T., Bird, D.F., and S. Sathyendranath. 1991. Critical depth and marine primary production.

Proceedings of the Royal Society B: Biological Sciences, 246, 205–217

Platt, T., and S. Sathyendranath. 1993. Estimators of primary production for interpretation of remotely sensed data on ocean color. Journal of Geophysical Research, 98(C8), 14561–14567

Platt, T., Fuentes-Yaco, C., and K. T. Frank. 2003. Spring algal bloom and larval fish survival. Nature, 243, 398 – 399

Prieur, L., and S. Sathyendranath. 1981. An optical classification of coastal and oceanic waters based on the specific spectral absorption curves of phytoplankton pigments, dissolved organic matter and other particulate materials. Limnology and Oceanography, 26, 671–689

Preisendorfer, R. W. 1976. Hydrologic Optics. National Oceanic and Atmospheric Administration, Honolulu, Hawaii.

Proshutinsky, A., Timmermans, M.-L., Ashik, I., Beszczynska-Moeller, A., Carmack, E., Frolov, I., Krishfield, R. et al. 2010. Ocean, in: Arctic Report Card. Ed. by J. Richter-Menge, and J.E.Overland. http://www.arctic.noaa.gov/reportcard

Rabe, B., Dodd, P. A., Hansen, E., Falck, E., Schauer, U., Mackensen, A., Beszczynska-Möller, A., Kattner, G., Rohling, E. J., and Cox, K., 2013. Liquid export of Arctic freshwater components through the Fram Strait 1998–2011. Ocean Science, 9, 91-109, doi:10.5194/os-9-91-2013

Redfield, A.C., Ketchum, B.H, and Richards, F.A. 1963. In: The Sea, Ideas and Observations, Vol. 2, 26-77. Interscience, New York.

Reigstad, M., Carroll, J., Slagstad, D., Ellingsen, I. H., Wassmann, P. 2011. Intra-regional comparison of productivity, carbon flux and ecosystem composition within the northern Barents Sea. Progress in Oceanography, 90 (1-4). ISSN 0079-6611.s 33 – 46.s, doi: 10.1016/j.pocean.2011.02.005.

Rey, F., Noji, T. T., and Miller, L. 2000. Seasonal phytoplankton development and new production in the central Greenland Sea. Sarsia 85: 329-344

Reynolds, C. S., Huszar, V., Kruk, C., Naselli-Flores, L., Melo, S. 2002. Towards a functional classification of the freshwater phytoplankton. Journal of Plankton Research, 24, 417–428

Riebesell ,U., Zondervan, I., Rost, B., Tortell ,P.D., Zeebe, R.E., Morel, F.M.M. 2000. Reduced calcification of marine plankton in response to increased atmospheric CO2. Nature, 407, 364–367.

Rigor, I. G., and J. M. Wallace. 2004. Variations in the age of Arctic sea-ice and summer sea-ice extent, Geophysical Research Letters, 31, L09401, doi:10.1029/2004GL019492

Robinson, C., Tilstone, G. H., Rees, A. P., Smyth, T. J., Fishwick, J. R., Tarran, G. A., Luz, B., Barkan, E., and D. Efrat, 2009. Comparison of in vitro and in situ plankton production determinations,

Aquatic Microbial Ecology, 54, 13–34, doi:10.3354/ame01250

Rudels, B., and D. Quadfasel. 1991. Convection and deep water formation in the Arctic Ocean - Greenland Sea system. Journal of Marine Systems, 2, 435-450

Rysgaard, S., Nielsen, T.G., and B.W. Hansen. 1999. Seasonal variation in nutrients, pelagic primary production and grazing in a high-Arctic coastal marine ecosystem, Young Sound, Northeast Greenland. Marine Ecology Progress Series, 179, 13– 25

Saba, V. S., et al. 2011. An evaluation of ocean color model estimates of marine primary productivity in coastal and pelagic regions across the globe. Biogeosciences, 8, 489–503, doi:10.5194/bg-8-489-2011

Sakshaug, E., Andersen, K., and Kiefer, D.A. 1989. A steady state description of growth and light absorption in the marine planktonic diatom *Skeletonema costatum*. Limnology and Oceanography, 34, 198-205

Sakshaug, E. 2004. Primary and secondary production in the Arctic seas. In: Stein R, Macdonald R (eds). The organic carbon cycle in the Arctic Ocean. Springer, Berlin, 57-81

Sathyendranath, S., and T. Platt, 1989. Computation of aquatic primary production: Extended formalism to include effect of angular and spectral distribution of light. Limnology and Oceanography, 34, 188-198

Sathyendranath, S., Caverhill, C.M., Warnock, R.E., and M.R. Lewis. 1989. Remote sensing of oceanic primary production: Computations using a spectral model. Deep-Sea Research, 36, 431-453

Sathyendranah, S., Cota, G., Stuart, V., Maass, H., and Platt, T. 2001. Remote sensing of phytoplankton pigments: a comparison of empirical and theoretical approaches. International Journal of Remote Sensing, 22: 249-273

Schandelmeier, L., and V. Alexander. 1981. An analysis of the influence of ice on spring phytoplankton population structure in the Southeast Bering Sea. Limnology and Oceanography, 26, 935-943

Schauer, U., Beszczynska-Möller, A., Walczowski, W., Fahrbach, E., Piechura, J., and Hansen, E. 2008. Variation of Measured Heat Flow Through the Fram Strait Between 1997 and 2006. In Arctic-Subarctic Ocean Fluxes: Defining the Role of the Northern Seas in Climate, 65-88

Schoemann, V., Besquevort, S., Stefels, J., Rousseau, V., and C. Lancelot. 2005. Phaeocystis blooms in the global ocean and their controlling mechanisms: a review. Journal of Sea Research, 53, 43-66

Segar D. 2007. Introduction to Ocean Sciences. (W. W. Norton & Company, New York). http://www.wwnorton.com/college

Sieburth, J. M., Smetacek, V., Lenz, J. 1978. Pelagic ecosystem structure: Heterotrophic compartments of the plankton and their relationship to plankton size fractions. Limnology and Oceanography, 23, 1256–1263

Simis, S. G. H., Tijdens, M., Hoogveld, H. L., and H. J. Gons. 2005. Optical changes associated with cyanobacterial bloom termination by viral lysis. Journal of Plankton Research, 27, 937–949, doi:10.1093/plankt/fbi068

Skogen, M. D., Budgell, W. P., Rey F. 2007. Interannual variability in Nordic seas primary production. ICES Journal of Marine Science, 64, 889-898

Slagstad, D., Ellingsen, I. H., and P. Wassmann. 2011. Evaluating primary and secondary production in an Arctic Ocean void of summer sea ice: An experimental simulation approach. Progress in Oceanography 90, 117–131, doi: 10.1016/j.pocean.2011.02.009

Smayda, T. J. 1997. What is a bloom? a commentary. Limnology and Oceanography, 42(5(2)), 1132–1136

Smedsrud, L. H., Sirevaag, A., Kloster, K., Sorteberg, A., and Sandven, S. 2011. Recent wind driven high sea ice area export in the Fram Strait contributes to Arctic sea ice decline. The Cryosphere, 5, 821–829, doi:10.5194/tc-5-821-2011

Smetacek, V., and S. Nicol. 2005. Polar ocean ecosystems in a changing world. Nature, 437, 362-368

Smith, R. C., and K. S. Baker. 1978. The bio-optical state of ocean waters and remote sensing. Limnology and Oceanography, 23, 247–259

Smith, R. C. and K. S. Baker. 1984. The analysis of ocean optical data. Ocean Optics (Bellingham, Wash.), 7, 119-126

Smith, W.O., Jr, Baumann, M.E.M., Wilson, D.L., and Aletsee, L. 1987. Phytoplankton biomass and productivity in the marginal ice zone of the Fram strait during summer 1984. Journal of Geophysical Research, 92, 6777-6786

Smith, W. O., and D. M. Nelson. 1985. Phytoplankton bloom produced by a receding ice edge in the Ross Sea : Spatial coherence with the density field. Science, 227, 163

Soltwedel, T., Bauerfeind, E., Bergmann, M., Budaeva, N., Hoste, E., Jaeckisch, N., Juterzenka, K., Matthiessen, J., Mokievsky, V., Noethig, E.-M., Queric, N., Sablotny, B., Sauter, E., Schewe, I., Urban, B., Wegner, J., Wlodarska-Kovalczuk, M., and M. Klages. 2005. HAUSGARTEN: multidisciplinary investigations at a deep-sea, long-term observatory in the Arctic Ocean. Oceanography, 18(3), 46-61

Spencer, J. W. 1971. Fourier series representation of the position of the sun. Search, 2, 172

Spreen, G., Kaleschke, L., and G. Heygster. 2008. Sea ice remote sensing using AMSR-E 89-GHz channels. Journal of Geophysical Research, 113, C02S-3

Steele, J. H. 1962. Environmental control of photosynthesis at the sea. Limnology and Oceanography, 7, 137-150

Steeman-Nielsen, E. 1951. Measurement of production of organic matter in sea by means of carbon-14. Nature, 267 (4252), 684-685, *doi*:*10.1038/167684b0*

Steemann-Nielsen, E. 1965. On the terminology concerning production in aquatic ecology with a note about excess production. Archiv für Hydrobiologie, 61, 184-189

Stramski, D., Reynolds, R. A., Babin, M., Kaczmarek, S., Lewis, M. R., Roettgers, R., Sciandra, A., Stramska, M., Twardowski, S., Franz, B. A., and H. Claustre. 2008. Relationships between the surface concentration of particulate organic carbon and optical properties in the eastern South Pacific and eastern Atlantic Oceans, Biogeosciences, 5, 171–201, doi:10.5194/bg-5-171-2008

Sugget, D. J., Oxborough, K., Baker, N. R., Macintyre, H. L., Kana, T. M., and Geider, R. J. 2003. Fast repetition rate and pulse amplitude modulation chlorophyll a measurements for assessment of photosynthetic electron transport in marine phytoplankton. European Journal of Phycology, 38, 371-384

Sverdrup, H. U. 1953. On conditions for the vernal blooming of phytoplankton. Journal du Conseil International pour l'Exploration de la Mer, 18, 287–295

Tanre, D., Herman, M., Deschamps, P.Y., De Leffe, A. et al. 1979. Atmospheric modelling for space measurements of ground reflectances, including bidirectional properties. Applied Optics, 18, 3587–3594

Tassan, S. and Ferrari, G. M. 1995. An alternative approach to absorption measurements of aquatic particles retained on filters, Limnology and Oceanography, 40, 1358–1368

Taylor, B. B., Torrecilla, E., Bernhardt, A., Taylor, M. H., Peeken, I., Röttgers, R., Piera, J., and A. Bracher. 2011. Bio-optical provinces in the eastern Atlantic Ocean and their biogeographical relevance, Biogeosciences, 8, 3609-3629, doi:10.5194/bg-8-3609-2011

Tran, S., Bonsang, B., Gros, V., Peeken, I., Sarda-Esteve, R., Bernhardt, A., and S. Belviso. 2013. A survey of carbon monoxide and non-methane hydrocarbons in the Arctic Ocean during summer 2010. Biogeosciences, 10, 1909-1935, doi:10.5194/bg-10-1909-2013

Tremblay, J.-É., Raimbault, P., Martin, J., Garcia, N. 2012. The Ecology and Biogeochemistry of

Subsurface Phytoplankton Layers in the Arctic Ocean. IPY2012. Conference - Montréal, Canada. 22-27 April 2012

Vaquer-Sunyer, R., Duarte, C. M., Regaudie-de-Gioux, A., Holding, J., García-Corral, L.S., Reigstad, M., Wassmann, P. 2013. Seasonal patterns in Arctic planktonic metabolism (Fram Strait - Svalbard region). Biogeosciences, 10. ISSN 1726-4170.s 1451 – 1469.s, doi: 10.5194/bg-10-1451-2013

Velleman, P. F., and Hoaglin, D. C. 1981. Applications, basics, and computing of exploratory data analysis. Belmont, CA: Duxbury Press

Walczowski W, Piechura J. 2007. Pathways of the Greenland Sea warming. Geophysical Research Letters, 34, L10608.

Walczowski, W., Piechura, J., Goszczko, I., Wieczorek, P. 2012. Changes in Atlantic water properties: an important factor in the European Arctic marine climate. ICES Journal of Marine Science, 69, 864-869

Wang, J., Cota, G. F., and D. A. Ruble. 2005. Absorption and backscattering in the Beaufort and Chukchi Seas. Journal of Geophysical Research-Oceans, 110, C04014, doi:10.1029/2002JC001653

Waniek, J. and N.P. Holliday. 2006. Large-scale physical controls on phytoplankton growth in the Irminger Sea. Part 2: model study of the physical and meteorological preconditioning. Journal of Marine Systems, 59, (3-4), 219-237

Wassmann, P. F., Slagstad, D., Wexels R. C., Reigstad, M. 2006. Modelling the ecosystem dynamics of the Barents Sea including the marginal ice zone. II. Carbon flux and interannual variability. Journal of Marine Systems, 59. ISSN 0924-7963.s 1 - 24

Wassmann, P. 2011. Arctic marine ecosystems in an era of rapid climate change. Progress in Oceanography, 90, (1-4). ISSN 0079-6611.s 1 – 17.s, doi: 10.1016/j.pocean.2011.02.002.

Wassmann, P., and M. Reigstad. 2011. Future Arctic Ocean seasonal ice zones and implications for pelagic-benthic coupling. Oceanography, 24(3), 220–231. doi: 10.5670/oceanog.2011.74

Webb, W. L., Newton, M., and D. Starr. 1974. Carbon dioxide exchange of *Alnus Rubra*: a mathematical model. Ecologia, 17, 281-291

Welschmeyer N., and C. Lorenzen. 1981. Chlorophyll-specific photosynthesis and quantum efficiency at subsaturating light intensities. Journal of Phycology, 17, 283–293

Weston, K., Fernand, L., Mills, D.K, Delahunty R., and J. Brown. 2005. Primary production in the deep chlorophyll maximum of the northern North Sea. Journal of Plankton Research, 27, 909 – 922

Williams, P. J. leB. 1993. On the definition of plankton production terms. In: Measurement of primary

production from the molecular to the global scale. Eds: W. K. W. Li and S. Y. Maestrini, 9-19, International Council for the Exploration of the Sea, Copenhagen, Denmark

Wiltshire, K. H., and B. F. J. Manly. 2004. The warming trend at Helgoland Roads, North Sea: phytoplankton response. Helgoland Marine Research, 58, 269–273

White, H. 1980. A heteroskedasticity-consistent covariance matrix estimator and a direct test for heteroskedasticity. Econometrica, 48 (4), 817–838. doi:10.2307/1912934.JSTOR 192112934

Wozniak B., Dera J., Ficek D., Majchrowski R., Kaczmarek S., Ostrowska M., Koblentz-Mishke O.-I. 1998. Modelling the influence of photo- and chromatic- acclimation on the absorption properties of marine phytoplankton. Ocean Optics Conference, Kailua-Kona, Hawaii, USA, 10-13 November 1998

Wright, J.C. 1959. Limnology of Canyon Ferry Reservoir: Phytoplankton standing crop and primary production. Limnology and Oceanography, 4, 235-245

Wu, Y. S., Peterson, I. K., Tang, C. C. L., Platt, T., Sathyendranath, S., and Fuentes-Yaco, C. 2007. The impact of sea ice on the initiation of the spring bloom on the Newfoundland and Labrador Shelves. Journal of Plankton Research, 29, 509–514

List of abbreviations

A&M 1996 standard	primary production calculated using Antoine and Morel (1996) model
A&M 1996 & Che 2013	primary production calculated using Antoine and Morel (1996) model with Cherkasheva et al. (2013a) parametrization
ACRI	Arctic Climate Regime Index
AMSR-E	Advanced Microwave Scanning Radiometer - Earth Observing System
AR	Autotrophic Respiration
ARCSS-PP	Arctic primary production in situ database
ARK-25	25th R/V Polarstern expedition to the Arctic
ART	Arctic in Rapid Transition
AO	Arctic Oscillation index
AWI	Alfred-Wegener-Institute for Polar and Marine Research, Bremerhaven
B&F 1997	primary production calculated using Behrenfeld and Falkowski (1997a) model
CDOM	Colored Dissolved Organic Matter
CHL	CHLorophyll-a
CTD	Conductivity Temperature Depth sensor
CZCS	Coastal Zone Color Scanner
DIN	Dissolved Inorganic Nutrients
EF	Eastern Fram Strait
EGC	East Greenland Current
FRRF	Fast Repetition Rate Fluorometer
GlobColour	The European Service for Ocean Colour
GPP	Gross Primary Production
GS_all	Greenland Sea sector of the Arctic
GSM	Garver-Siegel-Maritorena model
HPLC	High Performance Liquid Chromatography
MERIS	MEdium Resolution Imaging Spectrometer
MODIS	MODerate resolution Imaging Spectroradiometer
MOM-2	geophysical fluid dynamics laboratory Modular Ocean Model
NAO	North Atlantic Oscillation index
NAOSIM	North Atlantic/Arctic Ocean Sea-Ice Model

NCEP	National Centers for Environmental Prediction
NCP	Net Community Production
NOAA	National Oceanic and Atmospheric Administration
NPP	Net Primary Production
NSIDC	National Snow and Ice Data Center
NwAC	Norwegian Atlantic Current
OD	Optical Density
PABs	Particulate ABsorption
PAR	Photosynthetically Active Radiation
PHAROS	PHysical Analysis of RemOte Sensing images
PP	Primary Production
PPARR	Primary Production Algorithm Round Robin
PPC	Photo-Protecting Carotenoid
PSC	Photosynthetic Carotenoid
PUR	Photosynthetically Usable Radiation
R/V	Reseach Vessel
RAC	Return Atlantic Current
RMSD	Root Mean Square Difference
SeaWiFS	Sea-viewing Wide Field-of-view Sensor
SCM	Subsurface Chlorophyll Maximum
SIC	Sea Ice Concentration
SIT	Sea Ice Thickness
SSS	Sea Surface Salinity
SST	Sea Surface Temperature
TEOS-10	Thermodynamic Equation Of Seawater - 2010
TI	Time-Integrated primary production model
VGPM	Vertically Generalized Primary production Model
WF	Western Fram Strait
WIDI	Wavelength-Integrated-Depth-Integrated primary production model
WIDR	Wavelength-Integrated-Depth-Resolved primary production model
WRDR	Wavelength-Resolved-Depth-Resolved primary production model
WSC	West Spitsbergen Current

Acknowledgements

I would like to thank all those who made current study possible:

My PhD thesis supervisor Astrid Bracher and Antje Boetius for their willingness to review this thesis

Justus Notholt and Georg Heygster for providing me an opportunity to conduct this thesis

The team of graduate school POLMAR, and especially Claudia Sprengel and Claudia Hanfland for their support and advice all through PhD time, for funding my research, for providing an exceptional prolongation of funding, for sponsoring scientific stay at the Laboratory of Villefranche, for granting travel and accommodation support for conferences, and for giving me an opportunity to participate in soft skill courses, which were very valuable for the successful completion my PhD. Last but not least, I am thankful to them for making PhD Committees mandatory.

Gopika Suresh for proofreading all texts I have ever written since she entered IUP, for ideas I learned from her, brainstorming, and also for her generosity and energy which made my PhD time lighter

Christian Melsheimer for his positive and personal attitude, for guiding me in my first months in Germany and even before that, for helping me with administrative and scientific tasks, for always finding time for scientific discussions, makemap script, for careful reading of my manuscripts and conference contributions

My current supervisor Maria Hörhold for her understanding and for giving me the opportunity to finalize the thesis in tranquility

Astrid Bracher for giving the initial idea for my PhD project, for scientific freedom, for advising me on relevant literature and conferences, for starting collaboration with Eva-Maria-Nöthig and Antje Boetius, for organizing my participation in RV 'Polarstern' cruises and for reviewing the manuscripts.

PHAROS and PHYTOOPTICS groups for the friendly atmosphere. I am thankful to PHAROS group for satellite sea ice concentration data

Colleagues of the Laboratory of Villefranche: David Antoine for his ideas, for hosting me during the scientific stay in his laboratory, for the script of Morel (1991) model; and Bernard Gentili for processing the data in his free time and teaching me to use the script.

Antje Boetius for her help during R/V 'Polarstern' cruise, and when revising the manuscript, and an inspiration she gives students

Cornelia Köberle for promptly extracting NAOSIM datasets and explaining me how to handle them

Rüdiger Gerdes for the NAOSIM data and his helpful comments during the manuscript revision

Martin Losch for always participating in my PhD Committee meetings, for which he had to travel

Eva-Maria Nöthig for providing the chlorophyll-a data that she has been gathering for years and for her comments during the revision of our publications

Sonja Wiegmann, Ilka Peeken and Anja Bernhardt for processing in-situ PABs, HPLC CHL and PAR data

Mariana Altenburg Soppa for providing the publications that were not accessible by the University of Bremen library

Kevin Arrigo for suggesting to focus specifically on the Greenland Sea

Victor Foux and Alexey Koldunov from the St Petersburg State University for giving me my first insight into satellite oceanography

Birgit Teuchert for her quick help with administrative issues

Peter Grupe for technological assistance

Special thanks to all the crews, scientists, and Captains from R/V 'Polarstern' cruises, for offering helping hands onboard

ESA and NASA for the satellite chlorophyll-a, sea surface temperature and brightness temperatures data

Very special thanks to:

Anna Serdyuchenko for her encouragement and support, along with the recreational time with her pets

Victor Gorshelev for his sense of humor, for up to date info about current affairs, and for always helping me

Marcus Huntemann for his calmness, being the perfect officemate, for helping me with sea ice data and for sharing his expertise in IT

Nicolas Cassar for his RV 'Polarstern' lectures and for showing me the excitement of being a marine biologist

Larisa Istomina for keeping me healthy physically

Zhen Li and Mariugenia Salas for our time together

Tilman Hesse for his friendship and long talks

Olga Batura for her knowledge about visa and other bureaucratic issues

Olivia Serdeczny for her generous help onboard RV 'Polarstern' especially during the 20-hour shifts, and for her warm personality

Rosa Wilm for waking up in the middle of the night onboard RV 'Polarstern' to help me do the measurements, although she was not part of my working group

My sister for being an example of a person passionate about her work, for always being there for me, and her honesty

My parents for being my inspiration. I thank them for their love, patience, trust in me and for teaching me to never give up. I thank my mother for being my pillar of strength and support, for teaching me the various languages that I know, for building the creative side of mine and for teaching me how not to be afraid

Last, but not least, I thank my grandmother for telling me to always learn new things